THE SODIUM-O_2/CO_2 ELECTROCHEMICAL CELL

A Dissertation

Presented to the Faculty of the Graduate School

of Cornell University

In Partial Fulfillment of the Requirements for the Degree of

Doctor of Philosophy

by

Shaomao Xu

May 2016

THE SODIUM –O_2/CO_2 ELECTROCHEMICAL CELL

Shaomao Xu, Ph. D.

Cornell University 2016

Metal-air batteries, especially lithium and sodium air systems, have attracted significant research effort in the past decade. The high theoretical specific energy (3500Wh/kg for Li-O_2 and 1600Wh/kg for Na-O_2) and moderate equilibrium potential (2.96V for Li-O_2 and 2.3V for Na-O_2) make these chemistries attractive energy storage platforms for transportation, autonomous aircraft, and emergent robotics technologies. The term metal-air battery, however, is often used to describe the system which is actually a "metal-O_2" battery, for in most studies O_2 is used in place of air as the active material in the battery cathode. This change is employed to eliminate formation of electrochemically stable metal hydroxide and metal carbonate discharge products when CO_2 and moisture present in ambient air react with metal ions in the cathode. Therefore, when it comes to practical design and operation of metal-air battery, significant new complications that largely defeat the competitive advantages of this storage technology will be introduced into the metal-air battery system due to the impurities in the ambient air. Recent work has shown that when a mixture of O_2 and CO_2 is used as the active material in the cathode, it is possible to recharge a metal-O_2/CO_2 cell provided steps are taken to prevent electrolyte decomposition during the recharge.

In the current work, we studied electrochemical processes in model sodium-O_2/CO_2 (Na-O_2/CO_2) cells. We find that provided that with the formation of the electrochemically stable electrode/electrolyte interfaces, such cells are able to deliver both exceptional energy storage capacity and stable long-term charge-discharge cycling behaviors at room temperature. $NaHCO_3$ is shown to be the principal discharge product through in- and ex-situ chemical analysis of the cathode. The modification on the electrolyte to make it stable under high voltage is crucial for the rechargeability of the system. By means of differential electrochemical mass spectrometry (DEMS), we show that addition of as little as 10% of electrolyte additive extends the high-voltage stability of the electrolyte by at least 1 V, allowing recharge of the Na-CO_2/O_2 cells. We also report a novel primary Li-CO_2 battery that consumes pure CO_2 gas in its cathode. The battery exhibits a high discharge capacity of around 2500 mAh/g at moderate temperatures. The metal-O_2/CO_2 platform provides a novel approach for simultaneous capturing of CO_2 emissions and producing electrical energy.

BIOGRAPHICAL SKETCH

Shaomao Xu was born in April 1987 in Qingdao, China and graduated from China University of Petroleum in 2010 with a degree of Bachelor of Engineering in Chemical Engineering. After graduation, Shaomao came to Cornell University as a master of engineering student. After receiving a degree of Master of Engineering in Chemical Engineering in 2011, Shaomao stayed at Cornell University to pursue his PhD in Chemical Engineering.

Dedicated to my parents and family.

ACKNOWLEDGMENTS

First of all, I would like to express my gratefulness for all the guidance and support provided by my advisor, Professor Lynden Archer, for the past five years. His insightful advice has led me through various difficulties during the project, and his inspiration has been a great source of motivation for my research.

I also would like to thank Professors Yong Lak Joo and Jin Suntivich for serving as my committee members and their comments on my work are greatly appreciated. Many thanks are also due to the Archer group members/alumni: to Shyamal Das for helping me set up the initial experiments; to Zichao Yang and Yingying Lu for helpful discussions and experimental assistance; to Shuya Wei, Lin Ma, Zhengyuan Tu and Rajesh Mallavajula for their support in various ways; to MEng and undergraduate students Wenwen Liu, Yi Shi and Michael Statt for assisting with some of the experiments. I would like to thank collaborators Yingchao Yu and Hongsen Wang (Abruña group) for their effort.

Energy Materials Center at Cornell and KAUST-Cornell Center for Energy and Sustainability are acknowledged for financial support and Cornell Center for Materials Research for use of facilities.

Last but not least, I would like to thank my parents for their affection and care over the years, and my family for their support.

TABLE OF CONTENTS

LIST OF FIGURES

LIST OF TABLE

CHAPTER 1

Introduction

CO_2 and Ambient Air in Metal-Oxygen Batteries: Steps towards Reality

1.1 Abstract

Metal-air batteries, especially lithium and sodium air technologies, have gained significant research focus in the past decade. The high theoretical specific energy (3500Wh/kg for Li-O_2 and 1600Wh/kg for Na-O_2) and moderate equilibrium potential (2.96V for Li-O_2 and 2.3V for Na-O_2) make these chemistries attractive energy storage platforms for transportation, autonomous aircraft, and emergent robotics technologies. The term metal-air battery, however, hardly describes the cell designs under most active investigation by researchers, for in most studies O_2 is used in place of air as the active material in the battery cathode. This change, designed to eliminate formation of electrochemically stable metal hydroxide and metal carbonate discharge products when CO_2 and moisture present in ambient air react with metal ions in the cathode, introduce significant new complications for practical metal-air battery design and operations that largely defeat the competitive advantages of this storage technology. Recent work has shown that when a mixture of O_2 and CO_2 is used as the active material in the cathode, it is possible to recharge a metal-O_2/CO_2 cell provided steps are taken to prevent electrolyte decomposition during the recharge. In this chapter, we critically review the literature on metal-O_2/CO_2 cells, focusing on how the presence of CO_2 in the active cathode material changes electrochemistry at the cathode

and rechargeability of the cells. We also assess progress and future prospects for metal-air battery technologies involving ambient air as the cathode gas.

1.2 Introduction

With a theoretical energy density of 3505 Wh/kg [13], including the weight of oxygen during discharge, the rechargeable Li-air battery is considered among the most promising electrical energy storage platforms for electrified transportation. [1-3, 6-12] While it is understood that in actual practice only a fraction of this high theoretical energy density can be achieved in a reversible energy storage device, the much higher efficiency of electric motors [4, 5] over internal combustion engines means that an electric vehicle powered by a Li-air cell can still attain a usable energy density competitive with that of conventional fossil fuels, such as gasoline (1750 Wh/kg). [9] Unlike the Li-ion battery, however, which is based on highly reversible ion intercalation reactions at both the anode and cathode, the Li-air cell involves an interfacial electrochemical conversion reaction between lithium ions in an electrolyte and oxygen, dissolved in the electrolyte from ambient air, at a porous carbon cathode. At the anode, electrochemical stripping and plating of metallic lithium is the source and sink of lithium ions consumed during the discharge reaction and produced during the Li-air cell recharge.

These fundamental differences between the electrochemical processes at work in Li-ion and Li-air cells are largely responsible for the contrasting states of commercial readiness of the two technologies. On the anode side, it is known that reversible

stripping and plating of metallic lithium in liquid electrolytes is frustrated by multiple issues, including side reactions with the electrolyte that over time deplete the lithium and electrolyte and by uneven electrodeposition and dendrite proliferation in the cell, which may lead to internal short circuiting and is therefore a serious safety concern. [14, 15] Electrolyte decomposition may also be exacerbated by the formation of reactive $O_2^{\bullet-}$ species in the electrolyte. [16, 17] Additionally, the vast majority of the "Li-air" batteries that have been studied in the literature are in reality lithium-oxygen cells because these cells utilize pure oxygen, as opposed to ambient air, in the cathode. While this practice is important for advancing fundamental knowledge, the presence of significant amounts of moisture and CO_2 in ambient air, produces as fundamental changes in the chemistry of an actual Li-air cell, with new insulating species such as LiOH and Li_2CO_3 forming at the cathode, making the battery less rechargeable. [18, 19] It is possible to remove these complications in a practical Li-air cell by adding to the cell design a gas pretreatment/purification system to remove H_2O and CO_2 from ambient air or by including an on-board storage tank suitable for delivering pure oxygen as desired during battery operation. [20] Unsurprisingly, the introduction of these additional components lead to substantial increases in the weight and capital cost of a Li-air system, which cancel out the most important advantages of a Li-air battery, compared to the Li-ion system, for applications in transportation.

As a first step towards advancing knowledge of the effect of CO_2 in ambient air on the operations of the Li-air cell, several recent studies have focused on Li-O_2/CO_2 batteries, which utilize a mixture of oxygen and carbon dioxide at the cathode. An

added impetus for such work comes from the prospect of using such metal-O_2/CO_2 cells in a hybrid EV design where the battery plays the dual role of a carbon capture-conversion system able to reduce emissions and enhance the range of a conventional IC-based vehicle powered by fossil fuels. Indeed, while a variety of chemical and physical methodologies are under active investigation to capture and sequester the thousands of tons of CO_2 emitted every year in transportation, [21-23] the vast amount of energy consumed to regenerate the capture fluid or sorbent, is a common shortcoming of all approaches. Thus, without some form of government intervention to alter the economics of CO_2 capture from mobile sources, it is unlikely that any of the carbon capture technologies under development will find widespread use in transportation. A metal-air battery that utilizes a mixed fuel of O_2 and CO_2 therefore provides a model for studying the effects of CO_2 in ambient air on the Li-O_2 cell operation and at the same time, provides a novel hybrid platform for electrical energy generation and carbon capture. This chapter focuses on recent developments in both areas and highlights progress in metal-O_2/CO_2 and metal-ambient air batteries that are enabled by these works.

1.3 Metal-O_2/CO_2 Batteries

1.3.1 Li-O_2/CO_2 Battery

The first lithium-air battery system involving a mixture of O_2 and CO_2 gas in the cathode was reported by Takechi et al. [24] It is known that $O_2^{\bullet-}$ can be captured by CO_2 and this reaction has been widely used in CO_2 sensors, as well as in molten-carbonate fuel cells (MCFCs). [25, 26] Based on this reaction, the electrochemical

processes in the cathode of a Li-O_2/CO_2 battery have been argued to involve the following five-step reaction sequence [24]:

$$4O_2 + 4e^- \rightarrow 4{O_2}^{\bullet -} \quad (1)$$

$${O_2}^{\bullet -} + CO_2 \rightarrow {CO_4}^{\bullet -} \quad (2)$$

$${CO_4}^{\bullet -} + CO_2 \rightarrow {C_2O_6}^{\bullet -} \quad (3)$$

$${C_2O_6}^{\bullet -} + {O_2}^{\bullet -} \rightarrow {C_2O_6}^{2-} + O_2 \quad (4)$$

$${C_2O_6}^{2-} + 2{O_2}^{\bullet -} + 4Li^+ \rightarrow 2Li_2CO_3 + 2O_2 \quad (5)$$

The discharge product is therefore thought to be Li_2CO_3. One interesting fact about this Li-O_2/CO_2 battery is that the specific discharge capacity is two times higher than that of the Li-O_2 battery, as shown in Figure 1.1. It has also been observed that the void space in the cathode is fully filled by the discharge products, which is not the case for a Li-O_2 battery. The reason for this difference is believed to revolve around differences in the reaction rate. The first reaction in the proposed mechanism is common to both Li-O_2 and Li-O_2/CO_2 batteries. Following this reaction, in a Li-O_2 battery, the ${O_2}^{\bullet -}$ radical reacts with Li+ ion to form ${LiO_2}^{\bullet}$, and this reaction is believed to be slower than the reactions (2)-(4) in the analogous Li-O_2/CO_2 battery. Furthermore, although the intermediate products were not detected, it is believed that the intermediate ${C_2O_6}^{2-}$ compound can stably diffuse in the electrolyte, thus slowing down the precipitation of Li_2CO_3, allowing it to completely fill the void space in the cathode. Unfortunately, these studies are all based on carbonate electrolytes, which are now known to undergo additional electrochemical decomposition reactions during the recharge. This finding leads to the widespread, but incorrect, view that in contrast to the Li-O_2 battery, a Li-O_2/CO_2 battery is not rechargeable.

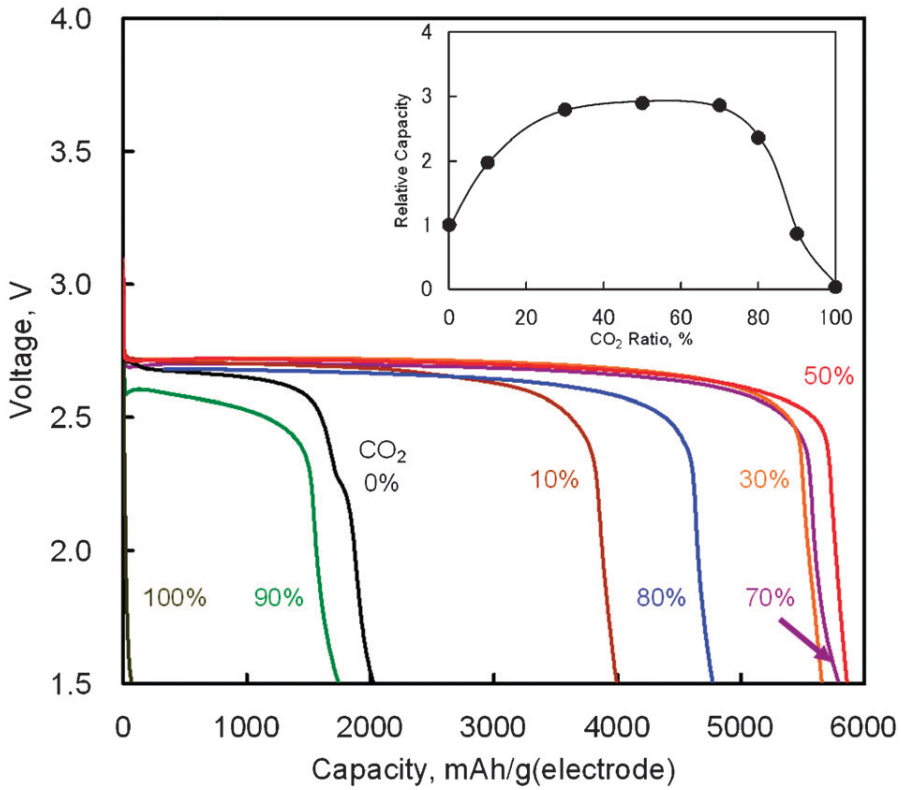

Figure 1.1 Discharge curves for the Li–O_2/CO_2 battery with various ratios of CO_2 in O_2/CO_2 mixed gas at 25 ℃ (current density: 0.2mA/cm^2). Inset shows how CO_2 composition in the cathode gas impacts relative discharge capacities, compared with the Li–O_2 battery (CO_2 0%). Adapted from [24].

The reaction mechanism of the Li-O_2/CO_2 battery has been reported to depend on the type of electrolyte used. Kim and Kang et al. studied Li-O_2/CO_2 cells with DME and DMSO electrolytes. [27] Using density functional theoretical (DFT) analysis, the authors contended that in low dielectric constant (ε) electrolytes such as DME (ε = 7.2) the $O_2^{\bullet-}$ radical is favored to react with Li+ and form $LiO_2^{\bullet}$, so the reaction mechanism in the Li-O_2/CO_2 battery is thought to be the same as in the Li-O_2 battery, with Li_2O_2 as the principal discharge product. However, in high ε electrolytes like carbonates and DMSO (ε = 47.2), the reaction between the $O_2^{\bullet-}$ radical and CO_2 is more favored, so in this case CO_2 does take part in the reaction, and the discharge product is Li_2CO_3 (Figure 1.2a). These predictions are consistent with the limited experimental data available. In the high-ε electrolyte (DMSO) case, it is worth noting that even though the discharge product is Li_2CO_3, which is thermodynamically stable and thought to be undegradable during recharge, the cells still exhibit some amount of rechargeability and were stably cycled for over 20 cycles, as shown in Figure 1.2b and c. The formation of the discharge product Li_2CO_3 was detected after discharge and the disappearance of the product after recharge was also observed. These findings therefore appear to demonstrate that the Li-O_2/CO_2 battery can be recharged, which opens the possibility for Li-O_2/CO_2 rechargeable cells to be used in more or less the same applications targeted for Li-O_2 and Li-air batteries.

For electrolytes such as DME, in which Li_2O_2 is the main discharge product, the amount of CO_2 in the O_2/CO_2 mixture has been reported to markedly influence cell

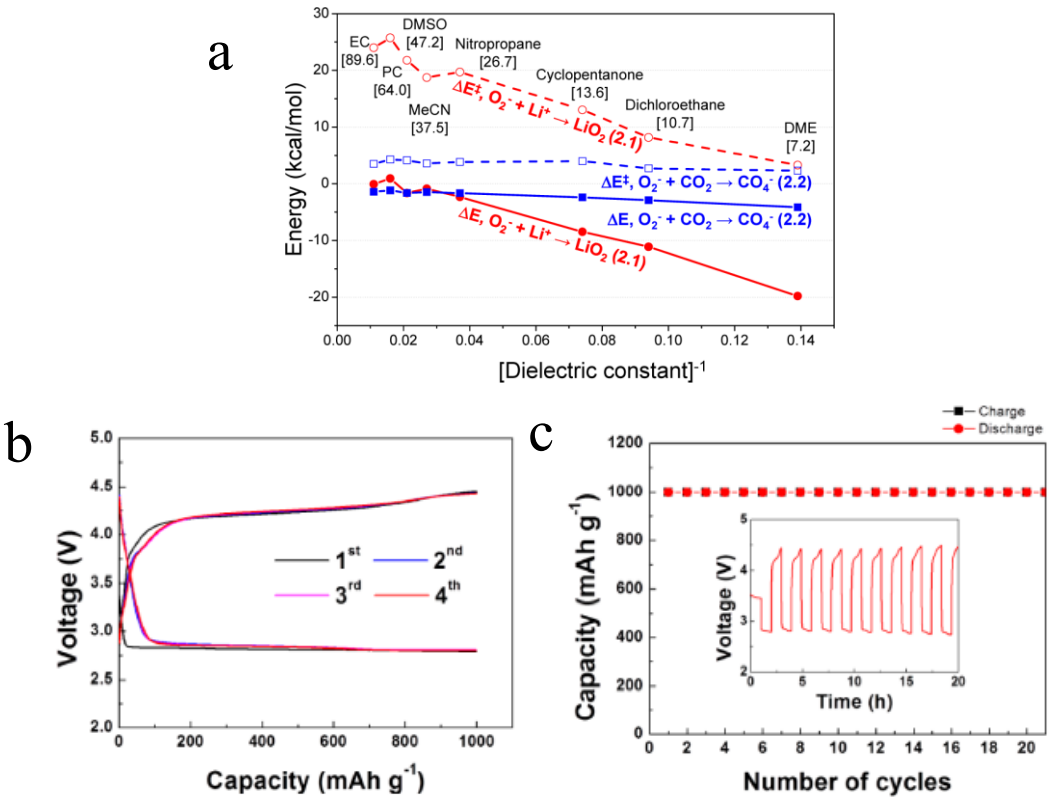

Figure 1.2 (a) DFT-predicted trend of activation barrier ($\Delta E^{\ddagger}$, dashed) and binding reaction energy (ΔE, solid) plotted against [dielectric constant]-1 for the initial complex formation (ICF) steps of reactions, forming LiO_2 (red, circle) and CO_4^- (blue, square), respectively. The values enclosed in brackets are the dielectric constants of various solvents. (b) The voltage profiles for the first four cycles and (c) the related cyclability of the Li-O_2/CO_2 battery with DMSO electrolyte. Current density=0.4mA/cm^2. Adapted from [27].

operation. Mekonnen et al. found that a 1% CO_2 atmosphere (99% O_2) increased the capacity of a Li-O_2 cell to ~120% of the pure O_2 case, but a 50% CO_2 atmosphere reduced the capacity to ~4% of the pure O_2 case, effectively deactivating the battery. [42] The complementary DFT study found that CO_2 adsorption is most favorable at the step valley sites of the $(1\bar{1}00)$ Li_2O_2 surface, with an adsorption energy of -0.73 eV. The authors conclude that low CO_2 concentrations block surface-active nucleation sites, which increases the capacity of the battery but at the expense of an increased overpotential. A follow-up DFT study of the Li_2CO_3@Li_2O_2 interface found that electron polaron hopping can occur within the peroxide side of the interface with a low energy barrier of less than 0.5 eV. [43] These interfaces may increase the discharge product conductivity versus pure Li_2O_2, offering another possible explanation for the extended capacity in the presence of CO_2.

1.3.2 Na-O_2/CO_2 Battery

The gradual depletion of lithium resources and anticipated rise in the cost of lithium has fueled interest in alternatives to metallic lithium as the anode in metal-air batteries. [28-32] Sodium has a high earth-abundance (sixth most abundant element), is relatively easy to extract, and is available at a fraction of the cost of lithium. It is therefore unsurprising that sodium-based battery systems are attracting significant attention from research groups worldwide. [33-35] With this increased interest, rising attention is being given to the benefits of Na-air and Na-O_2 cells as energy storage platforms that can compete with Li-O_2 technology. Das et al. reported the first example of the Na-O_2/CO_2 battery and pointed out how the lower cost and high

natural abundance of Na would enable potential use of such cells for simultaneously capturing CO_2 and generating electrical energy. [36] Consistent with what has been found for the Li-O_2/CO_2 battery, these authors reported that by adding between 40% and 63% CO_2 in the cathode gas streams, Na-O_2/CO_2 batteries with discharge capacity 2.1 and 2.6 times (Figure 1.3a and b) higher than the corresponding Na-O_2 cell are possible in the ionic liquid 1-ethyl-3-methylimidazolium trifluoromethanesulfonate and tetraglyme-based electrolytes, respectively. Postmortem analysis of the cathode using XRD showed that the specific choice of electrolyte chemistry profoundly influences the chemistry of the discharge product. In the IL-based electrolyte, the discharge product was found to be Na_2CO_3, while in a tetraglyme-based electrolyte, a mixture of Na_2CO_3 and $Na_2C_2O_4$ was argued to be the discharge product. The authors reported the following reaction mechanisms in the two electrolyte systems: (i) In the ionic liquid based electrolyte, the reaction is analogous to the reaction in Li-O_2/CO_2 battery.

$$4O_2 + 4e^- \rightarrow 4{O_2}^{\bullet -} \quad (6)$$

$${O_2}^{\bullet -} + CO_2 \rightarrow {CO_4}^{\bullet -} \quad (7)$$

$${CO_4}^{\bullet -} + CO_2 \rightarrow {C_2O_6}^{\bullet -} \quad (8)$$

$${C_2O_6}^{\bullet -} + {O_2}^{\bullet -} \rightarrow {C_2O_6}^{2-} + O_2 \quad (9)$$

$${C_2O_6}^{2-} + 2{O_2}^{\bullet -} + 4Na^+ \rightarrow 2Na_2CO_3 + 2O_2 \quad (10)$$

(ii) In the tetraglyme-based electrolyte, the reactions above occur in tandem with the reaction summarized below, during the discharge.

$$O_2 + 2e^- \rightarrow {O_2}^{2-} \quad (11)$$

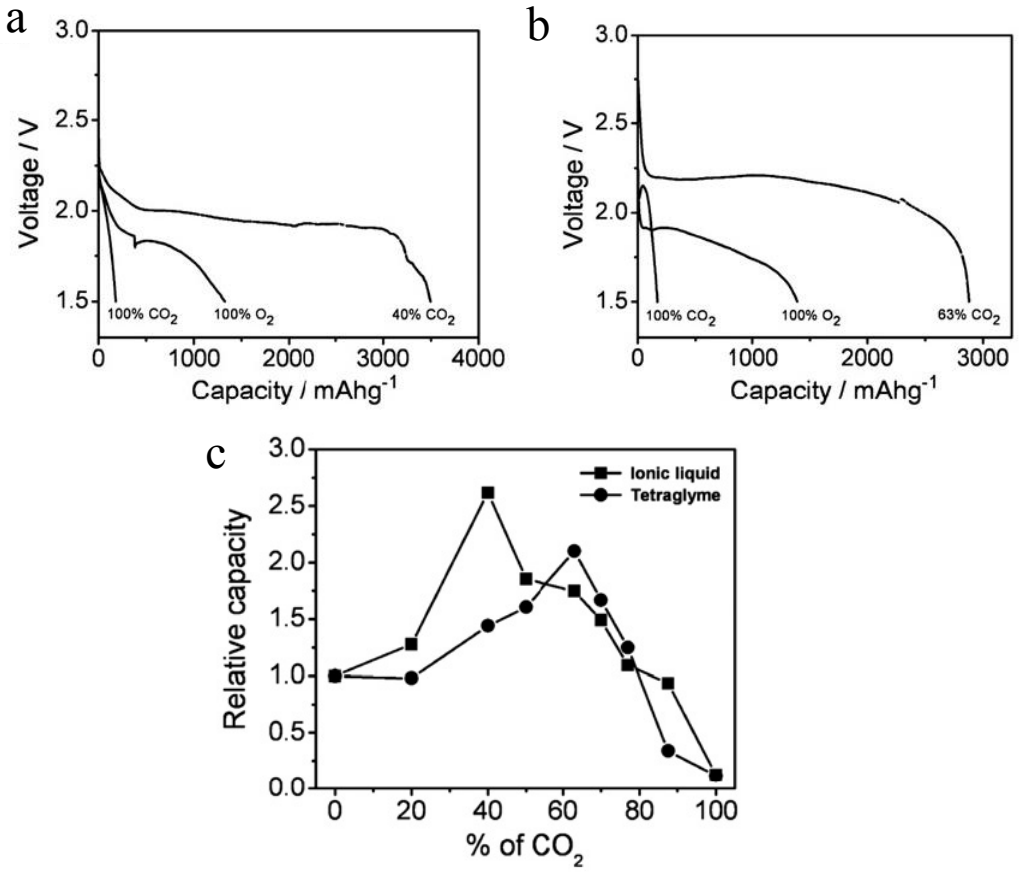

Figure 1.3 Galvanostatic discharge profiles for Na–CO_2/O_2 cells operated with a mixed O_2/CO_2 gas feed. (a) Measurements performed in an electrolyte based on the Ionic Liquid (IL) 1-ethyl-3-methylimidazolium trifluoromethanesulfonate and (b) Measurements performed in tetraglyme-based electrolytes; (c) variation of capacity with CO_2 concentration. Adapted from [36].

$$CO_2 + {O_2}^{2-} \rightarrow {CO_4}^{2-} \quad (12)$$

$${CO_4}^{2-} + CO_2 + 2Na^+ \rightarrow Na_2C_2O_4 + O_2 \quad (13)$$

In this case, the discharge product is a mixture of Na_2CO_3 and $Na_2C_2O_4$.

Due to the stability of the sodium oxides, the charge potential of the Na-O_2/CO_2 battery is above 4.5V (vs. Na/Na+), which is beyond the stability window of most electrolytes. As a consequence, it is difficult to develop a rechargeable Na-O_2/CO_2 battery based on conventional electrolyte systems. The Archer group have reported that addition of ionic liquid tethered silica nanoparticles as additive in propylene carbonate-based electrolytes can enhance high-voltage stability of the electrolyte. [50, 51] Figure 1.4a illustrates how such SiO_2-tethered ILs can be used as electrolyte additives in Na-O_2/CO_2 batteries and Figure 1.4(b) and 4(c) show how addition of the additives leads to rechargeablity of the Na-O_2/CO_2 battery. [37] In particular, with the addition of 10% of the SiO_2-IL additive to a propylene carbonate based electrolyte, the cathodic stability of the electrolyte was increased by almost 1V. Therefore, even though the charge potential is above 4.5V, no electrolyte decomposition is observed and the Na-O_2/CO_2 battery can be stably recharged for over 20 cycles. Besides, during recharge of the battery, the evolution of both O_2 and CO_2 is detected, which means the gases that took part in the discharge get released during recharge. This again proves the rechargeability of the battery. Postmortem analyses of the cathode using XRD and vibration spectroscopy indicate that the discharge product is $NaHCO_3$ and that it decomposes upon cell recharge. Trace amounts of H_2O introduced during the preparation of electrolyte is thought to be the source of $NaHCO_3$ as the principal

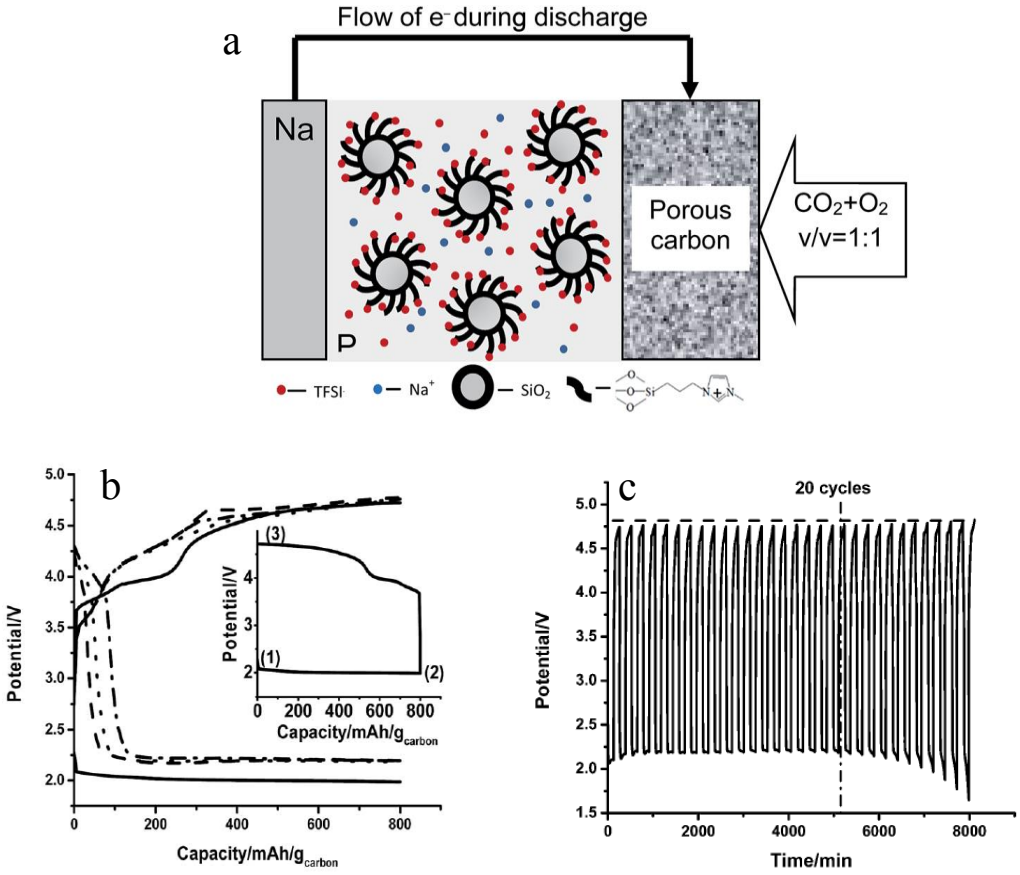

Figure 1.4 (a) Schematic diagram of the Na–O_2/CO_2 rechargeable battery; (b) Discharge–charge profiles for the Na–O_2/CO_2 battery in the first cycle (solid line), 5th cycle (dash line), 10th cycle (dot line) and 20th cycle (dash dot line); (c) Cycling profiles for Na–CO_2/O_2 battery with SiO_2-IL-TFSI/PC electrolyte. The dash line shows the trend of change of the charge potential. The dash-dot line indicates the 20th cycle where the battery shows a stable cycling. The current density employed is 200 mA/g and the capacity cutoff is 800 mA h/g_{carbon}. Adapted from [37].

discharge product. The relatively instability of $NaHCO_3$, compared to Na_2CO_3, may be a reason for the rechargeability of the Na-O_2/CO_2 battery. However, considering the fact that in a Li-O_2/CO_2 battery Li_2CO_3 can be decomposed during recharge, it is possible that even if the cell discharge product is the more stable Na_2CO_3, a rechargeable Na-O_2/CO_2 battery is perhaps still possible.

1.4 Li-/CO_2 Battery

In early studies of Li-O_2/CO_2 batteries, it was shown that with pure CO_2 as the cathode gas, the battery has very low capacity. [24] A report from Xu et al. is to our knowledge among the first to disclose a high-temperature Li-CO_2 battery system that exhibits attractive electrochemical energy storage capacity. [38] High temperature operation was possible using a 1-butyl-3-methylimidazolium bis(trifluoromethanesulfonyl)imide IL-based electrolyte. It is found that whereas the Li-CO_2 battery has a very low storage capacity at room temperature, by increasing the operating temperature to 60 ℃-100 ℃, the discharge capacity increases dramatically (Figure 1.5a). It is believed that operating the Li-CO_2 battery at high temperature brings about two beneficial effects. Firstly, the solubility of discharge product is thought to increase with temperature, thus limiting the thickness of the insulating deposition on the cathode surface. Additionally, a high temperature is thought to improve electrode kinetics by lowering transport barriers at the electrolyte-cathode interface. Based on thermodynamic analysis, it is believed that the discharge product is Li_2CO_3 and carbon:

$$4Li + 3CO_2 \rightarrow 2Li_2CO_3 + C \qquad (14)$$

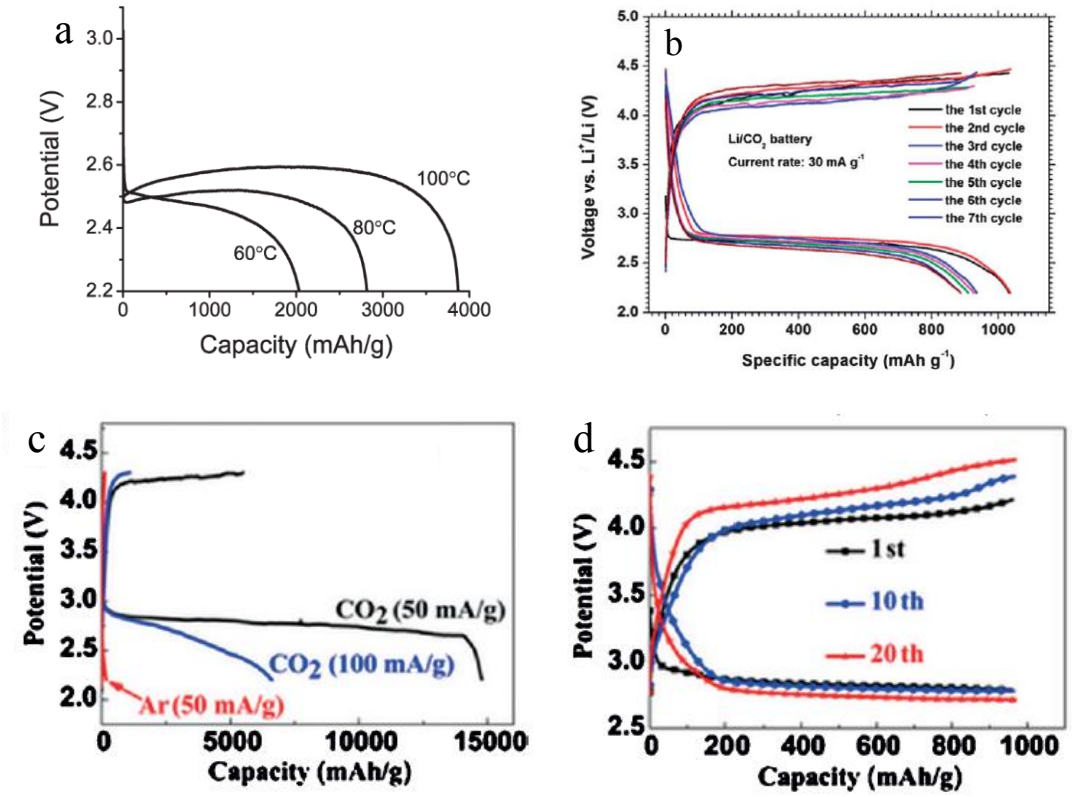

Figure 1.5 (a) Galvanostatic discharge curves for Li-CO_2 cells operated at various temperatures in the range 60-100 ℃ at a current density of 0.05 mA/cm^2 to the potential of 2.2 V. (b) Charge–discharge voltage profiles for the Li-CO_2 battery with cut-off voltage of 2.2 V at room temperature. (c) The initial discharge curves for the batteries with graphene cathodes at a current density of 50mA/g and 100mA/g in CO_2 atmosphere, as well as at 50mA/g in Ar atmosphere (d) Voltage profiles for the 1st, 10th, 20th cycle with a curtailing capacity of 1000mAh/g at a current density of 50mA/g. Adapted from [38-40]

Li_2CO_3 was found to deposit on the surface of cathode, meaning it is one of the major discharge products. However, since carbon cathode was utilized in this study, the formation of carbon is hard to detect.

Li et al. studied the Li-CO_2 battery using a porous gold cathode. [39] After discharge, the formation of amorphous carbon was detected on the cathode, consistent with expectations based on the mechanism in reaction (14). Apart from this, the authors found that with a conventional tetraglyme based electrolyte, the Li-CO_2 battery still shows decent capacity of around 1,000 mAh/g, as shown in Figure 1.5b. Even though the discharge product forms a thick layer of fibers on the surface of the cathode, it can still be decomposed during the recharge and the battery can stably cycle. In order to increase the capacity of the Li-CO_2 battery, Zhou et al. introduced graphene as the cathode material. [40] Due to the exceptional catalytic activity of graphene, the Li-CO_2 battery shows an incredibly high capacity of over 14,000 mAh/g. With a cutoff capacity of 1,000 mAh/g, the battery can be stably cycled for over 20 cycles (Figure 1.5c and d). Even though the Li-CO_2 cells used in the study were investigated only at low current density (J = 50-100mAh/g) and with a high overpotential, a growing consensus is that with additional research the Li-CO_2 battery has the potential to become a prominent member among the new generation of energy storage systems.

1.5 Li-air battery with ambient air

Ambient air introduces yet another impurity to the Li-O_2 battery: water. The amount of water in the air can reach up to 4% depending on humidity, and is generally much

greater than the amount of CO_2 (400 ppm or 0.00040%) in ambient air. [44] Thus, it is important that the effects of water on Li-O_2 cell electrochemistry are studied at the fundamental level. Meini et al. performed one of the earliest of these studies by comparing the discharge performance of Li-O_2 cells in a dry environment to those exposed to water vapor. [45] They observed that the presence of water vapor increased the first cycle capacity of the cell by a factor of ten. The authors proposed that the superoxide radical, $O_2^{\bullet-}$, reacts preferentially with the trace water in the electrolyte to form soluble reaction products. A detailed study by Aetukuri et al. also observed a clear and consistent increase in discharge capacity as a function of water content, shown in Figure 1.6b. [46] XRD analysis of the discharge product confirmed that Li_2O_2 is the dominant species and SEM imaging of the cathode revealed that the Li_2O_2 forms as toroid-shaped particles, which increase in size as the water content in the electrolyte rises. This phenomenon was ascribed to the ability of water to solvate O_2^-, which promotes a solution-phase mechanism in which LiO_2 can disproportionate to produce Li_2O_2 without the need for a direct electron conduction pathway, as illustrated in Figure 1.6a. Linear sweep voltammetry (LSV) appears to confirm this hypothesis. The anhydrous cell produces a sharp peak at a higher potential (Figure 1.6c), agreeing with the theoretically predicted curve for the surface mechanism, while the cell with 4,000 ppm of water produces a broader peak at a reduced potential (Figure 1.6d), consistent with the theoretically predicted curve for the solution mechanism.

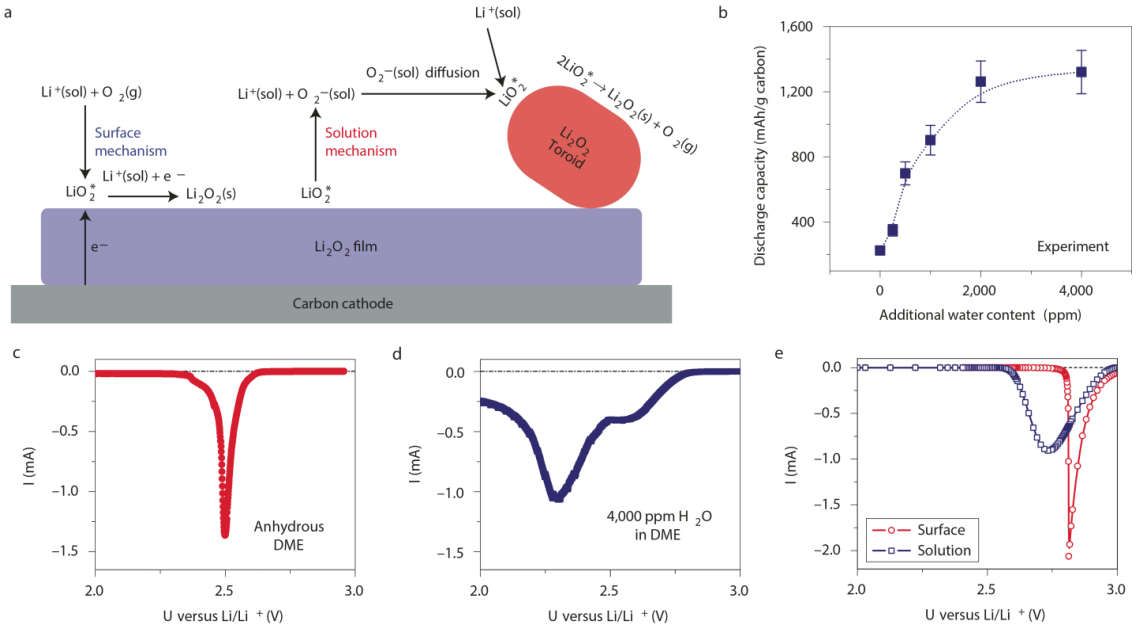

Figure 1.6 (a) Illustration of surface-mediated and solution-mediated Li_2O_2 formation mechanisms. The latter of which is promoted by the presence of water. (b) The dependence of discharge capacity on water content. Discharge linear sweep voltammetries (LSVs) of cells using (c) anhydrous DME electrolyte and (d) electrolyte with 4,000 ppm water added. (e) Discharge LSVs predicted by model for surface- and solution-mediated Li_2O_2 formation. Adapted from [46].

Trace amounts of water were also found to catalyze the oxygen evolution (charging) reaction. Li et al. constructed cells with a Super P carbon cathode containing ruthenium and manganese dioxide nanoparticles, an electrolyte containing 120 ppm of H_2O, and a $LiFePO_4$ anode. [47] Although $LiFePO_4$ could not be used in a practical cell, it was used in place of Li in this study to eliminate anodic side reactions. The presence of water was found to significantly decrease the charge overpotential from 0.70 V to 0.21 V. This was attributed to water acting as a redox mediator during charge. Specifically, Li_2O_2 reacts with water to form LiOH and H_2O_2, which are then oxidized on the Ru and MnO_2 nanoparticles, respectively. The result is a cathode and electrolyte system that could cycle 200 times with only a discharge/charge potential gap of 0.32 V.

With the increase in the understanding of effect of impurities in Li-O_2 battery, it is therefore becoming increasingly possible to develop a Li-air battery with ambient air as the cathode gas. By utilizing a hybrid electrolyte system with a lithium-ion conducting film separating the organic phase and aqueous phase, a rechargeable Li-air battery with ambient air has been reported. [48, 49] The presence of aqueous electrolyte in the cells, however, introduces extra complexity to the battery system, especially during the charge cycles. [49] Zhou et al. developed a rechargeable Li-air battery with ambient air. [41] The battery has a unique structure (Figure 1.7a) with a hybrid electrolyte: the catholyte is a solid conductor $Li_{1.35}Ti_{1.75}Al_{0.25}P_{2.7}Si_{0.3}O_{12}$ while the anolyte is a conventional EC based liquid electrolyte. With this electrolyte,

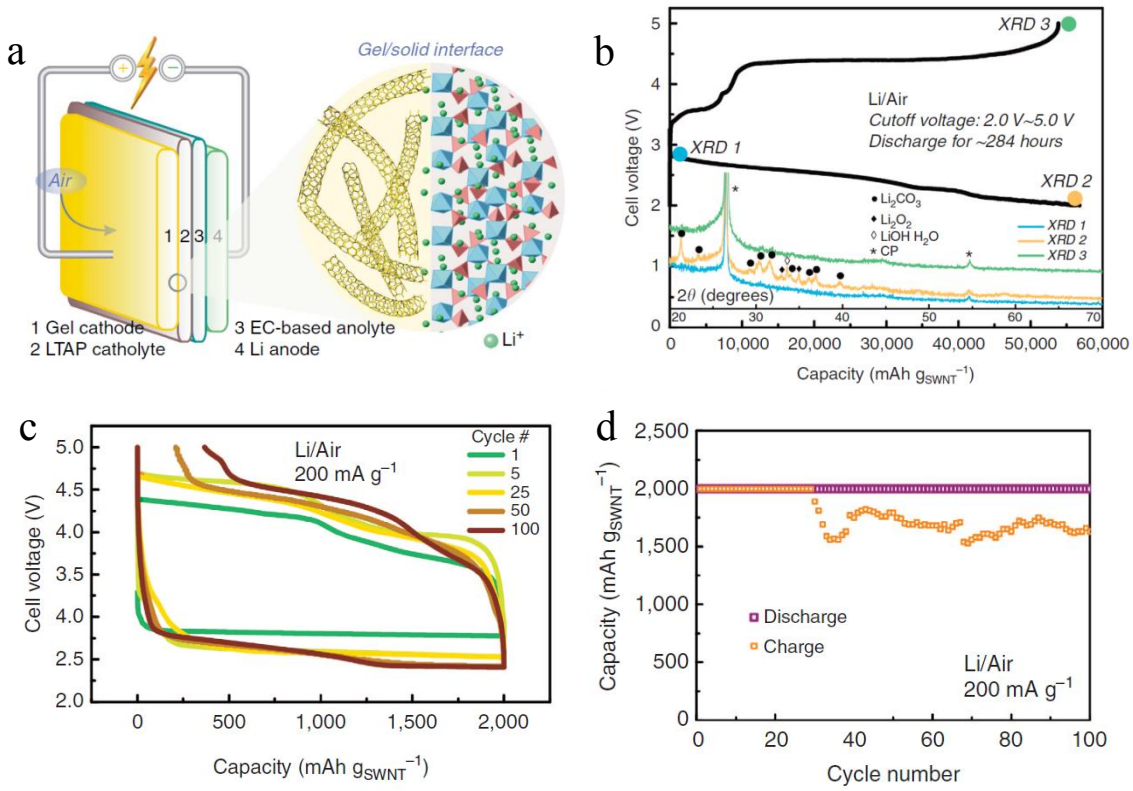

Figure 1.7 (a) Schematic illustration of Li-air battery with ambient air; (b) Discharge–charge profiles and XRD analysis for the Li-air battery in ambient air; (c) and (d) Cycling performance of Li-air battery in ambient air: (c) Voltage profiles and (d) cycling profiles under a capacity limitation of 2,000mAh/g_{SWNT} . Adapted from [41]

the authors contended that it is possible to prevent contact between the liquid electrolyte and O_2^- radical, so the problem of electrolyte decomposition is diminished.

Also, instead of a conventional carbon cathode, a Li-salt modified crosslinked network gel air cathode had been used, which consists of single-walled carbon nanotubes and ionic liquid of 1-ethyl-3-methylimidazolium bis(trifluoromethylsulfonyl)imide, is utilized in order to form a stable electrode-electrolyte interface. The battery exhibits exceptional performance, showing a discharge capacity of 56,800 mAh/g (Figure 1.7b) and stable rechargeability of over 100 cycles with a capacity cutoff of 1,000 mAh/g (Figure 1.7c and d). The discharge product is a mixture of Li_2O_2, LiOH, and Li_2CO_3 which in the end all convert to Li_2CO_3 due to CO_2 in the ambient air. Even though the existence of Li_2CO_3 leads to instability of charge in later cycles, the decomposition of the product during recharge is observed, the mechanism of which is still not clear. This shows that if problems such as electrolyte decomposition and Li parasitic reaction with air can be prevented, the Li-air battery can be operated with a high performance for many stable cycles.

1.6 Conclusions & Perspectives

The emergence of rechargeable metal-air batteries in which a mixture of O_2 & CO_2 gas or ambient air is the active material in the cathode is fueling renewed interest in the development of this storage technology for commercial applications. It also provides opportunities for designing novel electrochemical platforms for simultaneously storing electrical energy and for capturing CO_2 emissions from exhaust

streams from mobile and stationary sources. Using results from literature investigations of Li-O_2/CO_2 and Na-O_2/CO_2 electrochemical cells, we show that these systems exhibit two important traits that will drive significant future interest. First, at an optimum CO_2/O_2 composition close to 1/1, Li-O_2/CO_2 and Na-O_2/CO_2 electrochemical cells display higher energy storage capacities, compared to Li-O_2 or Na-O_2 technology. The source of the increase is shown to originate from new reactions enabled by CO_2 in the cathode which, depending on the electrolyte solvent utilized, produces metal carbonates and oxalates — instead of metal peroxides and oxides, as the principal discharge products. Second, even in the absence of redox mediators, the batteries are rechargeable and the discharge curves exhibit stable plateaus at voltages comparable to those in Li-O_2 and Na-O_2 batteries. A particularly important observation that deserves deeper studies is that rechargeability of Li-O_2/CO_2 and Na-O_2/CO_2 electrochemical cells hinges on the ability to stabilize the electrolyte from degradation during the recharge cycle. Additional research is also needed to more fully understand the electrode reaction mechanisms in these cells. For example, although metal carbonates are easily identified as the dominant discharge products in Li-O_2/CO_2 and Na-O_2/CO_2 cells, some studies have reported that in Na-O_2/CO_2 cells more soluble bicarbonates may also predominate in the discharge product, if there is a source of hydrogen (e.g. trace amounts of water) in the electrolyte. This finding means that concerns about the negative effects on metal-air battery performance of CO_2 and H_2O contaminants in ambient air may be misplaced and that with appropriate steps taken to protect the metallic anode from side reactions with these species in the electrolyte, they may ultimately prove beneficial for stable cycling. Finally the

electrically insulating nature and poor solubility of metal carbonates in commonly used electrolytes creates high over potential during recharge, which means that new electrolytes in which the voltage stability window is intrinsically high, or can be made high using additives introduced into the electrolyte or by surface modification of the electrodes, are required to achieve the thousands of cycles of trouble free charge and discharge required for applications in transportation.

1.7 Goals & Methods

This thesis will describe the details of the study of the metal-O_2/CO_2 electrochemical cells, including the fundamental studies of the reaction mechanisms in such electrochemical cells, the electrochemical cell performance of the cells and the rechargeability of the cells. Various techniques will be used for the characterization, including X-Ray techniques to determine crystalline phases, electron microscopy to study morphology, optical spectroscopy to investigate chemical bonding, mass spectrometry to identify gas phase component, gas adsorption/porosimetry studies for surface area/pore structure determination, and other methods such as electrical or mechanical measurements. Electrochemical characterization mainly involves galvanostatic charge-discharge cycling to determine energy density, rate capability and cycling performance and cyclic voltammetry and impedance measurements for mechanistic investigation.

1.8 Outline of dissertation

This thesis is organized as follows. Chapter 2 addresses the assist of carbon dioxide in a primary Na-O_2/CO_2 battery. The introduction of CO_2 leads to a very high discharge capacity of 6500-7000mAh/g. The reaction mechanism of the cell is studied by ex-situ characterization of the discharge product. We propose a reaction mechanism based on the discharge products.

Chapter 3 describes a rechargeable Na-O_2/CO_2 electrochemical cell using a carbon based cathode with imidazolium ionic liquid tethered silica nanoparticles as electrolyte additives. Chemical and physical characterization is performed on the cathodes and electrolytes to understand various properties of the electrochemical cell, including the chemical composition of the discharge product, morphology of the deposition of the product and gas phase evolution. Electrochemical performances of the cell is tested which show that it is able to maintain decent capacity after 20 cycles.

Chapter 4 focuses on the understanding of the mechanism of the Na-O_2/CO_2 electrochemical cell. With the introduction of a nickel foam cathode, the side reaction is eliminated from the cell, which provides the platform for the study of the reaction mechanism with minimal effect from side reactions. The special experiments are designed and performed, the results of which are discussed. The reaction mechanism in this case is elucidated and the effect of CO_2 in the cell is well studied. Besides, with the introduction of a nickel cathode, the rechargeability of the cell shows significant improvement.

Chapter 5 discusses a high temperature Li-CO_2 system with no presence of O_2 enabled by an ionic liquid electrolyte. Under high temperature the CO_2 gas, which is considered to be highly inactive, can participate in the electrochemical reaction and be reduced to carbon. The reaction mechanism is studied via the analysis of the discharge product and the comparison with thermodynamic data. The effect of the operating temperature is also studied.

In conclusion, this thesis develops a rechargeable metal-O_2/CO_2 electrochemical cell. This electrochemical cell should shed light on a more applicable metal-air electrochemical cell. Also, it may give a hint to a potential novel approach for the combination of carbon capture and energy storage.

REFERENCES

1. Grande L.; Paillard E.; Hassoun J.; Park J.; Lee Y.; Sun Y.; Passerini S.; Scrosati *B., Adv. Mater.* **2015**, 27, 784.,
2. Choi N.; Chen N.; Freunberger S.; Ji X.; Sun Y.; Amine K.; Yushin G.;Nazar L. F.; Cho J.; Bruce P.G., *Angew. Chem. Int. Ed.* **2012** , *51* , 9994 .
3. Rahman A.; Wang X.; Wen C., *J. Appl. Electrochem.* **2014**, 44**,** 5
4. Anderman M.; Kalhammer F. R.; MacArthur D., **2000,** Advanced batteries for electric vehicles: an assessment of performance, cost, and availability. Prepared for State of California Air Resources Board, Sacramento
5. Taniguchi A.; Fujioka N.; Ikoma M.; Ohta A., *J. Power Sources,* **2001**, 100, 117.
6. Park M.; Sun H.; Lee H.; Lee J.; Cho J., *Adv. Energy. Mater.* **2012**, 2, 780.
7. Wang J.; Li Y.; Sun X., *Nano Energy,* **2013**, 2, 443.
8. Lee J.; Kim S.; Cao R.; Choi N.; Liu M.; Lee K.; Cho J., *Adv. Energy Mater.* **2011**, 1, 34.
9. Girishkumar G.; McCloskey B.; Luntz A. C.; Swanson S.; Wilcke W., *J. Phys. Chem. Lett.* **2010**, 1, 2193.
10. Padbury R.; Zhang X., *J. Power Sources*, **2011**, 196, 4436.
11. Black R.; Adams B.; Nazar L. F., *Adv. Energy Mater.* **2012**, 2, 801.
12. Lu Y.; Gallant B. M.; Kwabi D. G.; Harding J. R.; Mitchell R. R.; Whittingham M. S.; Yang S., *Energy Environ. Sci.,* **2013**, 6, 750.

13. Bruce, P. G.; Freunberger, S. A.; Hardwick, L. J.; Tarascon, J.-M. *Nat. Mater.* **2012**, *11* (1), 19.

14. Aurbach D.; Zinigrad E.; Teller H.; Dan P., *J. Electrochem. Soc.* **2000**, 147, 1274.

15. Tarascon J.-M.; Armand M., *Nature,* **2001**, 414, 359.

16. Freunberger S.; Chen Y.; Peng Z.; Griffin J.; Hardwick L.; Barde F.; Novak P.; Bruce P. G., *J. Am. Chem. Soc.* **2011**, 133, 8040.

17. Freunberger S.; Chen Y.; Drewett N.; Hardwick L.; Barde F.; Bruce P. G., *Angew. Chem. Int. Ed.* **2011**, 50, 8609.

18. Aurbach D.; Gofer Y.; Ben-Zion M.; Aped P., *J. Electroanal. Chem.* **1992**, *339*, 451.

19. Aurbach D.; Weissman I.; Zaban A.; Chusid O., *Electrochim. Acta,* **1994**, *39*, 51.

20. Gallagher K.; Goebel S.; Greszler T.; Mathias M.; Oelerich W.; Eroglu D.; Srinivasan V., *Energy Environ. Sci.*, **2014**, 7, 1555

21. Scharg D. P., *Science*, **2007**, 315, 812.

22. Gough C., *Int. J. Greenhouse Gas Control*, **2008**, 2, 155.

23. Benn S. M.; Orr F. M., *MRS Bull.,* **2008**, 33, 297.

24. Takechi K.; Shiga T.; Asaoka T., *Chem. Commun.,* **2011**, 47, 3463.

25. Roberts J. L.; Calderwood T. S.; Sawyer D. T., *J. Am. Chem. Soc.,* **1984**, 106, 4667.

26. Wadhawan J. D.; Welford P. J.; McPeak H. B.; Hahn C. E. W.; Compton R. G., *Sens. Actuators, B*, **2003**, 88, 40.

27. Lim H.; Lim H.; Park K.; Seo D.; Gwon H.; Hong J.; Goddard W.; Kim H.; Kang K., *J. Am. Chem. Soc.* **2013**, 135, 9733−9742

28. Palomares V.; Serras P.; Villaluenga I.; Hueso K. B.; Gonzalez J. C.; Rojo T., *Energy Environ. Sci.,* **2012**, 5, 5884

29. Pan H.; Hu Y.-S.; Chen L., *Energy Environ. Sci.,* **2013**, 6, 2338.

30. Ellis B. L.; Nazar L. F., *Curr. Opin. Solid State Mater. Sci.,* **2012**, 16, 168.

31. Park Y.-U.; Seo D.-H.; Kwon H.-S.; Kim B.; Kim J.; Kim H.; Kim I.; Yoo H.-I.; Kang K., *J. Am. Chem. Soc.*, **2013**, 135, 13870.

32. Xiong H.; Slater M. D.; Balasubramanian M.; Johnson C. S.; Rajh T., *J. Phys. Chem. Lett.,* **2011**, 2, 2560.

33. Das S. K.; Lau S.; Archer L. A., *J. Mater. Chem. A,* **2014**, 2, 12623

34. Hartmann P.; Bender C.; Vracar M.; Durr A. K.; Garsuch A.; Janek J.; Adelhelm P., *Nat. Mater.,* **2013**, 12, 228.

35. Peled E.; Golodnitsky D.; Mazor H.; Goor M.; Avshalovmov S., *J. Power Sources,* **2011**, 196, 6835.

36. Das S. K.; Xu S.; Archer L. A., *Electrochem. Commun.,* **2013**, 27, 59.

37. Xu S.; Lu Y.; Wang H.; Abruna H. D.; Archer L. A., *J. Mater. Chem. A*, **2014**, 2, 17723

38. Xu S.; Das S. K.; Archer L. A., *RSC Advances*, **2013**, 3, 6656

39. Liu Y.; Wang R.; Lyu Y.; Li H.; Chen L., *Energy Environ. Sci.,* **2014**, 7, 677

40. Zhang Z.; Zhang Q.; Chen Y.; Bao J.; Zhou X.; Xie Z.; Wei J.; Zhou Z., *Angew. Chem. Int. Ed.* **2015**, 54, 6550.

41. Zhang T.; Zhou H., *Nat. Commun.* **2013**, 4, 1817

42. Mekonnen, Y. S.; Knudsen, K. B.; Mýrdal, J. S. G.; Younesi, R.; Højberg, J.; Hjelm, J.; Norby, P.; Vegge, T. *J. Chem. Phys.* **2014**, 140 (12), 121101.

43. Mekonnen, Y. S.; Garcia-Lastra, J. M.; Hummelshøj, J. S.; Jin, C.; Vegge, T. *J. Phys. Chem. C* **2015**, 119, 18066.

44. Dlugokencky, E.; Tans, P. *NOAA/ESRL* (www.esrl.noaa.gov/gmd/ccgg/trends/).

45. Meini, S.; Piana, M.; Tsiouvaras, N.; Garsuch, A.; Gasteiger, H. a. *Electrochem. Solid-State Lett.* **2012**, *15* (4), A45.

46. Aetukuri, N. B.; McCloskey, B. D.; García, J. M.; Krupp, L. E.; Viswanathan, V.; Luntz, A. C. *Nat. Chem.* **2014**, *7* (1), 50.

47. Li, F.; Wu, S.; Li, D.; Zhang, T.; He, P.; Yamada, A.; Zhou, H. *Nat. Commun.* **2015**, *6*, 7843.

48. Wang, Y.; He, P.; Zhou, H., *Energy Environ. Sci*. **2011**, 4, 4994.

49. Wang, Y.; Zhou, H. *J. Power Sources,* **2010**, 195, 358.

50. Lu, Y.; Das, S. K.; Moganty, S. S.; Archer L. A., *Adv. Mat.*, **2012**, 24, 4430.

51. Lu, Y.; Korf, K.; Kambe, Y.; Tu, Z.; Archer, L. A., *Angew. Cheme. Int. Ed.,* **2014**, 53, 488.

CHAPTER 2

Carbon Dioxide Assist for Non-Aqueous Sodium-Oxygen Batteries

2.1 Abstract

This chapter reports a novel non-aqueous Na – air battery that utilizes a gas mixture of CO_2 and O_2. The battery exhibits a high specific energy of 6500 – 7000 $Whkg^{-1}$ (based on the carbon mass) over a range of CO_2 feed compositions. The energy density achieved is higher, by 200% to 300%, than that obtained in pure oxygen. Ex-situ XRD analysis reveals that Na_2O_2, $Na_2C_2O_4$ and Na_2CO_3 are the principal discharge products. The Na-CO_2/O_2 and Mg-CO_2/O_2 battery platforms provide a promising, new approach for CO_2 capture and generation of electrical energy.

2.2 Introduction

Growing interest in electrochemical energy storage for transportation and grid storage has resulted in an intensive search for alternative energy storage technologies that offer specific energies above those achievable (~200 Whkg−1) with state-of-the-art lithium-ion batteries. More than a decade of research into such storage platforms has helped define the magnitude of the challenges that must be overcome for lithium-ion batteries to achieve specific energies in the 500 – 700 Whkg−1 range [1]. In this context, metal – air batteries are gaining focus because of their exceptionally high

specific energies [2,3]. Among the various metal – air batteries, the Li – air and Zn – air technologies have attracted most attention.

An air battery utilizing Na as anode is attractive because of the high earth abundance, modest cost, and relatively high electrode potential (−2.71 V vs SHE) that may be achieved. Coupled with O_2, Na has the ability to deliver a specific energy of 1600 Whkg−1 ($2Na^+ + O_2 + 2e^- \rightarrow Na_2O_2$ at 2.33 V; estimated based on the weight of both Na and O_2 consumed). Until 2011, the potential of the Na – O_2 couple remained less explored, in comparison to the Li – O_2 battery. A report by Peled et al. demonstrated a Na – O_2 cell based on liquid Na in combination with polymer electrolytes and operated at 100 ℃ [4]. Fu et al. proposed an alternative Na – O_2 cell configuration that operates at room temperature in ethylene carbonate/dimethyl carbonate as electrolyte [5]. They reported a stable discharge plateau at 2.3 V, corresponding to Na_2O_2 formation.

CO_2 is a greenhouse gas and has been implicated in global climate change [6]. A variety of chemical and physical methodologies are under development for capturing and sequestering the thousands of metric tons of the gas emitted per annum [6 – 8]. A metal – air battery that utilizes a mixed fuel of CO_2 and O_2 provides a potentially novel platform for electrical energy generation and carbon capture [9]. Recently, researchers at Toyota reported that incorporation of CO_2 with O_2 improves the energy

density of a Li – O_2 battery [10], indicating that there may be other benefits for incorporating CO_2 in other metal – air batteries.

Herein, we describe novel Na – CO_2/O_2 and Mg – CO_2/O_2 batteries operated at room temperature utilizing tetraglyme and an ionic liquid as electrolyte. Unlike the Li – O_2/CO_2 battery [10], which specifically aims to use CO_2 to enhance the energy density of the Li – O_2 cell, the current work focuses on metal – CO_2/O_2 batteries as platforms for CO_2 capture in a technology that also produces electrical energy. Both of these goals are met using a "primary" battery, i.e. one that removes/concentrates CO_2 from an effluent gas mixture, and therefore does not require the cathode reactions to be reversible. While the economics of such a battery based on lithium anode may be impractical, they can become viable for anodes based on a variety of earth abundant materials such as Na, Mg, Al, Zn, Ca, Cu, and Fe [11]. As with other CO_2 capture technologies, we envision metal – CO_2/O_2 batteries as the first step in a systematic program for CO_2 capture and sequestration, which ultimately uses chemical, biological, or geological approaches for CO_2 sequestration.

2.3 Experimental

The investigated Na – CO_2/O_2 battery configuration is similar to our previously reported Li – O_2 battery [12]. The air cathode consists of 90% Super P (TIMCAL) carbon and 10% PVDF binder. Mechanically perforated coin cells were used for electrochemical experiments. 1 M $NaClO_4$/tetraethylene glycol dimethylether and 0.75

M $NaCF_3SO_3$/1-ethyl-3-methyl imidazolium trifluromethanesulfonate (IL) were used as electrolytes. The cells were assembled in an argon-filled glove box. Required concentrations of CO_2 and O_2 were premixed in a chamber at 1 atm before introducing the gas feed into the battery chamber. Galvanostatic experiments were performed at 25 ℃ and at a current density of 70 mAg−1. The porous carbon electrode dimension is 1.95 cm^2 with typical carbon loading of 0.76 – 1.28 mg cm^{-2} and thickness of 5 μm. Ex-situ TEM, FTIR and XRD analyses used discharged electrodes that were vacuum dried.

2.4 Electrochemical Analyses

Figure 2.1 reports the galvanostatic discharge profiles of Na – CO_2/O_2 cells operated under various concentrations of O_2 and CO_2. Figure 2.1A and B correspond, respectively, to cells using ionic liquid and tetraglyme-based electrolytes. Under a 100% O_2 environment, the two varieties of Na – air cells exhibit discharge capacities of 1315 mAhg−1 and 1390 mAhg−1, respectively (estimated based on carbon mass). Unlike Fu et al. [5], the discharge profiles with pure O_2 feed show a less well-defined voltage plateau at 2.3 V. This difference might be attributed to the electrolytes and air cathode employed in our studies, since the current rates are similar [12]. The Na – CO_2 cells also show low discharge capacities of 183 and 173 mAhg−1 under pure CO_2 environment. Sluggish reaction kinetics between Na+ ions and CO_2 at room temperature is anticipated [9], which may explain the latter observation. Remarkably, the discharge capacities of both the IL and tetraglyme based Na – CO_2/O_2 cells based

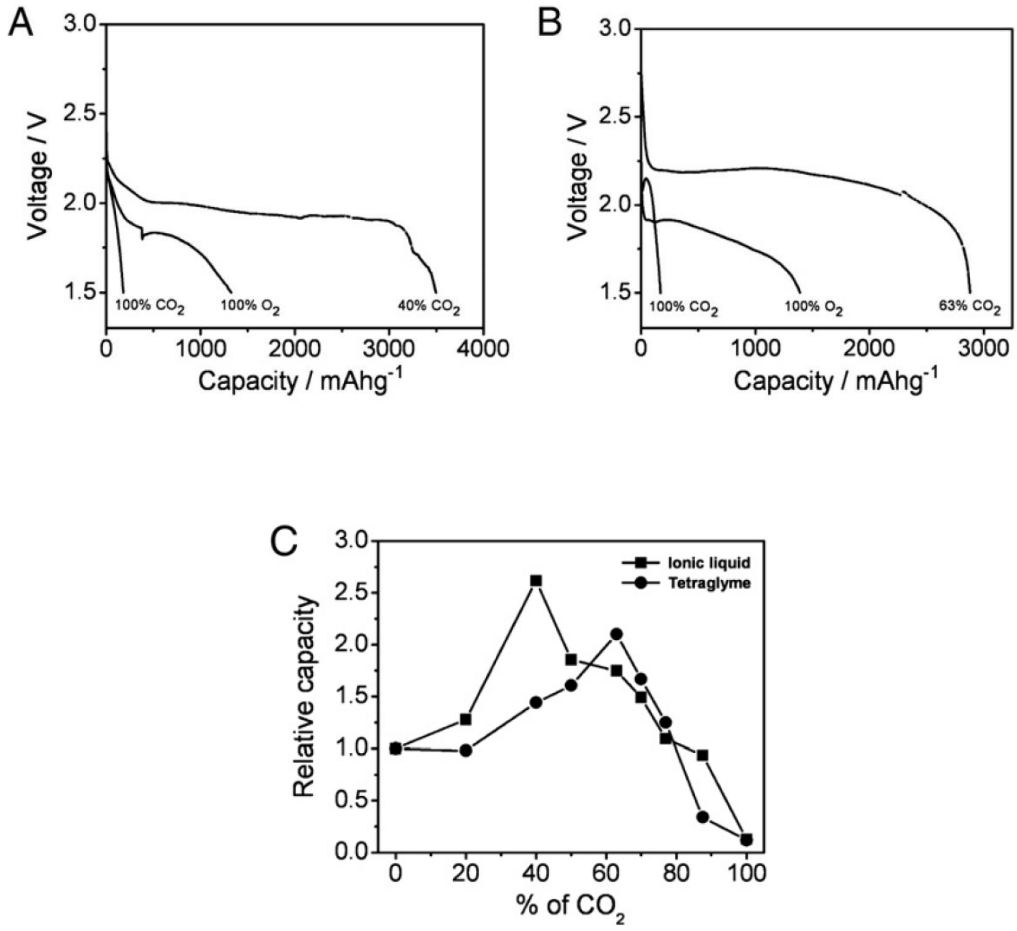

Figure 2.1 Galvanostatic discharge profiles for Na-O_2/CO_2 cells operated with a mixed O_2/CO_2 feed with (A) ionic liquid electrolyte and (B) tetraglyme electrolyte. (C) Variation of discharge capacity with respect to CO_2 concentration.

on feed streams containing 40% and 63% CO_2 are respectively 3500 and 2882 mAhg−1; an increase of 2.6 and 2.1 times compared to the Na-100% O_2 case. Figure 2.1C reports the relative discharge capacities as a function of CO_2 concentration. The variation in capacity depends on the chemical composition of the electrolytes, but displays a similar trend for the tetraglyme- and IL-based electrolytes, with the highest discharge capacities observed at intermediate CO_2 compositions. It demonstrates that the specific energy of a Na – air cell can be significantly enhanced, by factors of 2 to 3, by introducing optimized concentrations of CO_2. It is also apparent that the optimal ratio of CO_2/O_2 for the largest discharge capacity lies between 40% and 70% CO_2 and depends on the composition of the electrolyte. The optimal CO_2/O_2 feed composition is also expected to be a function of temperature [12].

2.5 Characterization of Discharge Products

To obtain deeper insights into the overall electrochemistry and role of CO_2 the discharged carbon electrodes were harvested and investigated by TEM, XRD, and FTIR spectroscopy. Ex-situ TEM images (Figures 2.2B and C), indicate that the porous carbon electrodes are filled with discharge products. Figure 2.3 shows that additional X-ray diffraction peaks emerge in every case (Figure 2.3b – d). The peaks can be indexed to crystalline phase of Na_2O_2 (ICDD no. 083-0597) in case of Na-100% O_2 cells (Figure 2.3). Remarkably, however, no signature of Na_2O_2 is found in electrodes from the O_2/CO_2 mixed gas feed. Instead, diffraction peaks for Na_2CO_3 (ICDD no. 075-6816) and $Na_2C_2O_4$ (ICDD no. 075-3639) are observed. Additionally,

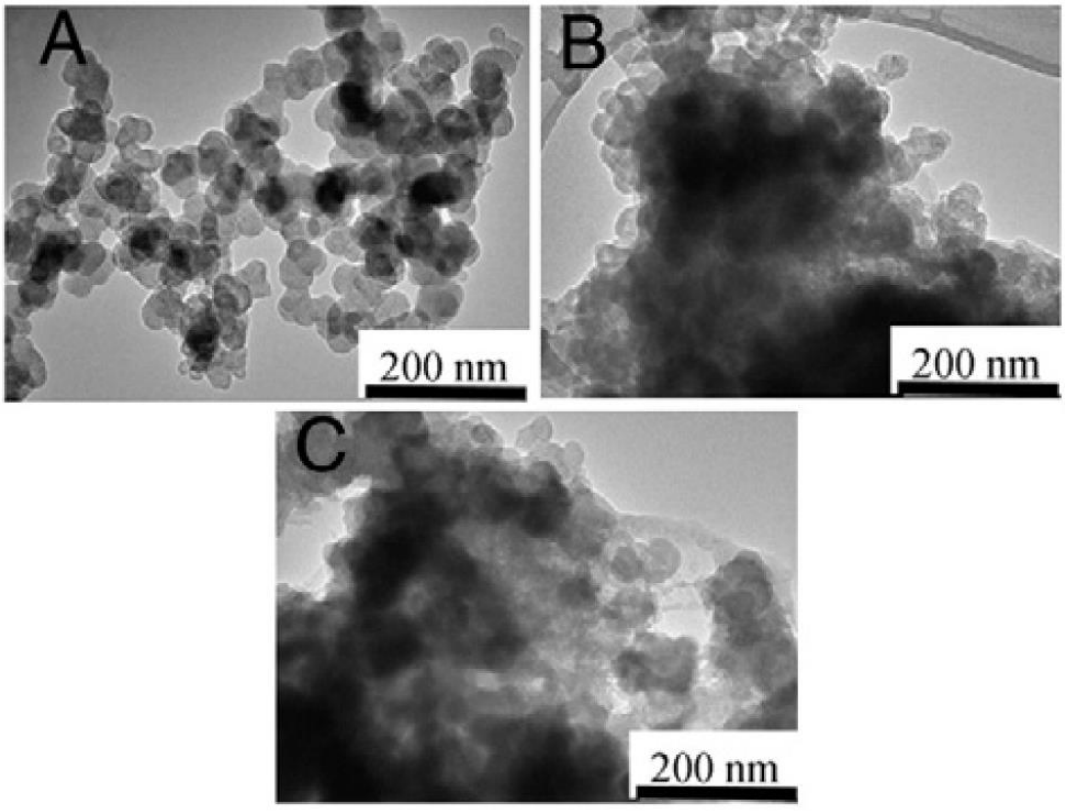

Figure 2.2 Ex-situ TEM micrographs of Super P carbon (A), discharged carbon electrodes harvested from IL (B) and tetraglyme (C) cells.

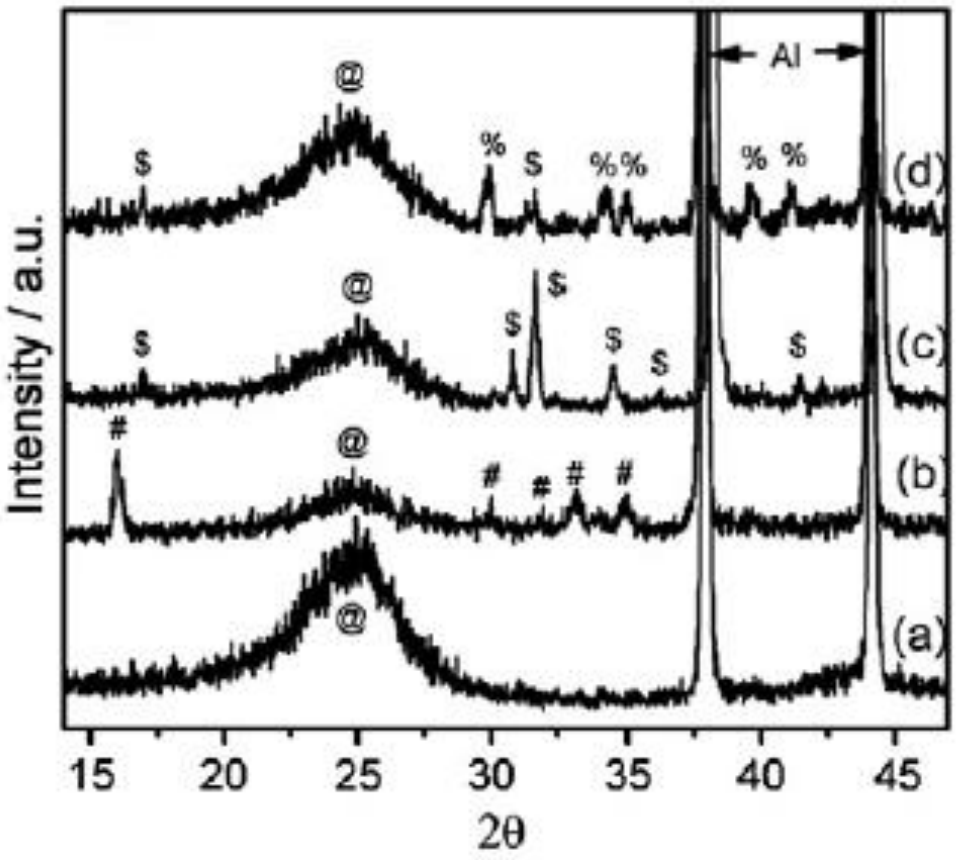

Figure 2.3 Ex-situ XRD of Super P electrode (a), and electrodes obtained from Na – O_2 IL cell (b), Na – CO_2/O_2 IL cell (c) and Na – CO_2/O_2 tetraglyme cell (d); @, #, $, and % denote graphitic carbon, Na_2O_2, $Na_2C_2O_4$, and Na_2CO_3 phases respectively.

while Na_2CO_3 and $Na_2C_2O_4$ coexist for the tetraglyme based Na – O_2/CO_2 cells (Figure 2.3d), $Na_2C_2O_4$ is the dominant phase for cells using the IL electrolyte (Figure 2.3).

The XRD and FTIR results suggest that the following electrochemical reaction may occur in cells that employ pure O_2: $O_2+2e^-+2Na^+ \rightarrow Na_2O_2$ [5]. The processes by which Na_2CO_3 and $Na_2C_2O_4$ are formed for O_2/CO_2 mixed gas feed are likely more complex. Electrochemical reduction of O_2 and CO_2 is known to involve complicated elementary reactions and also depends on the solvent and electrode material [14,15]. It should be noted nonetheless that the fact that only $Na_2C_2O_4$ forms in IL based electrolytes, whereas both Na_2CO_3 and $Na_2C_2O_4$ coexist in tetraglyme cells indicates that the reactions are not hopelessly complex. Various research groups have reported on the electrochemical reduction of O_2 and CO_2 [14,15]. Based on the reported results and the observations above, we propose the following preliminary view of the reaction mechanisms for the Na – O_2/CO_2 cell.

(i) In the ionic liquid based electrolyte, the reaction is analogous to the reaction in Li-O_2/CO_2 battery.

$$O_2 + 4e^- \rightarrow 4O_2^{\bullet -} \quad (1)$$

$$O_2^{\bullet -} + CO_2 \rightarrow CO_4^{\bullet -} \quad (2)$$

$$CO_4^{\bullet -} + CO_2 \rightarrow C_2O_6^{\bullet -} \quad (3)$$

$$C_2O_6^{\bullet -} + O_2^{\bullet -} \rightarrow C_2O_6^{2-} + O_2 \quad (4)$$

$$C_2O_6^{2-} + 2O_2^{\bullet -} + 4Na^+ \rightarrow 2Na_2CO_3 + 2O_2 \quad (5)$$

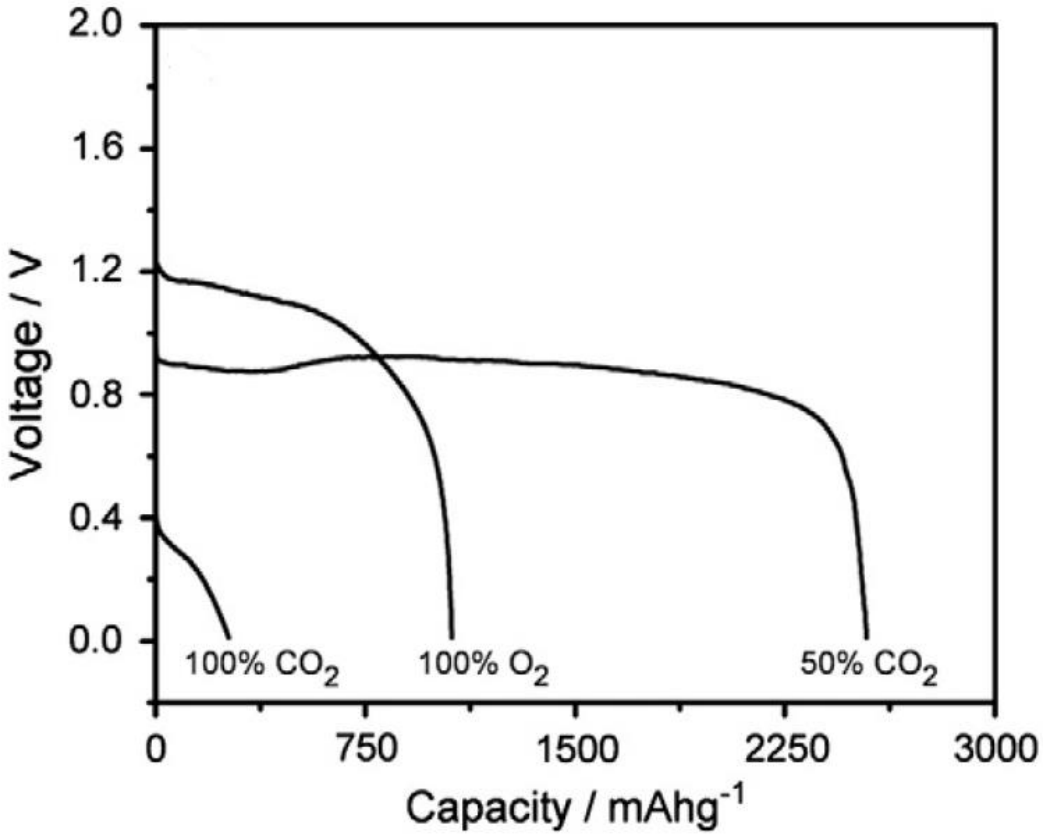

Figure 2.4 Galvanostatic discharge curves for Mg-air cells.

(ii) In the tetraglyme-based electrolyte, the reactions above occur in tandem with the reaction summarized below, during the discharge.

$$O_2 + 2e^- \rightarrow {O_2}^{2-} \quad (6)$$

$$CO_2 + {O_2}^{2-} \rightarrow {CO_4}^{2-} \quad (7)$$

$${CO_4}^{2-} + CO_2 + 2Na^+ \rightarrow Na_2C_2O_4 + O_2 \quad (8)$$

2.6 Mg-O_2/CO_2 Battery

The same ideas would lead one to expect that electrochemical properties of non-aqueous primary metal – air cells based on other earth-abundant metals, e.g. Mg, may also be enhanced by introduction of CO_2. To evaluate this idea, we assembled a Mg – air cell as a proof of concept. 1 M $Mg(ClO_4)_2$-propylene carbonate is used as electrolyte. As illustrated in Figure 2.4, the Mg – air cell shows a discharge voltage plateau of ~0.9 V and close to a factor of 250% enhancement in specific energy with introduction of 50% CO_2, underscoring its promise.

2.7 Conclusions

In summary, we investigated a primary non-aqueous Na – CO_2/O_2 battery as a dual platform for converting a CO_2-rich gas stream to electrical energy and for capturing the CO_2. With different electrolytes, the Na – air battery shows enhancements of 200 to 300% when a mixture of CO_2/O_2 gas with high CO_2 content is used as fuel. The discharge product of the battery is also affected by the utilization of different electrolytes. Preliminary postmortem structural analysis indicates that Na_2CO_3 is

formed as the discharge product when ionic liquid is used as the electrolyte, while $Na_2C_2O_4$ is formed in the cells with tetraglyme as the electrolyte. The reaction mechanism is proposed based on the discharge products. In the ionic liquid electrolyte the mechanism is similar to that of a Li-O_2/CO_2 battery, while the use of tetraglyme as the electrolyte results in an extra reaction that leads to the formation of $Li_2C_2O_4$. We further show that metal – air batteries based on other, earth-abundant metals may also benefit from CO_2-enriched air.

REFERENCES

1. C.-X. Zu, H. Li, *Energy Environ. Sci.,* **2011**, 4, 2614.

2. T. Ogasawara, A. Debarte, M. Holzapfel, P. Novak, P.G. Bruce, *J. Am. Chem. Soc.,* **2006**, 128, 1390;

   P.G. Bruce, S.A. Freunberger, L.J. Hardwick, J.-M. Tarascon, *Nat. Mat.,* **2012**, 11, 19.

3. J.S. Lee, S.T. Kim, R. Cao, N.S. Choi,M. Liu, K.T. Lee, J. Cho, *Adv. Energy. Mater.,* **2011**, 1, 34.

4. E. Peled, D. Golodnitsky, H. Mazora, M. Goora, S. Avshalomov, *J. Power Sources*, **2011**, 196, 6835.

5. Q. Sun, Y. Yang, Z.-W. Fu, *Electrochem. Commun.,* **2012**, 16, 22.

6. D.P. Scharg, *Science*, **2007**, 315, 812.

7. C. Gough, *International Journal of Greenhouse Gas Control*, **2008**, 2, 155.

8. S.M. Benn, F.M. Orr, *MRS Bulletin*, **2008**, 33, 30.

9. S. Xu, L.A. Archer, Cornell University Invention Disclosure 5889 (2012) “Metal‐CO2 batteries for energy generation and carbon capture”.

10. K. Takechi, T. Shiga, T. Asaoka*, Chem. Commun.,* **2011**, 47, 3463.

11. D. Linden, T.B. Reddy, Handbook of Batteries, third ed. McGraw-Hill, 2002.

12. S.K. Das, S. Xu, A.-H. Emwas, Y.Y. Lu, S. Srivastava, L.A. Archer, *Energy Environ. Sci.,* **2012**, 5, 8927.

13. E.G. Brame, S. Cohen, J.L. Margrave, V.W. Meloche, *Journal of Inorganic and Nuclear Chemistry*, **1957**, 4, 90.

14. J.D. Wadhawana, P.J. Welforda, H.B. McPeak, C.E.W. Hahn, R.G. Compton, *Sensors and Actuators B*, **2003**, 88, 40.

15. R. Ortiz, O.P.Marquez, J.Marquez, C.Gutierrez, *Journal of Electroanalytical Chemistry*, **1995**, 390, 99.

CHAPTER 3

A Rechargeable Sodium-CO_2/O_2 Battery Enabled By Stable Nanoparticle Hybrid Electrolytes

3.1 Abstract

In this chapter we report on rechargeable batteries that use metallic sodium as the anode, a mixture of CO_2 and O_2 as the active material in the cathode, and an organic-inorganic hybrid liquid as electrolyte. The batteries are attractive among energy storage technologies because they provide a mechanism for simultaneously capturing CO_2 emissions while generating electrical energy. Through in- and ex-situ chemical analysis of the cathode we show that $NaHCO_3$ is the principal discharge product, and that its relative instability permits cell recharging. By means of differential electrochemical mass spectrometry (DEMS) based on ^{12}C and ^{13}C we further show that addition of as little as 10% of 1-methyl-3-propylimidazolium bis(trifluoromethanesulfone)imide ionic liquid tethered to SiO_2 nanoparticles extends the high-voltage stability of the electrolyte by at least 1 V, allowing recharge of the Na-CO_2/O_2 cells.

3.2 Introduction

Due to its exceptional charge storage capacity, the Li-air battery has been studied by research teams worldwide as among the most promising electrochemical storage technologies for meeting growing energy demands for transportation [1-4]. It is

understood that the large storage capacity of Li-air cells stems from the high electronegativity and lightweight of the metallic lithium anode and the fact that the active cathode material, O_2, is harnessed continuously from the surroundings. An air battery in which metallic lithium is replaced by sodium as the anode is attractive for a variety of reasons. First, sodium is one of the most abundant metals in earth's crust and is available in practically all corners of the earth. Consequently, the price of sodium is less than 10% that of lithium [5]. Second, the electrode potential of Na/Na+ (-2.7V vs. SHE) though less negative than that of Li/Li+ (-3.0V vs. SHE) is still quite high. Finally, although the higher molecular weight of sodium relative to lithium lowers the gravimetric energy density of a Na-O_2 cell relative to Li-O_2, the theoretical energy density of a Na-air battery is considerable (1600Wh/kg, $2Na + O_2 \rightarrow Na_2O_2$ at 2.33V, estimated based on the weight of both Na and O_2 consumed); it is even more attractive on a volumetric basis. These considerations among others have fueled research interests in Na-air batteries, particularly in the past three years.[6] Peled et al. reported a Na-O_2 cell utilizing molten Na metal as the anode and a solid-state polymer electrolyte operated at temperature exceeding 100 ℃ [7]. Fu et al. reported an alternative Na-O_2 cell at room temperature using conventional carbonate electrolyte. [8-9] Hartmann et al. demonstrated a high capacity rechargeable Na-O_2 battery in which NaO_2 is the principal discharge product [10-11].

CO_2 is now understood to be a leading greenhouse gas and its rising emissions have been implicated in global climate change [12]. Various chemical and physical methodologies are currently under development to capture and sequestrate thousands of tons of CO_2 gas emitted per year [12-14]. All of these approaches are challenged by

the vast amounts of energy required to regenerate the capture fluid or sorbent, which increases cost of all currently-used capture technologies to levels such that government intervention is required to increase the economic appeal of CO_2 capture by utilities that use conventional fossil fuels for energy generation. In the previous chapter we reported that introducing CO_2 gas into the cathode stream of a metal-air battery provides a novel platform for simultaneously capturing the CO_2 and generating substantial amounts of electrical energy [15-17]. A practical limitation of the approach is that the batteries cannot be recharged [18]. In particular, the irreversible loss of storage capacity due to formation of stable metal carbonates and the proliferation of unwanted side reactions, such as the decomposition of electrolyte and carbon cathode [19-20] - both initiated by CO_2 - lead to batteries with little or no ability to be recharged. This is a serious limitation, particularly in electrochemical cells such as in the Li-CO_2/O_2 battery [15, 17-18] that employ an expensive (both in terms of cost and volume of CO_2 emissions during production) anode material. It is also problematic in cells that use less expensive metals such as sodium as anode, primarily because of the large amounts of CO_2 generated during production of the metal from naturally occurring salts or ores.

By stabilizing the electrolyte using a previously reported nanoparticle-tethered ionic liquid material chemistry [21-22], Figure 3.1, we herein show that it is possible to create Na-CO_2/O_2 batteries capable of being recharged for many cycles at potentials as high as 5V, without electrolyte decomposition. We also report that under these conditions, $NaHCO_3$ is the discharge product of the Na-CO_2/O_2; to our knowledge the first such report of a bicarbonate as the discharge product in a metal-air battery

system. We hypothesize that the stability of the electrolyte at the high cell recharge potential and the instability of $NaHCO_3$ compared to Na_2CO_3, make it possible to recharge the Na-CO_2/O_2 battery with an attractive capacity of 800mAh/g_{carbon}. Recent reports in fact suggest that the latter (instability of the $NaHCO_3$) is not a requirement for recharge, as it has been observed that for both Li-air and Na-air cells it is possible to decompose the carbonates that form as a result of electrolyte decomposition and other processes by charging the batteries at an appropriate, high voltage [23-24]. It seems plausible that even a metal-CO_2/O_2 battery where the discharge product is a carbonate may exhibit some degree of rechargeability.

3.3 Configuration of the Na-O_2/CO_2 Cell

The cell configuration used in the present study is similar to our previously reported Li-O_2 and Li-CO_2 battery [15-16] (see Figure 3.1). It is composed of a sodium metal anode, a glass fiber separator and a porous carbon cathode. A nanoparticle hybrid electrolyte comprised of propylene carbonate (PC) containing 10 v% SiO_2 nanoparticles densely functionalized (1.2 tethered ligands/nm^2 of SiO_2) with the ionic liquid 1-methyl-3-propylimidazolium bis(trifluoromethanesulfone)imide was used as the base electrolyte fluid for the study. Previous research shows that reinforced with a 1M LiTFSI salt, SiO_2-IL-TFSI/PC hybrid electrolytes with comparable particle loadings display room-temperature ionic conductivities in excess of 3mS/cm and exhibit attractive abilities to stabilize electrodeposition of lithium [22]. It has been hypothesized that this feature stems from the formation of a particle-enriched SEI

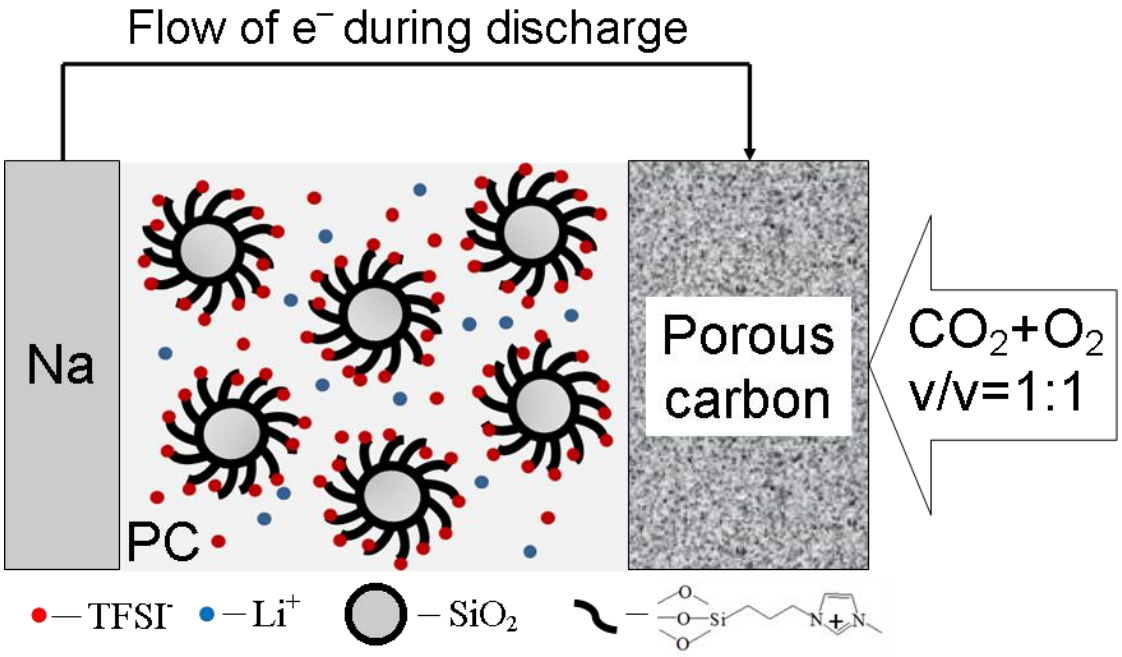

Figure 3.1 Schematic diagram of the Na-CO_2/O_2 rechargeable battery.

layer on Li, which simultaneously lowers the electric field gradients across the SEI and imparts favourable transport properties and mechanical toughness to the SEI. For the present studies using Na-CO_2/O_2 cells, 1M solutions of NaTFSI in either the hybrid SiO_2-IL-TFSI/PC electrolyte base fluid or in a conventional propylene carbonate liquid electrolyte medium were formulated. All cell components were assembled in a coin cell with a porous cathode cap and enclosed in a sealed stainless steel chamber filled with a symmetric gas mixture of CO_2 and O_2 (v/v=1:1).

3.4 Stability of the Electrolyte

Figures 3.2 and 3.3 illustrate the importance of the SiO_2-IL-TFSI additive in the PC-NaTFSI electrolyte. It can be clearly seen from the linear sweep scan voltammetry in the conventional PC electrolyte that at a potential around 5.2 V (vs Na/Na+) the current diverges and becomes unstable, an indication that the electrolyte undergoes massive decomposition at around this potential. For the SiO_2-IL-TFSI/PC-NaTFSI electrolyte, the catastrophic electrolyte decomposition is not seen and the only evidence of a divergent current is at a potential 5.8V, but even then the currents generated are at least one order of magnitude lower. These qualitative conclusions are reinforced using in-situ differential electrochemical mass spectrometry (DEMS) (Figure 3.3). These measurements were performed at a fixed scan rate of 0.5mV/s using a pristine porous carbon cathode with Na metal as both the reference and counter electrode, and fresh electrolyte. Comparison of Figures 3.2(c) and 3.2(d) reveals that while substantial amounts of CO_2 is generated, beginning at around 4V, for the conventional PC electrolyte, no CO_2 evolution is detected even at a potential as

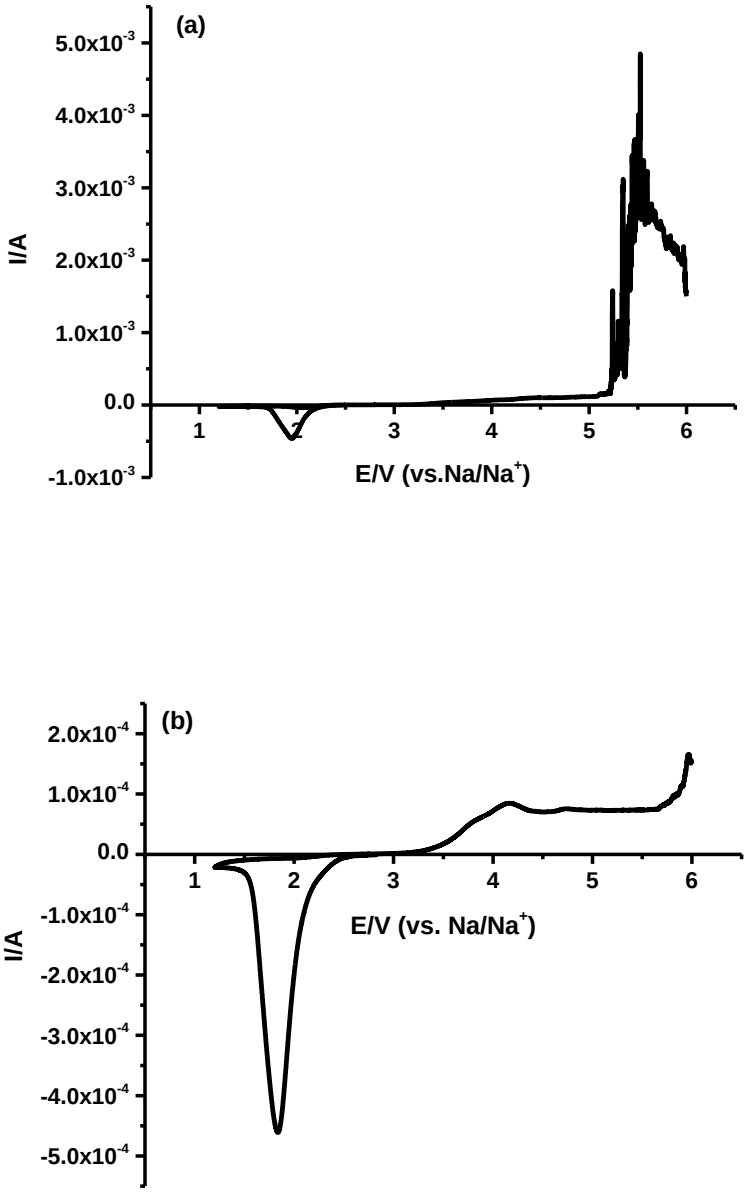

Figure 3.2 The comparison between the linear scan voltammetry of (a) conventional PC electrolyte and (b) the SiO_2-IL-TFSI/PC electrolyte under an O_2/CO_2 (v/v=1:1) mixture gas atmosphere.

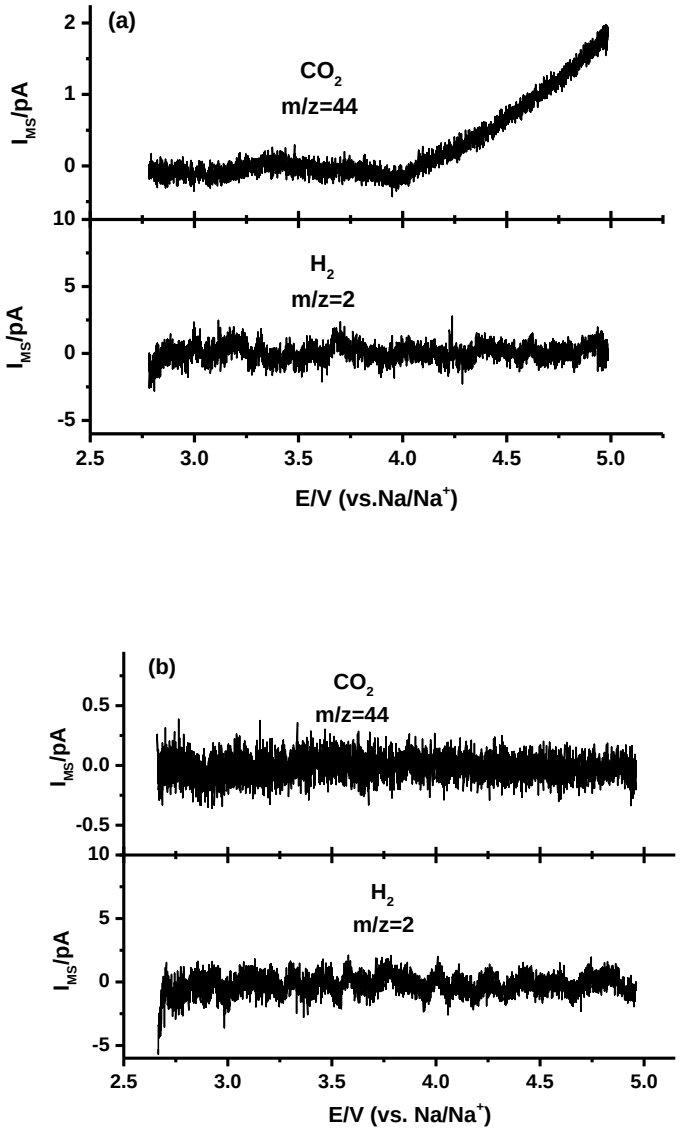

Figure 3.3 The comparison between the DEMS result of the positive scan of (a) conventional PC electrolyte and (b) the SiO_2-IL-TFSI/PC electrolyte.

high as 5.0V (vs Na/Na+), which is higher than the upper limit used for galvanostatic cycling experiments described next for the Na-CO_2/O_2 cells. It is notable that hydrogen is not detected in DEMS measurements performed in either the hybrid or conventional PC-based electrolytes. These results nicely demonstrate the remarkable stabilizing effect of the SiO_2-IL-TFSI particles on the carbonate electrolyte. Because of the importance of electrolyte stability in enabling recharge of the Na-CO_2/O_2 cell and the broader potential relevance of the SiO_2-IL-TFSI particles for stabilizing other carbonate-based electrolytes for high voltage cathodes such as $LiNi_{0.5}Mn_{1.5}O_4$ [25] and $LiCoPO_4$ [26] of current interest for lithium ion batteries, we believe the observations reported in Figure 3.3 are among the most important reported in the paper.

3.5 Cycling of the Cell

Figure 3.4 reports on the galvanostatic cycling behavior of the Na-CO_2/O_2 battery with different feed and electrolyte compositions at a low charge/discharge rate of 200mA/g. It shows that whereas the Na-CO_2/O_2 cells with the SiO_2-IL-TFSI/PC-NaTFSI hybrid electrolyte (Figure 3.4(c)) exhibit consistent charge potentials for 20 cycles, Na/O_2 cells based on SiO_2-IL-TFSI/PC-NaTFSI and Na-CO_2/O_2 cells containing PC-NaTFSI as electrolyte exhibit a steady increase in charge potential (i.e. the round trip efficiency of the cell falls with increased number of charge/discharge cycles as ohmic losses rise). This is another indication of electrolyte decomposition in the latter two cells. The decomposition of the PC-NaTFSI electrolyte has already been discussed via linear sweep voltammetry and DEMS, so it is straightforward to explain

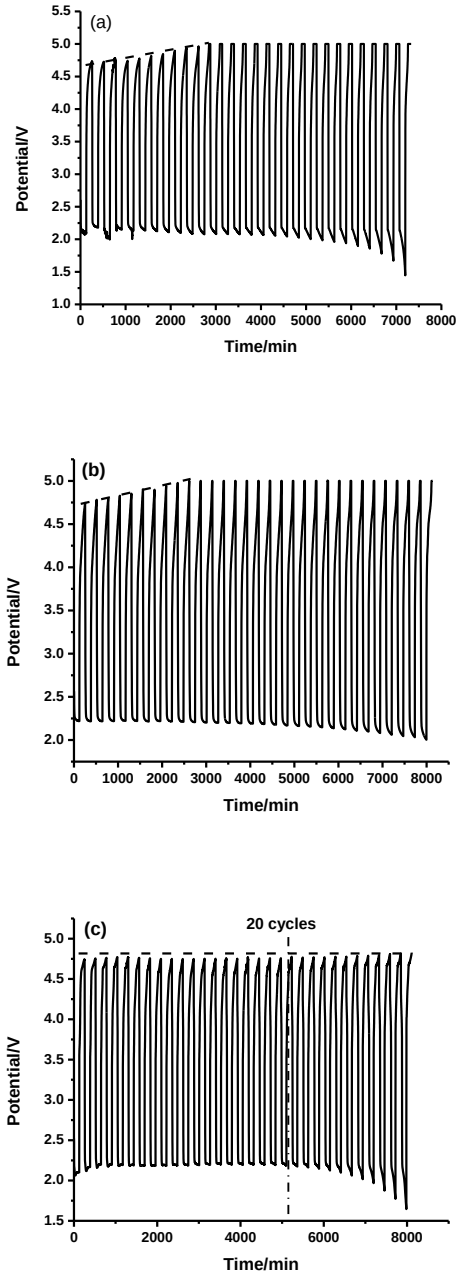

Figure 3.4 Cycling profiles for (a) Na-O_2 battery with SiO_2-IL-TFSI/PC electrolyte, (b) Na-CO_2/O_2 battery with PC electrolyte, (c) Na-CO_2/O_2 battery with SiO_2-IL-TFSI/PC electrolyte. The dash line shows the trend of change of the charge potential. The dash-dot line in (c) indicates the 20th cycle where the battery shows a stable cycling. The current density employed is 200mA/g and the capacity cutoff is 800mAh/gcarbon. The charge potential limit is 5V.

why the Na-CO_2/O_2 battery with PC electrolyte is unstable. It has been reported previously that the imidazolium group is not stable in the Li-O_2 battery [27]. Since the ionic particle in the SiO_2-IL-TFSI/PC electrolyte is functionalized with 1-methyl-3-propylimidazolium bis(trifluoromethanesulfone)imide, it is also perhaps straightforward to understand the gradual rise of the charge of the charge in terms of the decomposition of imidazolium in the O_2 rich atmosphere. Support for this conclusion comes from FTIR analysis of the three electrolytes after cell discharge. In particular, results shown in Figure 3.5 indicate that when used with the Na-O_2 cells, the SiO_2-IL-TFSI/PC electrolyte shows an extra IR absorbance at 1650cm^{-1} after cell discharge. This mode corresponds to the C=O bond stretch in an amide molecule, which is consistent with the idea that the $O_2^{\cdot}$ radical formed during the discharge could oxidize the imidazolium groups [27]. One can explain the absence of this IR band for the electrolytes used in the Na-CO_2/O_2 cells in terms of the proposed reaction mechanism of a generic metal-CO_2/O_2 battery [16, 18, 29], wherein the $O_2^{\cdot}$ radical binds with CO_2 gas to form CO_4- and C_2O_6- according to the following processes:

$$O_2 + e^- \rightarrow {O_2}^{\cdot -}$$

$${O_2}^{\cdot -} + CO_2 \rightarrow {CO_4}^{\cdot -}$$

$${CO_4}^{\cdot -} + CO_2 \rightarrow {C_2O_6}^{\cdot -}$$

Therefore, the existence of CO_2 in the cathode gas can be thought to impart some degree of protection of the electrolyte additive, probably stabilizing it against degradation during discharge.

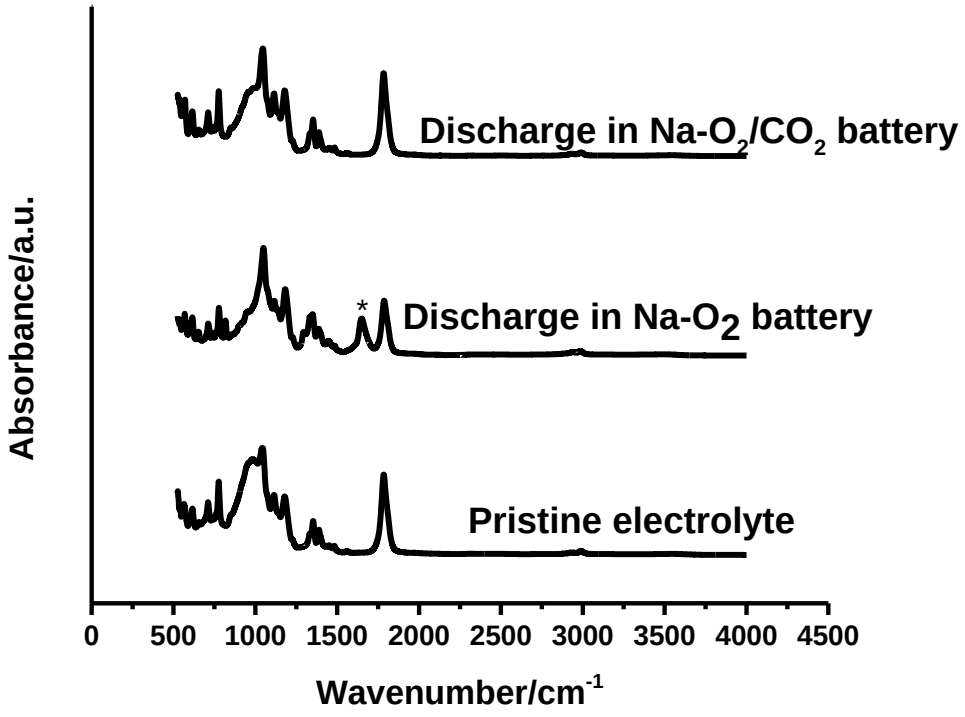

Figure 3.5 Ex-situ FTIR spectra for the SiO_2-IL-TFSI/PC-NaTFSI hybrid and PC-NaTFSI electrolytes after discharge in different battery systems. The * indicates the C=O peak in the electrolyte after discharge of the Na-O_2 cell.

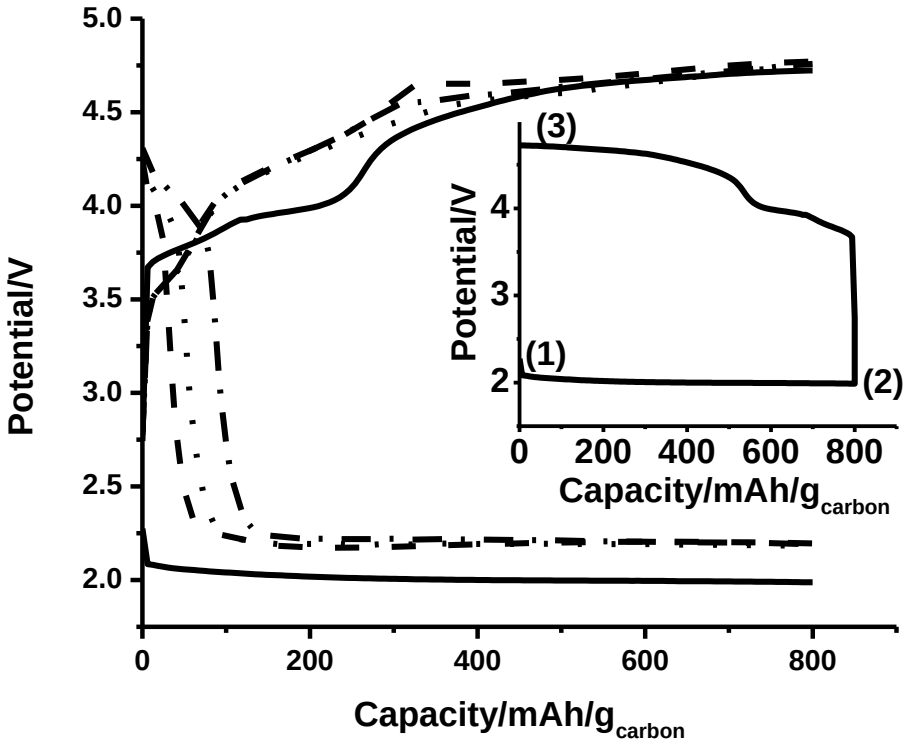

Figure.3.6 Discharge-charge profiles for the Na-O_2/CO_2 battery in the first cycle (solid line), 5th cycle (dash line), 10th cycle (dot line) and 20th cycle (dash dot line). Inset shows the point of the post-mortem study.

3.6 Post-mortem Characterization

The discharge-charge profiles for Na-CO_2/O_2 battery cycled at a fixed current density of 200mA/g are reported in Figure 3.6. The discharge and charge plateaus are observed at around 2.1V and 4.5V respectively, which is very close to what we observed in the linear scan voltammetry (Figure 3.2(b)). In order to analyze the discharge product, post-mortem X-ray diffraction (XRD) and FTIR (supporting information) were used to explore the nature of the product; the results are shown in Figure 3.7. The XRD profiles are unambiguously assigned to the nahcolite phase of $NaHCO_3$ (ICDD card #15-700). Notwithstanding the unambiguous assignment possible from XRD, it is surprising that the discharge product of the Na-CO_2/O_2 battery is sodium bicarbonate ($NaHCO_3$) since there is no previous report demonstrating bicarbonate as the discharge product in metal-air batteries containing added CO_2 or in which CO_2 is generated by decomposition of the electrolyte. Reports on metal-air battery utilizing PC electrolyte typically show that a carbonate salt is the discharge product [19, 28].

To determine the source of the hydrogen in the $NaHCO_3$ discharge product we consider and subsequently evaluate four very different hypotheses: (i) Hydrogen or hydrogen containing compounds capable of reacting with Na+ at the cathode electrolyte interface to produce $NaHCO_3$ are created from initial chemical reactions between the electrolyte and sodium electrode during the SEI interface formation process; (ii) Hydrogen is produced by electrode reactions involving residual moisture in the electrolyte, entrained by the 1-methyl-3-propylimidazolium

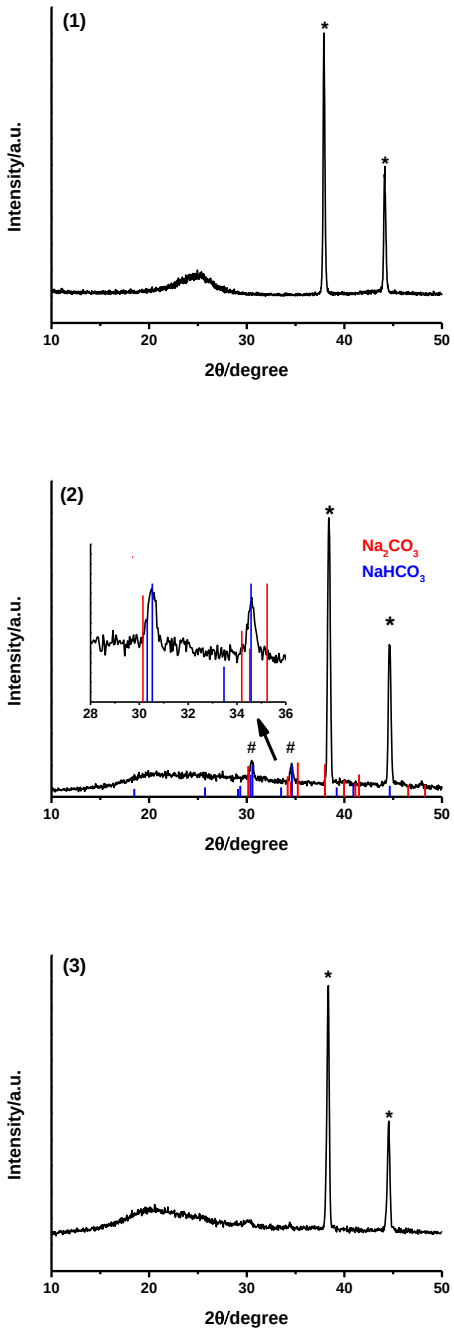

Figure 3.7 Post-mortem XRD of the cathodes under different conditions. (1) Pristine cathode (2) Cathode after discharge (3) Cathode after recharge. # indicates the characteristic peaks of $NaHCO_3$ and * indicates the characteristic peaks of Al current collector. Colored lines indicates the characteristic peaks of Na_2CO_3 (red) and $NaHCO_3$ (blue).

bis(trifluoromethanesulfone)imide and/or SiO_2 additives. Considering that the synthesis of the SiO_2-IL-TFSI particles is carried out in water this is a realistic possibility that has been studied in some detail in reference 22. (iii) Although both FTIR and DEMS indicate that electrolyte decomposition or H_2 generation do not occur in the potential range where the battery operates, the instability of imidazolium in an O_2 rich atmosphere near the porous cathode/electrolyte interface may produce small levels of hydrogen-containing decomposition products, which cannot be detected by the mentioned facilities, but which provide sufficient amounts of hydrogen to sustain the reaction at the cathode. (iv) A side reaction between the NaTFSI salt and aluminum current collector introduce hydrogen-containing side products 30 that may lead to $NaHCO_3$.

Residual water levels in the SiO_2-IL-TFSI/PC electrolyte have been the subject of previous intensive study [22] and treatment with various physical and chemical agents, including molecular sieves and metallic sodium, have been employed to produce the electrolytes used in the present study. Infrared spectra in the H_2O-characteristic 3500cm-1 and electrochemical analysis centered around the characteristic voltage range where H_2O decomposes were previously shown to imply undetetectable moisture levels in electrolytes dried using these approaches. Figure 3.2(b) report the I-V curves for the SiO_2-IL-TFSI/PC-NaTFSI used in the present work, which consistent with the earlier reports, are completely silent in the important 3.9V region where electrochemical decomposition of water is expected. Figure 3.5 further shows that the FTIR spectra are silent near the 3500cm-1 shift associated with the strong IR-active

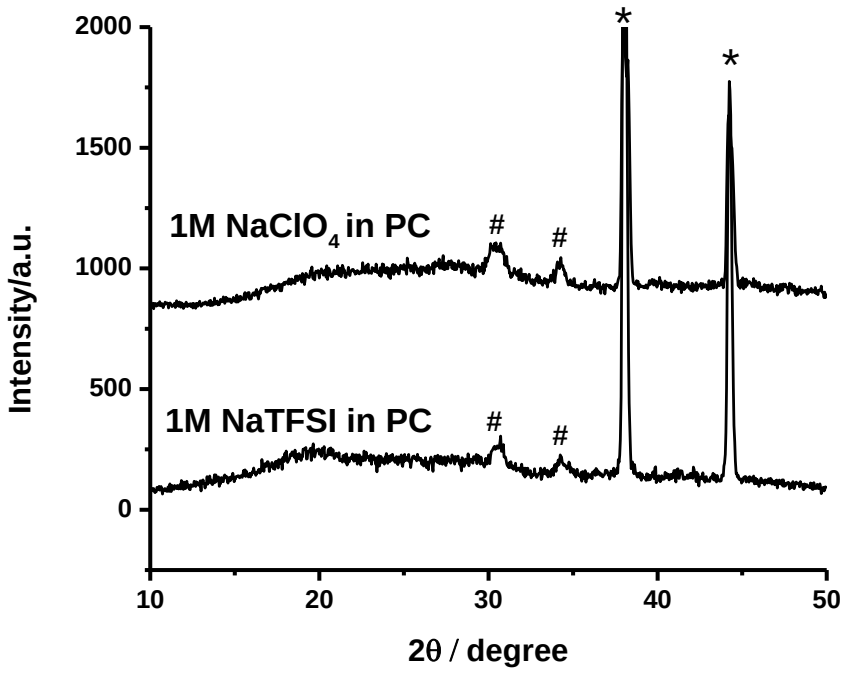

Figure 3.8 Ex-situ XRD analysis of cathodes after discharge in Na-CO_2/O_2 cells with different electrolytes. The # symbol identifies the characteristic peaks of $NaHCO_3$ and the * symbol identifies the characteristic peaks for the Al current collector.

longitudinal vibration mode of O-H groups. Besides, 17O-NMR also showed no signs of the existence of water in the electrolyte (Figure 3S4).

To further assess hypothesis (i) and to partially test (iii) and (iv), we constructed cells using alternative electrolytes in which the SiO_2-IL-TFSI particles were eliminated and/or $NaClO_4$ used as the salt to eliminate the possibility of side reactions with the aluminum current collector. Ex-situ XRD was performed on the resulting cathode and the results are also shown in Figure 3.8. It can be seen that the discharge product remains $NaHCO_3$, ruling out three of our four hypotheses and implying that hydrogen or a hydrogen containing compound capable of reacting with Na+ at the cathode electrolyte interface to produce $NaHCO_3$, is most likely generated during the SEI formation process.

The discharge potential in an electrochemical cell operating under equilibrium conditions provides an additional means for understanding the chemistry in the cell. We employed a galvanostatic intermittent titration technique (GITT) [31] to determine the equilibrium potential. The results are presented in Figure 3.9 and indicate that the equilibrium potential is around 2.7V. This means that the Na-CO_2/O_2 cells operate with an approximately 0.6 V discharge overpotential, which is comparable to that seen in Li-air batteries in the absence of catalyst. The dotted lines in Figure 3.9 are the theoretical potential based on thermodynamic calculations for the stated reactions. It is apparent from the comparisons that a reaction that includes molecular H_2 gas at the cathode yields an overall cell discharge potential closer to the measured equilibrium

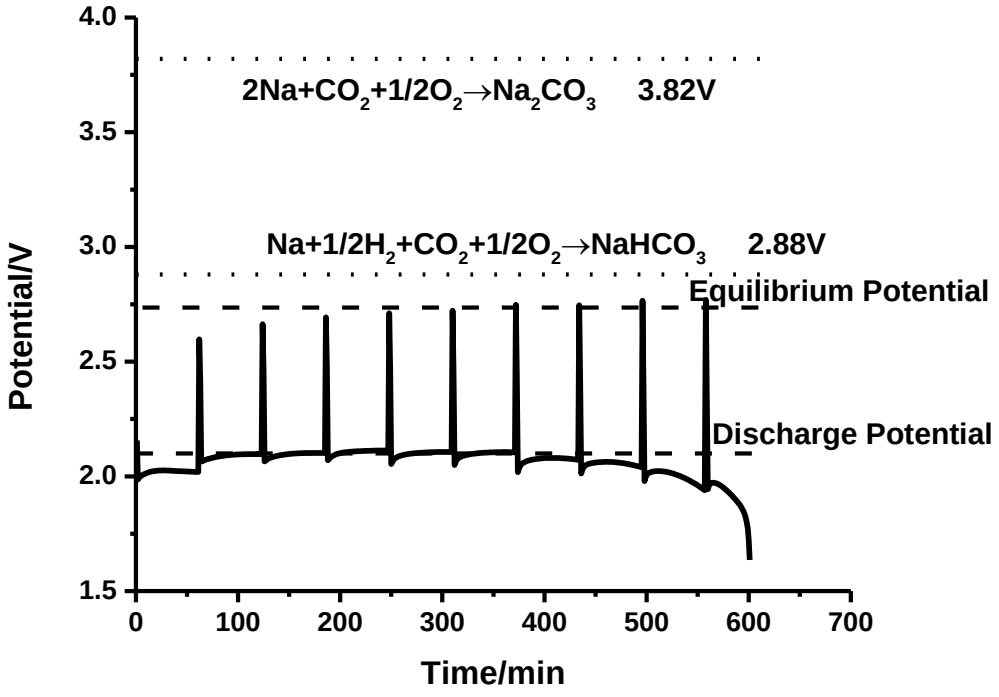

Figure 3.9 GITT discharge profile for Na-CO_2/O_2 cell. The dashed/broken line demarcates the equilibrium potential of the cell and the dotted lines correspond to the theoretical potential calculated based on thermodynamic data [32].

value than the equivalent value under the more normal assumptions leading to Na_2CO_3 as the principal discharge product.

That the Na-CO_2/O_2 cells are rechargeable, lends additional support to $NaHCO_3$ as the principal discharge product. Specifically, post-mortem XRD analysis reported in Figure 3.7 shows that the peaks associated with the discharge product disappear almost completely after recharging the cell. SEM images (Figure 3.10) of the cathode taken in the same sequence convey a similar understanding. These results show that the pristine cathode is composed of individual carbon particles aggregated together. After discharge, the inter particle space is seen to be occupied by discharge product, which makes the structure of the cathode more sheet-like. After recharge, the carbon particles are again seen to be separate; consistent with expectations if the discharge product decomposes completely during the charge process. Thus, consistent with the electrochemical measurements, both the XRD and SEM results strongly support rechargeability of the Na-CO_2/O_2 battery.

DEMS measurements provide additional insights about the electrochemical processes in Na-CO_2/O_2 cells. In particular, we carried out ex-situ DEMS measurements to characterize gaseous products that evolve during the charge cycle. For these measurements, the cells were discharged under normal Na-CO_2/O_2 cell operating conditions (Figure. 3.1) and the cathodes were taken out after the discharge and used in the DEMS cell, operated under vacuum, for the recharge. CO_2 evolution is obvious from Figure 3.11(a), but no O_2 or H_2 can be detected. Based on the proposed reaction

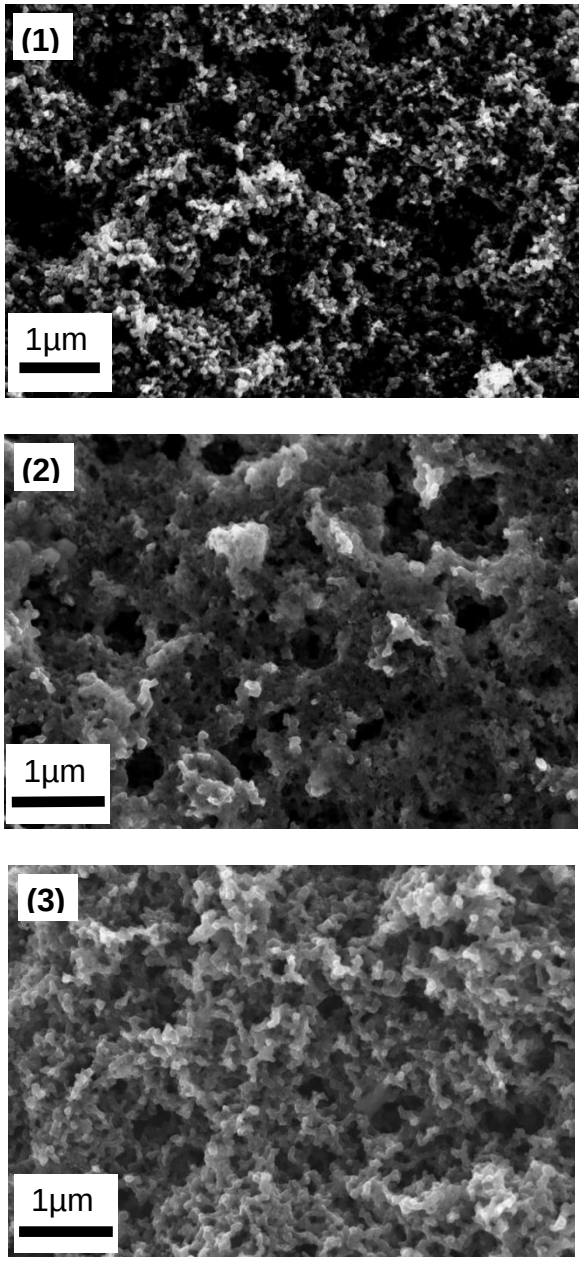

Figure 3.10 Post-mortem SEM images of the cathodes under different conditions. (1) Pristine cathode (2) Cathode after discharge (3) Cathode after recharge.

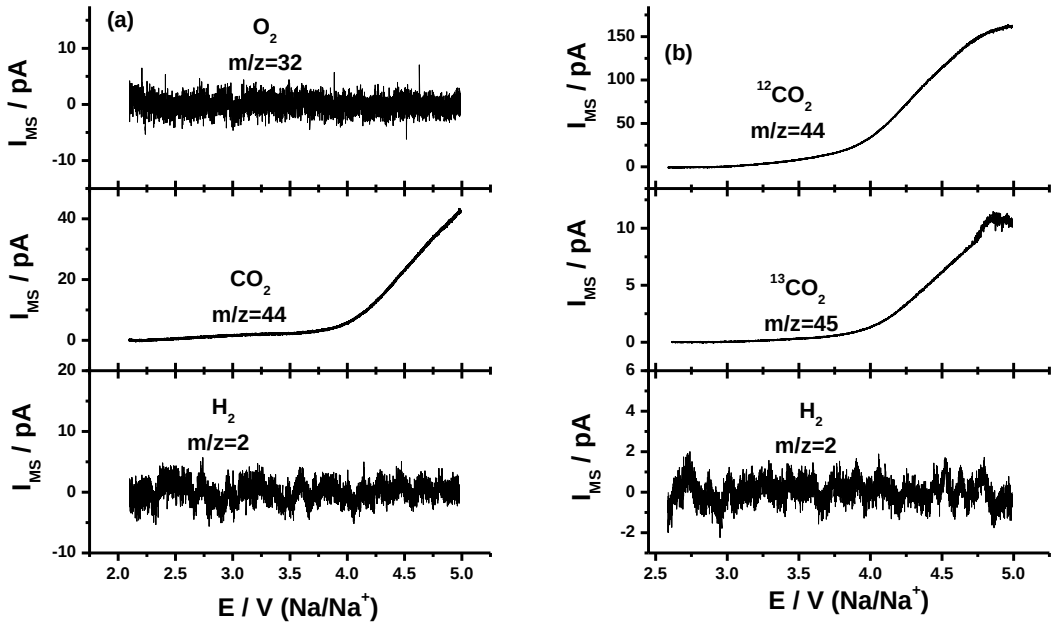

Figure 3.11 DEMS measurements of charge of the Na-CO_2/O_2 battery with different carbon cathodes. (a) Carbon black (super-P) cathode. (b) Porous ^{13}C cathode.

mechanism and the fact that O_2 is an important component of the cathode gas feed during discharge, and as such we would expect some amount of Na_2O_2 or Na_2O to be also formed during the discharge, and some amount of O_2 should be generated gas during recharge.

It has been reported that under O_2 rich atmosphere, carbon cathode can be oxidized and form CO_2 at high voltage [20], which raises the possibility that any O_2 generated in the charge cycle might be reduced by the carbon cathode during the recharge to generate CO_2. To study this possibility, a porous high-surface area carbon cathodes comprised of isotopic carbon (^{13}C) was used in DEMS measurements in the same manner as before to differentiate between the two potential sources of CO_2 upon cell recharge. Figure 3.11(b) indicates that this experiment yields relatively high levels of, $^{12}CO_2$ (MW=44), which we believe arises from decomposition of the discharge product from the higher pore-volume cathode. The figure also nicely shows that $^{13}CO_2$ (MW=45) is also unambiguously created, but at amounts roughly 10% of $^{12}CO_2$. These levels are evidently much higher than the proportion of ^{13}C in nature (~1%), and roughly consistent with orders of magnitude type expectations based on the relative amounts of CO_2 and O_2 in the gas feed. Considering Al was used as the current collector, which also has the possibility of reacting with evolved O_2, we believe that the fairly high amount of generated $^{13}CO_2$ is from the oxidation of the ^{13}C cathode by the generated O_2 during charge. Therefore, the cathode gas reacted during discharge can be regenerated during the recharge. Since the discharge product is $NaHCO_3$, it is expected that H_2 generation may also exist. However, no H_2 evolution

was detected during charge in either case, leaving the complete recharge mechanism yet to be understood.

3.7 Conclusions

In summary, we report a rechargeable Na-CO_2/O_2 battery that provides a potentially novel platform for capturing CO_2 emissions while generating large amounts of electrical energy. The battery utilizes a SiO_2-IL-TFSI/PC-NaTFSI hybrid electrolyte and is rechargeable for over 20 cycles. We show through conventional electrochemical and differential electrochemical mass spectrometry measurements that the rechargeability of the Na-CO_2/O_2 cell is facilitated by SiO_2-IL-TFSI nanoparticles seeded into the electrolyte, which increases its electrochemical stability at the high cell voltages needed for recharge. We further show that the principal discharge product in these cells is $NaHCO_3$ and, through postmortem XRD analysis demonstrate that the material is formed during cell discharge and consumed during recharge. DEMS based on ^{12}C and ^{13}C indicate that decomposition of $NaHCO_3$ during the charge process is accompanied by CO_2, and to a smaller extent O_2, emission. Finally, through analysis of the cell reactions using a galvanostatic intermittent titration technique (GITT) we tentatively conclude that H_2 may play an important role in the formation of $NaHCO_3$ and rechargeability of the cells. We hypothesize that the H_2 gas is created from decomposition of electrolyte during the SEI formation process, but concrete empirical support for this mechanism requires further work.

3.8 Methods

The investigated Na-CO_2 battery configuration is similar to the Li-air and Li-CO_2 cells reported earlier [23-24]. In particular, coin-type cells mechanically perforated on the cathode side were used for electrochemical experiments. The cathode material was created by blending conductive carbon, either super P-Li carbon black or amorphous ^{13}C, with a PVDF polymer binder in NMP. A fixed mass ratio of carbon to PVDF of 9:1 was used for all of the systems studied. The NMP slurry was cast on a gas diffusion layer or an aluminum mesh substrate (diameter 2 cm) and dried. The synthesis, purification, and characterization of the SiO_2-IL-TFSI/PC electrolyte have been reported previously [22]. The cells were assembled in an argon filled glove box. The assembled cells were then sealed into a customized stainless steel chamber filled with O_2 and CO_2 gas (1atm pressure, v/v=1:1) and connected to the battery tester. Neware CT-3008 battery tester was used for battery discharge-charge, cycling and GITT tests. The tests were run at a current density of 200mA/g and a capacity cutoff of 800mAh/gcarbon. The linear sweep scan was performed using CHI600D electrochemical analyzer with a scan rate of 0.1mV/s. X-ray diffraction (XRD) and Fourier transform infrared (FTIR) spectrum were utilized to characterize the cathode and electrolyte. The XRD was acquired using Scintag Theta-Theta X-ray diffractometer. The FTIR spectrum was obtained by Thermo Scientific Nicolet iZ10 spectrometer. Differential electrochemical mass spectrum (DEMS) was used to analyze the gas phase product. The scanning electron microscopy was employed to analyze the morphology of the cathodes. The images were obtained using LEO 1550 FESEM. The DEMS set-up has been described elsewhere [33]. For in-situ DEMS on

the electrolyte, a pristine porous carbon electrode was employed as the working electrode. For ex-situ DEMS on the cathode, firstly battery discharge was performed in a normal coin cell. After that the coin cell was disassembled and the cathode after discharge was put into the DEMS cell for recharge. The counter electrode and reference electrode are both Na metal and fresh electrolyte was used in DEMS measurement. The scan rate of DEMS is 0.5mV/s.

REFERENCES

1. K. M. Abraham, and Z. Jiang, *J. Electrochem. Soc.,* **1996**, 143, 1.
2. T. Ogasawara, A. Débarte, M. Holzapfel, P. Novák and P. G. Bruce, *J. Am. Chem. Soc.,* **2006**, 128, 1390.
3. P. G. Bruce, S. A. Freunberger, L. J. Hardwick and J. M. Tarascon, *Nat. Mater.,* **2012**, 11, 19.
4. G. Girishkumar, B. McCloskey, A. C. Luntz, S. Swanson and W. Wilcke, *J. Phys. Chem. Lett.,* **2010**, 1, 2193.
5. V. Palomares, P. Serras, I. Villaluenga, K. B. Hueso, J. Carretero-González and T. Rojo*, Energy Environ. Sci.*, **2012**, 5, 5884.
6. S.K. Das, S. Lau, L.A. Archer, *J. Mater. Chem. A.,* **2014**, 2 12623
7. E. Peled, D. Golodnitsky, R. Hadar, H. Mazor, M. Goor and L. Burstein, J. Power Sources, 2013, 244, 771; E. Peled, D. Golodnitsky, H. Mazora, M. Goora and S. Avshalomov, *J. Power Sources*, **2011**, 196, 6835.
8. Q. Sun, Y. Yang, Z. Fu, *Electrochem. Commun.,* **2012**, 16, 22.
9. W. Liu, Q. Sun, Y. Yang, J. Xie and Z. Fu, *Chem. Commun.,* **2013**, 49, 1951.
10. P. Hartmann, C. L. Bender, M. Vračar, A. K. Dürr, A. Garsuch, J. Janek and P. Adelhelm, *Nat. Mater.,* **2013**, 12, 228.
11. P. Hartmann, C. L. Bender, J. Sann, A. K. Dürr, M. Jansen, J. Janek and P. A. Adelhelm, *Phys. Chem. Chem. Phys.,* **2013**, 15, 11661.
12. D. P. Scharg, *Science,* **2007**, 315, 812.
13. C. Gough, *International Journal of Greenhouse Gas Control,* **2008**, 2, 155.

14. S. M. Benn and F. M. Orr, *MRS Bulletin*, **2008**, 33, 297.

15. S. Xu, S. K. Das and L. A. Archer, *RSC Advances*, **2013**, 3, 6656.

16. S. K. Das, S. Xu and L. A. Archer, *Electrochem. Commun*., **2013**, 27, 59.

17. S. Xu, W. I. A. Al Sadat, S. K. Das and L. A. Archer, US Patent Application, No. PCT/US13/68469

18. K. Takechi, T. Shiga and T. Asaoka, *Chem. Commun*., **2011**, 47, 3463.

19. W. Xu et al., *J. Power Sources,* **2012**, 215, 240.

20. M. M. Ottakam Thotiyl, S. A. Freunberger, Z. Peng and P. G. Bruce, *J. Am. Chem. Soc.*, **2013**, 135, 494.

21. Y. Lu, S. K. Das, S.S. Moganty and L. A. Archer, *Adv. Mater.*, **2012**, 24, 4430.

22. Y. Lu, K.S. Korf, Y. Kambe, Z. Tu and L. A. Archer, *Angew. Chem. Int. Ed.,* **2014**, 126, 498; K.S. Korf, Y. Lu, Y. Kambe, L.A. Archer, *J. Mater. Chem. A.* **2014**, 2 11866

23. T. Zhang and H. Zhou, H., *Nat. Commun.,* **2013**, 4, 1817.

24. H. Lim, H. Lim, K. Park, D. Seo, H. Gwon, J. Hong, W. A. Goddard, H. Kim and K. Kang, *J. Am. Chem. Soc.,* **2013**, 135, 9733.

25. Z. Zhang, L. Hu, H. Wu, W. Weng, M. Koh, P. C. Redfern, L. A. Curtiss and K. Amine, *Energy Environ. Sci.,* **2013**, 6, 1806.

26. J. Wolfenstine and J. Allen, *J. Power Sources*, **2005**, 142, 389.

27. S. K. Das, S. Xu, A. Emwas, Y. Lu, S. Srivastava and L. A. Archer, *Energy Environ. Sci.*, **2012**, 5, 8927.

28. J. Kim, H. Lim, H. Gwon and K. Kang, *Phys. Chem. Chem. Phys.,* **2013**, 15, 3623.

29. E. G. Brame, S. Cohen, J. L. Margrave and V. W. Meloche, *J. Inorg. Nucl. Chem.*, **1957**, 4, 90.

30. K. Xu, *Chem. Rev.,* **2004**, 104 (10), 4303.

31. W. Weppner and R. A. Huggins*, J. Electrochem. Soc.,* **1977**, 124, 1569.

32. M. W. Chase Jr., "NIST-JANAF Thermochemical Tables, Fourth Edition", *J. Phys. Chem. Ref. Data*, **1998**.

33. H. Wang, E. Rus and H. D. Abruña, *Anal. Chem.,* **2010**, 82, 4319.

APPENDIX

Supporting Figures for Chapter 3

1. GITT Measurement

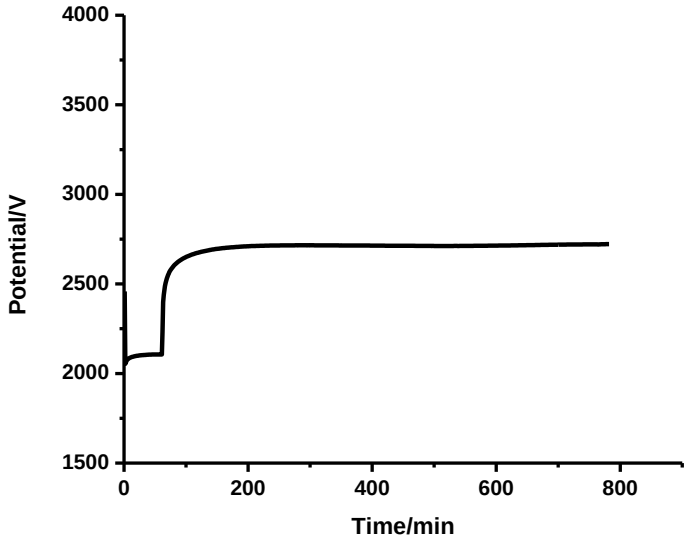

Figurev3.S1 Discharge pulse and relaxation of the galvanostatic intermittent titration technique (GITT) measurement. The stable plateau of the relaxation indicates that the rest time is sufficient.

2. Ex-situ FTIR Spectrum

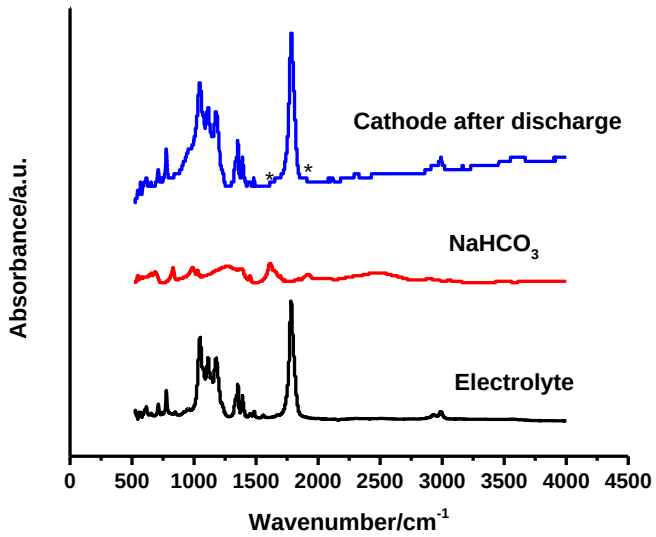

Figure 3.S2 Ex-situ FTIR of cathode after discharge in Na-O_2/CO_2 battery. * shows the peaks from $NaHCO_3$.

.

3. Ex-situ EDX Spectrum

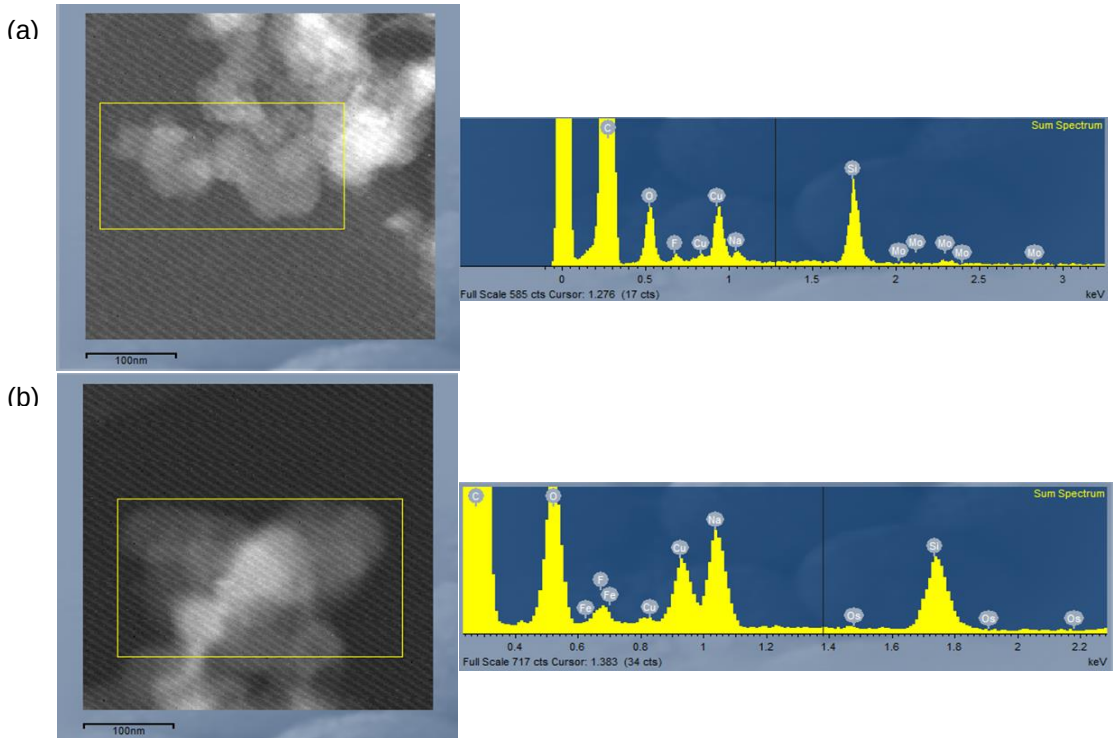

Figure 3.S3 Dark field TEM images and EDX spectra of particle-like structure (a) and sheet-like structure (b) on the cathode after discharge.

4. ^{17}O-NMR on the Electrolyte

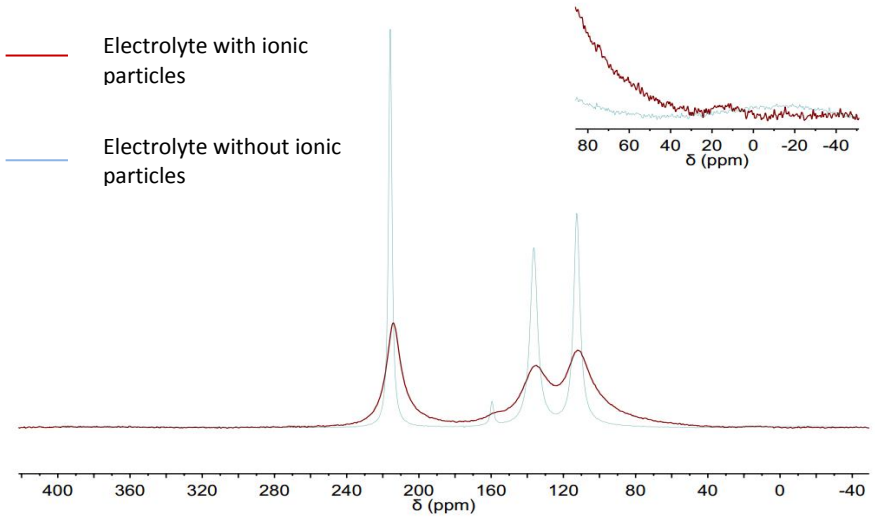

Figure 3.S4 ^{17}O-NMR on the electrolyte with no ionic particles (blue) and the electrolyte with 10% ionic particles (red). Inset shows the weak peak due to the ionic particles in the electrolyte.

CHAPTER 4

The Sodium-O_2/CO_2 Electrochemical Cell based on a Nickel Foam Cathode

4.1 Abstract

Electrochemical cells that utilize metals in the anode and an ambient gas as the active material in the cathode blur the lines between fuel cells and batteries. Such cells are under active consideration worldwide because they are considered among the most promising platforms for energy storage for electrified transportation. Lithium-Air (Li-Air) batteries are among the most actively investigated cells in this class, but long-term challenges associated with carbon-dioxide (CO_2) contamination of the cathode gas and associated loss of rechargeability due to metal carbonate formation adds significant gas-treatment infrastructure burdens to the Li-air cell that bring into question its viability. In contrast, several recent studies have shown that the presence of substantial fractions of CO_2 in the cathode gas stream can have significant benefits, including increasing the already high specific energy of a Li-oxygen cell by as much 200%. In this report, we consider electrochemical processes in model sodium-O_2/CO_2 (Na-O_2/CO_2) cells and find that provided that the electrode/electrolyte interfaces are electrochemically stable, such cells are able to deliver both exceptional energy storage capacity and stable long-term charge-discharge cycling behaviors at room temperature.

4.2 Introduction

An electrochemical cell in which metallic lithium serves as the anode and oxygen from ambient air is utilized as the active material in the cathode can reversibly store up to 11.4kWh of electrical energy per kg of the carbon substrate at which the electrochemical reaction $\boldsymbol{4Li + O_2 \rightarrow 2Li_2O}$ occurs. The specific energy storage capacity of such cells compare favorably with corresponding values from combustion reactions (e.g. coal (6.7kWh/kg) and commercial grade gasoline (13kWh/kg)), which has created interest in Li-Air cells as an alternative energy storage technology to fossil fuels for powering transportation. Following the first demonstration of Li-Air cells in non-aqueous carbonate electrolytes by Abraham and his colleagues [1], there has been an upsurge in research activity in the field [2-7], with the most important efforts focused on understanding electrochemical reactions at the cathode [8-10], electrolyte stability of the electrolyte [11-13], and the conditions required for achieving rechargeability [14-16]. Nothwithstanding the outstanding progress that has been made over the last decade, a quiet concession in the field is that barring a break-through in separations technology that allows oxygen from ambient air to be separated from other components, most notably CO_2 and moisture, with minimal pressure losses, such cells cannot live up to their theoretical potential based on the reactions at the anode and cathode. A consequence is that the term Lithium-air cell has gradually been replaced with the more accurate description Lithium-Oxygen battery, which also has an impressive theoretical energy density of 3.5kWh/kg, when the mass of oxygen and that anode material involved in the reaction at the cathode are included; this value becomes uninterestingly low however if the mass of the associated infrastructure for

carrying oxygen on board the cell, as opposed to harvesting it from ambient air, is included in the analysis. A conventional perspective, nonetheless, is that contamination from CO_2 and moisture in ambient air are to be avoided in such cells because they compete with oxygen for lithium ions at the cathode and react to form insulating metal carbonates and hydroxides [17] in the cathode, which limit cell capacity and rechargeability. On the basis of these ideas it is then reasonable to conclude that the long-term outlook for Li-Air cells is bleak.

Sodium is the 6th most abundant element in the earth's crust and costs about 10% that of lithium, the 25th most abundant element. [18] The standard electrode potential of Na/Na+ (-2.7V vs. SHE) is less negative than that of lithium (-3.0V vs. SHE), but it also undergoes a spontaneous reaction with O_2 from ambient air ($\boldsymbol{2Na + O_2 \rightarrow NaO_2}$) to yield a specific energy of 1.6kWh/kg, at 2.33V, when the weight of both Na and O_2 involved during the discharge reaction at the cathode are taken into account. Peled et al. were among the first to report a working Na-O_2 cell utilizing melted Na metal as the anode and a solid-state polymer electrolyte operated at over 100 ℃. [19-20] Subsequent work by Fu et al. demonstrated that Na-O_2 cells able to operate at room temperature are possible if conventional carbonate electrolytes are employed. [21-22] Hartmann and colleagues demonstrated a high capacity rechargeable Na-O_2 battery, which has Na-O_2 as the discharge product. [23-24] Despite the lower cost of the anode material, as is the case of Li-O_2 cells, a Na-O_2 cell that included the weight and cost of the infrastructure required to generate pure O_2

from ambient air or to carry an O_2 supply onboard the cell, would remove any of the advantages these cells offer of electrochemical energy storage.

An important recent result from theory [25] indicates that the discharge capacity of a Li-O_2 cell has very little to do with the electronic conductivity of the dominant discharge product, Li_2O_2, now known to be present in the cathode. This analysis further suggests that the rechargeability of a Li-O_2 cell is a much stronger function of the availability of uncovered surface area on the cathode substrate at the end of discharge and the associated ability to retain electrochemical contact with the highly insulating discharge product Li_2O_2. Support for this perspective comes from a rapidly growing list of experimental contributions which show that Li-O_2 cells with exceptional rechargeability can be achieved if only a fraction of the storage capacity is utilized in an interrupted discharge protocol. Support also comes from a smaller number of studies which show Li-O_2/CO_2 or Na-O_2/CO_2 cells, which utilize a mixture of O_2 and CO_2 as the active cathode gas, can deliver substantially higher capacity than the corresponding metal-CO_2 cells at O_2/CO_2 compositions near 1/1 [26, 27]. Researchers at Toyota [26] for example showed that incorporation of CO_2 with O_2 in Li-air cells increase the specific capacity by 200%, while a previous report by Das et al. showed that a CO_2/O_2 mixture with O_2/CO_2 composition of around 3/2 increased the discharge capacity of Na-air cells by as much as 150%. [27] A weakness of all of these studies is that the decomposition of the carbon substrate [28-30] in the recharge reaction yields either no or limited rechargeability relative to the metal-O_2 counterparts.

The results presented in this chapter contest these views and show that provided the cathode substrate and anode/electrolyte interface in a Na-O_2/CO_2 cell remain stable during the recharge cycle, it is possible to create metal-O_2/CO_2 cells that exhibit enhanced capacity to store electrochemical energy and which are rechargeable over at least 100 cycles of charge and discharge. Through detailed analysis of the discharge product morphology and chemical composition, we further illustrate the operating mechanisms for such cells. These results are encouraging not only for their expected large impacts on development of practical metal-air batteries that adhere to the original design of harnessing active cathode materials from ambient air, but also because such cells provide novel opportunities as dual function devices for capturing CO_2 and generating electrical energy in a fully reversible context. [31]

4.3 Cell Structure

The Na-CO_2/O_2 electrochemical cell configuration used in the study is depicted in Figure 4.1. It is similar to previously reported Li-O_2 and Li-CO_2 systems. [32-34] It is composed of a sodium metal anode, a glass fiber separator and a porous carbon cathode. The electrolyte consists of a previous reported SiO_2-IL-TFSI/propylene carbonate(PC)-1M NaTFSI electrolyte [35], created by blending silica nanoparticles densely functionalized with the ionic liquid 1-methyl-3-propylimidazolium bis(trifluoromethanesulfone)imide with a conventional propylene carbonate (PC)/NaTFSI liquid electrolyte. Due to the interaction between the tethered ionic liquid and sodium metal, the silica particles form a protective layer on the anode surface, which was shown previously to enhance the stability window of the

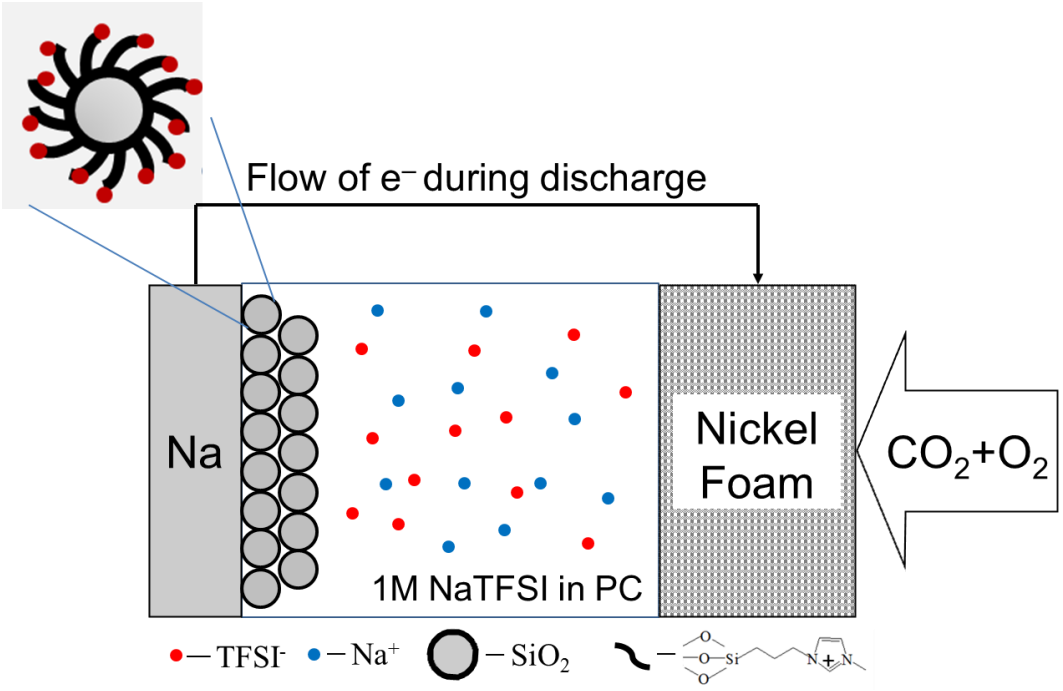

Figure 4.1 Schematic diagram of the Na-CO_2/O_2 electrochemical cell.

electrolyte by at least 1 volt, making it possible for the cell to be charged even under high overpotentials, without electrolyte degradation.

4.4 Characterization of Cathode Products

The nickel foam cathode is advantageous for a variety of reasons, including its smooth surface, which makes it possible to analyze the growth of discharge product by observing the morphology of the product layer (Figure 4.2). It can be clearly seen from the SEM images that the discharge product grows from nanometer size nuclei to 2 μm size spherical particle, and finally cover the whole surface of the cathode, when the steep drop on the discharge curve happens. This is consistent with the nucleation and growth model that was developed by Lau et al. [25] At the start of the discharge, the initial electrochemical reaction yields nanometer size nuclei. With the progress of the discharge, existing nuclei grow and at the same time new nuclei are formed. When the surface of the cathode is covered by the discharge product, the resistivity of the cathode increases rapidly, leading to the sharp downturn of the discharge curve that terminates the discharge. The discharge product was characterized via ex-situ XRD and EDX and found to be $NaHCO_3$. We hypothesize that trace amounts of water in the electrolyte (<50ppm, by Karl Fisher Titration) participate in the cathode reaction. Previous works have shown that in both Li-air and Na-air cells even with carbonate as the discharge product, it is still possible for the product to be decomposed to some extent during recharge [36-39].

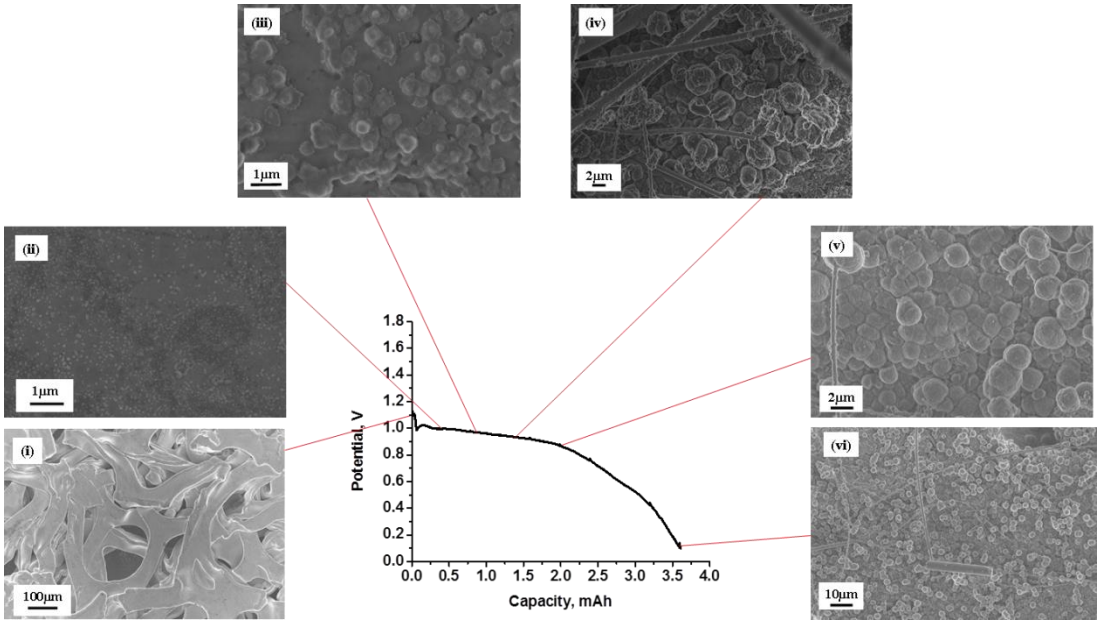

Figure 4.2 Discharge profile for Na-O_2/CO_2 cell with a nickel cathode and the SEM images of cathodes (i) before discharge, (ii) after 10% discharge, (iii) after 20% discharge, (iv) after 40% discharge, (v) after 60% discharge, (vi) after full discharge. The cell was discharged under 50 μA/cm^2 current density and the cathode gas is a mixed gas of O_2 and CO_2 with a molar ratio of 1:1.

4.5 Effect of Cathode Gas Composition

The effect of O_2:CO_2 molar ratio in the cathode gas was previously reported. [26, 27] In order to study the effect of CO_2 on the electrochemical cell, the discharge of cells with different gas feed from the cathode was performed. The comparison of the discharge capacity is shown in Figure 4.3a. It can be clearly seen that there is a maximum capacity happening at 1:1 O_2 to CO_2 ratio, which is consistent with previous results. The SEM images of cathodes after discharge in different atmosphere are shown in Figure 4.3b. With low CO_2 concentration the discharge product tend to form a sheet like structure on the cathode surface, while with high CO_2 concentration the discharge product forms separate spherical particles. With this observation, it is reasonable to hypothesize that the reaction in these cells are different. With ex-situ XRD and XPS this hypothesis can be proved (results shown in supporting information). For the highest capacity case, i.e. 1:1 O_2 to CO_2 ratio, both XRD and XPS clearly show the characteristic peak of $NaHCO_3$. For the lower capacity cases, XRD does not provide much information, most likely because the discharge products in these cases do not have crystalline structure. From the XPS though, it is clear that in the low CO_2 concentration case (O_2:CO_2=2:1) Na_2O_2 is a component of discharge product, while in the high CO_2 concentration case (O_2:CO_2=1:2) the peak of $Na_2C_2O_4$ appears in the spectrum. This is consistent with the previous findings that $Na_2C_2O_4$ can be formed as a product of CO_2 reduction. (27)

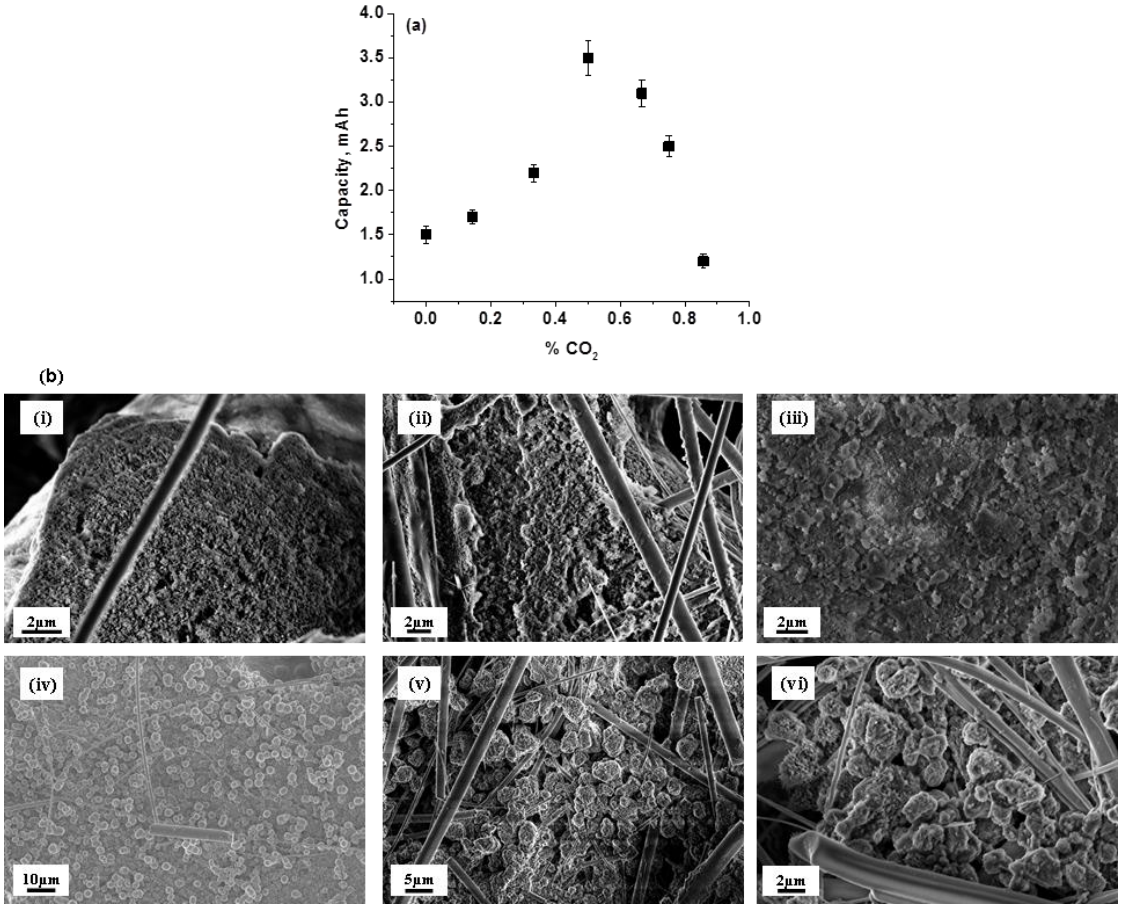

Figure 4.3 (a) The comparison of discharge capacity of Na-O_2/CO_2 cells with different cathode gas compositions. (b) The SEM images of cathodes after discharge in Na-O_2/CO_2 cell with different cathode gas compositions. (i) Pure O_2, (ii) O_2:CO_2=3:1, (iii) O_2:CO_2=2:1, (iv) O_2:CO_2=1:1, (v) O_2:CO_2=1:2, (i) O_2:CO_2=1:3.

4.6 Reaction Mechanism of the Cell

In order to understand how CO_2 increases the cell discharge capacity, experiments were performed wherein cells were first discharged galvanostatically to different stages in a pure O_2 atmosphere then the cathode gas was switched to a 1:1 O_2/CO_2 mixture and the discharge continued. The total capacity measured for these cells is compared in Figure 4.4. It is noted that if the gas switch happens during the discharge plateau, the total capacity is close to that of a Na-O_2/CO_2 cell with the O_2/CO_2 ratio (1:1) of the final cathode gas. However, if the gas switch is implemented near the end of the discharge in pure O_2, the ultimate discharge capacity obtained for the O_2/CO_2 mixed gas feed remains close to that of a Na-O_2 battery. A related and important observation is that in the Na-O_2/CO_2 cells the deposition of discharge products is promiscuous – it not only happens on the conductive surface of the cathode, but also in the pores of the insulating separator (Figure 4.4c). This phenomenon has also been observed in Li-O_2 batteries.[40-41], where it is thought to stem from the fact that the intermediate product LiO_2 is soluble in the electrolyte, can diffuse in the separator where it undergoes chemical reaction, $\mathbf{2LiO_2 \rightarrow Li_2O_2 + O_2}$ to produce insoluble Li_2O_2, which can deposit on any surface. We expect that a similar process may occur in the Na-O_2/CO_2 cell. However, unlike LiO_2, NaO_2 is insoluble in the electrolyte and can be the final discharge product of a Na-O_2 battery.[23, 24] With the presence of CO_2 in the cathode gas, NaO_2 can undergo additional reaction to form another intermediate compound $Na_2C_2O_6$, which is believed to be soluble and able to freely diffuse in the electrolyte. [26] The reaction mechanism may therefore be summarized as follows [26, 27, 42]:

$$4O_2 + 4e^- \rightarrow 4{O_2}^{\bullet -} \quad (1)$$

$${O_2}^{\bullet -} + CO_2 \rightarrow {CO_4}^{\bullet -} \quad (2)$$

$${CO_4}^{\bullet -} + CO_2 \rightarrow {C_2O_6}^{\bullet -} \quad (3)$$

$${C_2O_6}^{\bullet -} + {O_2}^{\bullet -} \rightarrow {C_2O_6}^{2-} + O_2 \quad (4)$$

$${C_2O_6}^{2-} + 2{O_2}^{\bullet -} + 4Na^+ \rightarrow 2Na_2CO_3 + 2O_2 \quad (5)$$

With the existence of moisture and excess CO_2, the discharge product can be converted to sodium bicarbonate:

$$Na_2CO_3 + CO_2 + H_2O \rightarrow 2NaHCO_3 \quad (6)$$

Since reactions (2)-(5) are chemical reactions, which do not require a conductive substrate to proceed, the final discharge product, which is $NaHCO_3$ due to the trace amount of water in the electrolyte, can be deposited in the network of insulating separator. This also explains the results of the gas switching experiments. If CO_2 is introduced during the plateau region of the discharge, the surface of the cathode is not yet fully occupied by the discharge product. Thus with the introduction of CO_2 reactions (2)-(5) can happen and because of the solubility of $Na_2C_2O_6$ the surface of the cathode can be freed for further reaction, leading to a high discharge capacity close to a Na-O_2/CO_2 cell. If CO_2 is introduced after the falling of discharge potential, the surface of the cathode is fully covered by the discharge product, which is Na_2O_2 due to the reaction $\boldsymbol{2NaO_2 \rightarrow Na_2O_2 + O_2}$. In this case, the introduction of CO_2 only converts Na_2O_2 to Na_2CO_3, without forming the soluble $Na_2C_2O_6$. Thus, the surface

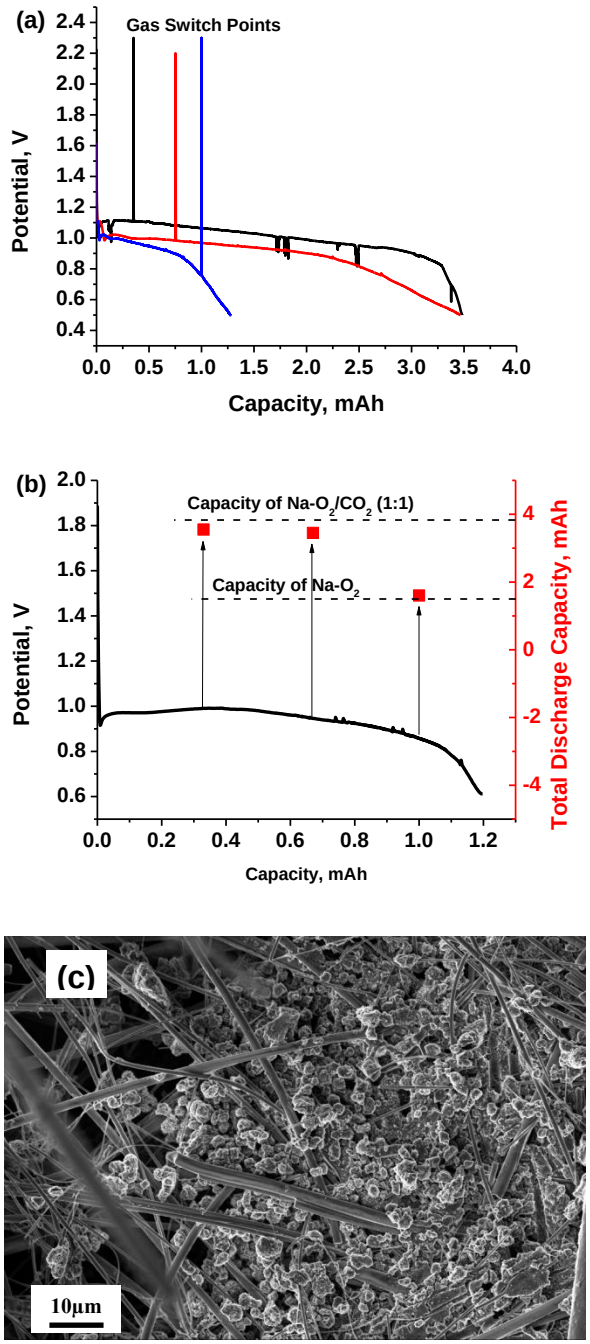

Figure 4.4 (a) Discharge curves of the electrochemical cells with gas switch during discharge. (b) Comparison of total discharge capacities of the cells with gas switch at different stages of discharge. The arrows indicate the point of gas switch with respect to a Na-O_2 cell. (c) SEM image of separator after discharge in a Na-O_2/CO_2 cell, indicating the deposition of discharge product on the separator.

of the cathode is still covered by an insulating layer preventing further discharge, leading to no increase in the discharge capacity.

4.7 Stability of the Nickel Cathode

The instability of carbon cathodes has been previously reported. It is believed that the highest voltage the Li-O_2 system with a carbon cathode can reach is 3.5V vs. Li/Li+ without cathode decomposition. [28-30] However, due to the high resistivity of the carbonate compound, the charge potential of Na-O_2/CO_2 cell without any catalysts or redox mediators can be as high as 4.5V vs. Na/Na+ (equivalent to 4.8V vs. Li/Li+), which is much higher than the voltage a carbon cathode can sustain. The decomposition of carbon cathode was studied using differential electrochemical mass spectrometry (DEMS) with isotopic carbon. [29, 32] It was found that during recharge of the cell, no O_2 evolution was detected due to the side reaction between carbon cathode and evolved O_2. After the introduction of a carbon cathode with ^{13}C, the evolution of CO_2 with both ^{13}C and ^{12}C was detected. The CO_2 with ^{12}C is from the decomposition of discharge product, whereas the CO_2 with ^{13}C is the result of degradation of cathode. This proves the instability of carbon cathode during the recharge of the Na-O_2/CO_2 cell. The stability of the nickel cathode is also studied with DEMS. The DEMS setup has been described in previous studies. [43, 44] The Na-O_2/CO_2 cell was first discharged in a coin cell apparatus, after which the nickel cathode was taken out and set up in the DEMS apparatus for charge. The results in Figure 4.5 clearly shows the evolution of both O_2 and CO_2, meaning the gas absorbed during discharge is breathed out during recharge without any side reactions. With this

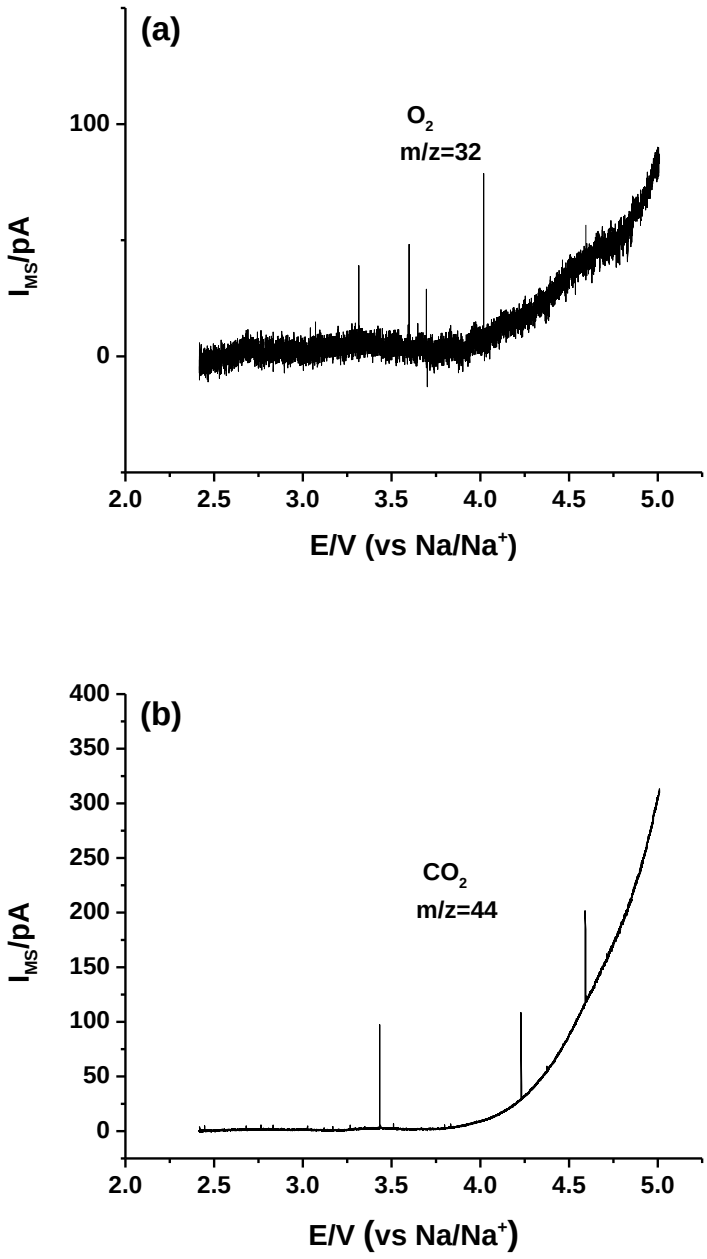

Figure 4.5 The evolution of (a) O_2 and (b) CO_2 detected from differential electrochemical mass spectrometry (DEMS).

result, it can be concluded that with the involvement of nickel cathode in Na-O_2/CO_2 cell, cathode decomposition is avoided.

4.8 Rechargeability of the Cell

The rechargeability of the Na-O_2/CO_2 system has previously been studied with a carbon cathode. [32] The cell was able to stably cycle for over 25 cycles while capacity fade still happened after 30 cycles due to the decomposition of the carbon cathode. With the introduction of a nickel foam cathode, the rechargeability of the cell is significantly improved. As is shown in the cycling profile (Figure 4.6), the cell with a nickel cathode can be very stably operated for over 100 cycles with a capacity cutoff of 200mAh/gcathode, which is comparable to 1000mAh/gcarbon with a carbon cathode. The charge-discharge profiles (Figure 4.7a) are identical from the 1st cycle to the 100th cycle, and the anodic and cathodic peaks in the cyclic voltammetry (Figure 4.7b) show almost no shift throughout 10 cycles. These facts further prove the rechargeability of the Na-O_2/CO_2 electrochemical cell. The evidence of rechargeability can also be found in SEM images of cathode after cycling (Figure 4.8). It can be clearly seen that after discharge the smooth surface of the nickel cathode is covered by spherical shape product particles which disappear after the recharge, indicating the decomposition of discharge product during charge. The cathode surface after 1 cycle, 10 cycles, and even 100 cycles remains clean and smooth, showing that the decomposition of the discharge product is complete in each cycle and that the Na-O_2/CO_2 cell is truly rechargeable.

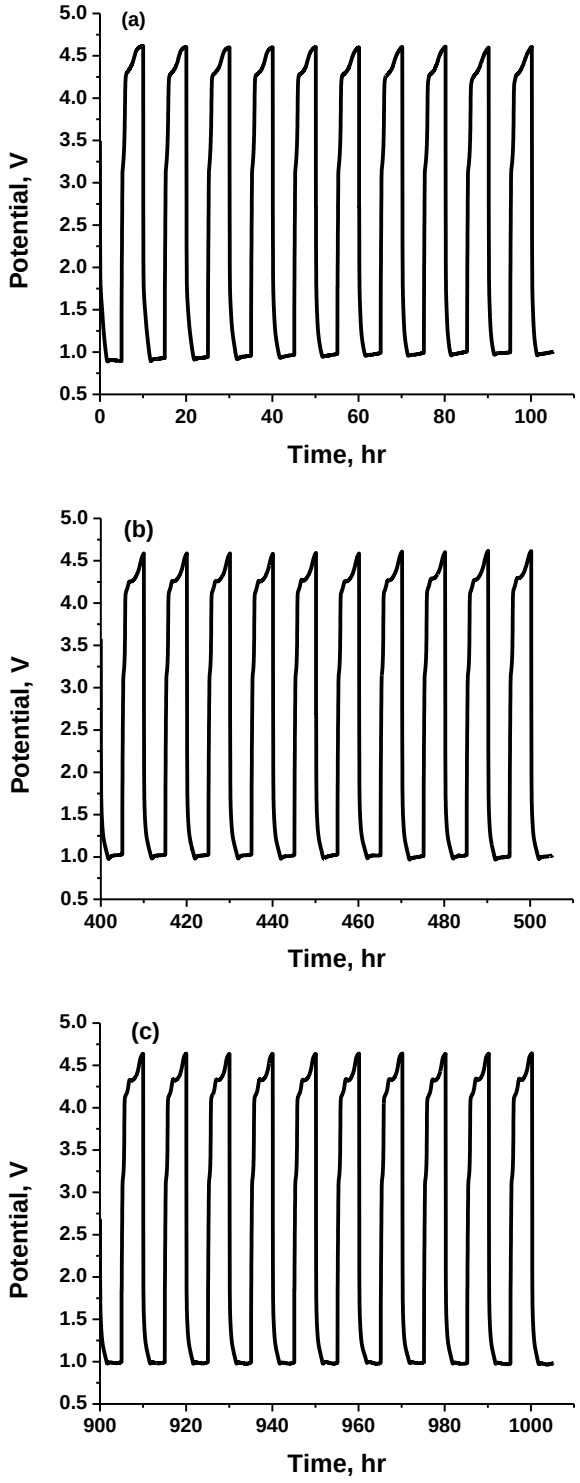

Figure 4.6 The cycling profiles for the Na-O_2/CO_2 cell. (a) 1st-10th cycle, (b) 41st-50th cycle, (c) 91st-100th cycle.

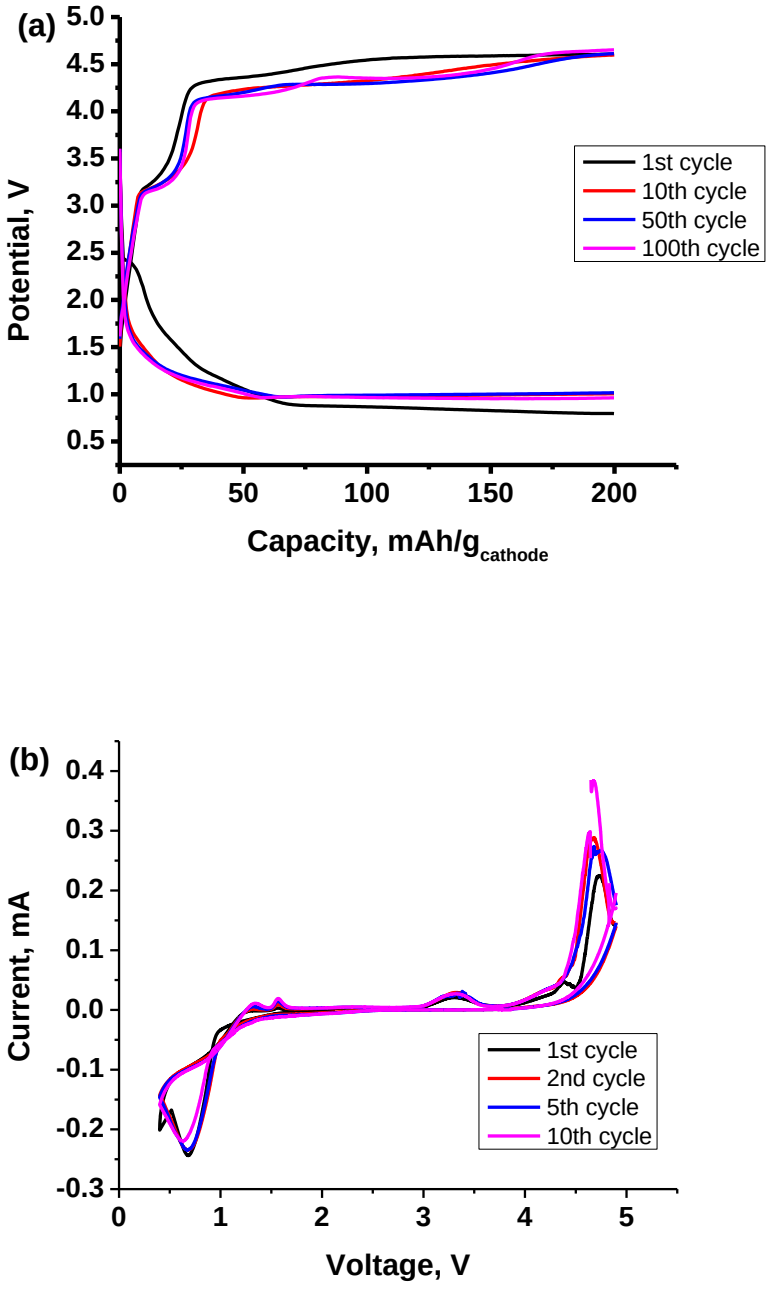

Figure 4.7 (a) Charge-discharge profiles of the 1st cycle, 10th cycle, 50th cycle and 100th cycle. The cell was operated with a current density of 50 μA/cm^2 and a capacity cutoff of 200mAh/gcathode. (b) Cyclic voltammetry of the 1st, 2nd, 5th, and 10th cycle. The scan rate was 0.1mA/s.

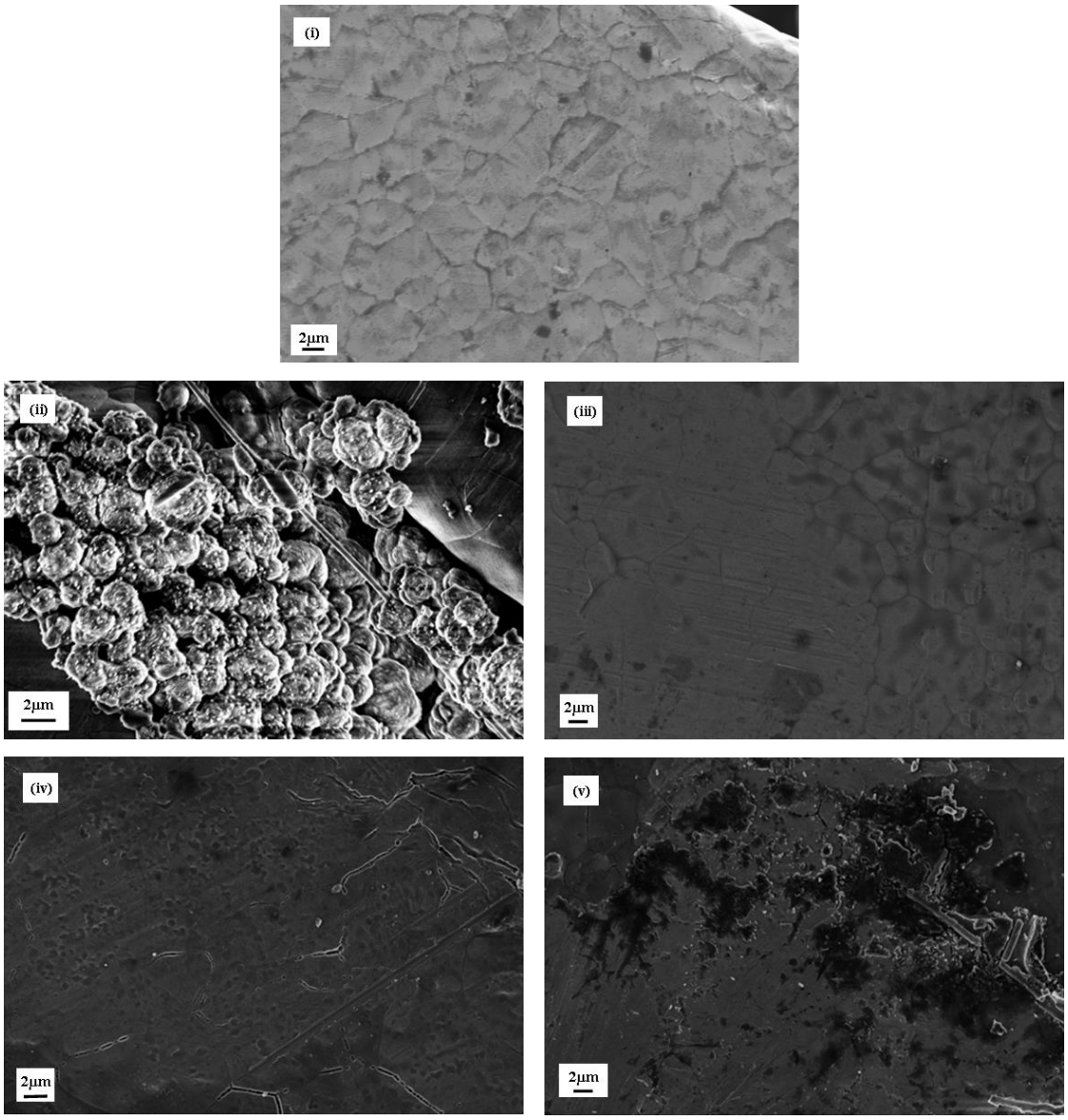

Figure 4.8 SEM images of cathodes (i) before discharge, (ii) after the 1st discharge, (iii) after the 1st recharge, (iv) after 10 cycles and (v) after 100 cycles.

4.9 Conclusions

In summary, we report a Na-O_2/CO_2 electrochemical cell utilizing a nickel foam cathode. With the introduction of nickel cathode, we can characterize the discharge product on the cathode and find that the deposition of discharge product is consistent with the nucleation and growth model previous raised for Li-air battery. Also, we report the effect of CO_2 concentration on the discharge capacity. The increase in the capacity with the existence of CO_2 is explained by the solubility of intermediate product $Na_2C_2O_6$, which is also proved by a gas switching experiment and the deposition of discharge product in the network of insulating separator. The nickel cathode also eliminates cathode decomposition, which helps improve the rechargeability significantly, making the cell stably run for over 100 cycles without any catalysts or redox mediators. The gas phase product was also investigated using DEMS, which indicates the gas absorbed during discharge is released during recharge, which proves the rechargeability of the Na-O_2/CO_2 cell from the other perspective.

REFERENCES

1. K. M. Abraham and Z. Jiang, *J. Electrochem. Soc.* **1996**, *143*, 1.
2. L. Grande, E. Paillard, J. Hassoun, J. Park, Y. Lee, Y. Sun, S. Passerini, B. Scrosati, *Adv. Mater.* **2015**, *27*, 784.
3. P. G. Bruce, S. A. Freunberger, L. J. Hardwick and J. M. Tarascon, *Nat. Mater.,* **2012**, *11*, 19.
4. G. Girishkumar, B. McCloskey, A. C. Luntz, S. Swanson and W. Wilcke, *J. Phys. Chem. Lett.,* **2010,** *1*, 2193.
5. M. Park, H. Sun, H. Lee, J. Lee, J. Cho, *Adv. Energy. Mater.,* **2012**, *2*, 780.
6. Y. Lu, B. M. Gallant, D. G. Kwabi, J. R. Harding, R. R. Mitchell, M. S. Whittingham, Y. Shao-Horn, *Energy Environ. Sci.,* **2013***, 6*, 750.
7. B. Scrosati, J. Garche, L*J. Power Sources,* **2010***, 195*, 2419.
8. J. S. Hummelshøj, J. Blomqvist, S. Datta, T. Vegge, J. Rossmeisl, K. S. Thygesen, A. C. Luntz, K. W. Jacobsen and J. K. Nørskov, *J. Chem. Phys., **2010**, 132*, 071101.
9. R. Black, S. Oh, J. Lee, T. Yim, B. Adams and L. F. Nazar, *J. Am. Chem. Soc.*, **2012**, ***134***, 2902.
10. L. Johnson, C. Li, Z. Liu, Y. Chen, S. A. Freunberger, P. C. Ashok, B. B. Praveen, K. Dholakia, J. Tarascon and P. G. Bruce, *Nat. Chem.,* **2014**, *6*, 1091.
11. S. A. Freunberger, Y. Chen, N. E. Drewett, L. J. Hardwick, F. Bardé and P. G. Bruce, *Angew. Chem. Int. Ed.,* **2011**, *50*, 8609.
12. D. G.Kwabi et al., *J. Phys. Chem. Lett.,* **2014,** *5*, 2850.

13. J. R. Harding, C. V. Amanchukwu, P. T. Hammond and Y. Shao-Horn, *J. Phys. Chem. C,* **2015,** *119*, 6947.

14. Y. Lu, H. A. Gasteiger and Y. Shao-Horn, *J. Am. Chem. Soc.*, **2011**, *133*, 19048.

15. Y. Chen, S. A. Freunberger, Z. Peng, O. Fontaine and P. G. Bruce, *Nat. Chem.,* **2013**, *5*, 489.

16. T. Liu et al. *Science,* **2015**, *350*, 530.

17. P. Albertus, G. Girishkumar, B. McCloskey, R. S. Sánchez-Carrera, B. Kozinsky, J. Christensen and A. C. Luntz, *J. Electrochem. Soc*., **2011**, *158*, A343.

18. V. Palomares, P. Serras, I. Villaluenga, K. B. Hueso, J. Carretero-González and T. Rojo, *Energy Environ. Sci.*, **2012**, *5*, 5884.

19. E. Peled, D. Golodnitsky, H. Mazora, M. Goora and S. Avshalomov, *J. Power Sources,* **2011**, *196*, 6835.

20. E. Peled, D. Golodnitsky, R. Hadar, H. Mazor, M. Goor and L. Burstein, *J. Power Sources,* **2013**, *244*, 771.

21. Q. Sun, Y. Yang, Z. Fu, *Electrochem. Commun.,* **2012**, *16*, 22.

22. W. Liu,Q. Sun,Y. Yang,J. Xie and Z. Fu, *Chem. Commun.,* **2013**, *49*, 1951.

23. P. Hartmann, C. L. Bender, M. Vračar, A. K. Dürr, A. Garsuch, J. Janek and P. Adelhelm, *Nat. Mater.,* **2013**, *12*, 228.

24. P. Hartmann, C. L. Bender, J. Sann, A. K. Dürr, M. Jansen, J. Janek and P. Adelhelm, *Phys. Chem. Chem. Phys.,* **2013**, *15*, 11661.

25. S. Lau and L. A. Archer, *Nano Lett.* **2015**, *15*, 5995.

26. K. Takechi, T. Shiga, T. Asaoka, *Chem. Commun.,* **2011**, *47*, 3463.

27. S. K. Das, S. Xu and L. A. Archer, *Electrochem. Commun.,* **2013**, *27*, 59.

28. B. M. Gallant et al. *J. Phys. Chem. C,* **2012**, *116*, 20800.

29. M. M. Ottakam Thotiyl, S. A. Freunberger, Z. Peng and P. G. Bruce, *J. Am. Chem. Soc.,* **2013**, *135*, 494.

30. M. Leskes, A. J. Moore, G. R. Goward and C. P. Grey, *J. Phys. Chem. C,* **2013**, *117*, 26929.

31. S. Xu, W. I. A. Al Sadat, S. K. Das and L. A. Archer, US Patent Application, No. PCT/US13/68469

32. S. Xu, Y. Lu, H. Wang, H. D. Abruña and L. A. Archer, *J. Mater. Chem. A*, **2014**, *2*, 17723.

33. S. K. Das, S. Xu, A. Emwas, Y. Lu, S. Srivastava and L. A. Archer, *Energy Environ. Sci.,* **2012**, *5*, 8927.

34. S. Xu, S. K. Das and L. A. Archer, *RSC Advances*, **2013**, *3*,6656.

35. Y. Lu , S. K. Das , S. S. Moganty and L. A. Archer, *Adv. Mater.,* **2012**, *24*, 4430.

36. Z. Zhang, Q. Zhang, Y. Chen, J. Bao, X. Zhou, Z. Xie, J. Wei and Z. Zhou, *Angew. Chem. Int. Ed.,* **2015**, *54*, 6550.

37. Y. Liu, R. Wang, Y. Lyu, H. Li and L. Chen, *Energy Environ. Sci.,* **2014**, *7*, 677.

38. H. Lim, H. Lim, K. Park, D. Seo, H. Gwon, J. Hong, W. Goddard, H. Kim and K. Kang, *J. Am. Chem. Soc.,* **2013**, *135*, 9733.

39. T. Zhang and H. Zhou, *Nat. Commun.,* **2013**, *4*, 1817.

40. W. Ryu, F. S. Gittleson, M. Schwab, T. Goh and A. D. Taylor, *Nano Lett.*, **2015**, *15*, 434.

41. B. D. Adams, C. Radtke, R. Black, M. L. Trudeau, K. Zaghib and L. F. Nazar, *Energy Environ. Sci.,* **2013**, *6*, 1772.

42. E.G. Brame, S. Cohen, J. L. Margrave and V.W. Meloche, *J. Inorg. Nucl. Chem.,* **1957**, *4*, 90.

43. H. Wang, E. Rus and H. D. Abruña, *Anal. Chem.,* **2010***, 82,* 4319.

44. H. Wang, E. Rus, T. Sakuraba, J. Kikuchi, Y. Kiya and H. D. Abruña, *Anal. Chem.,* **2014***, 86,* 6197.

APPENDIX

Supporting Information for Chapter 4

1. Methods

The investigated Na-O_2/CO_2 cell configuration is similar to the Li-air and Li-CO_2 cells reported earlier [1-4]. In particular, coin-type cells mechanically perforated on the cathode side were used for electrochemical experiments. The cathode material was purchased from MTI. The synthesis of the SiO_2-IL-TFSI/PC electrolyte has been reported previously [5]. The cells were assembled in an argon filled glove box. The assembled cells were then sealed into a customized stainless steel chamber filled with O_2 and CO_2 gas (1atm pressure) and connected to the battery tester.

Neware CT-3008 battery tester was used for battery discharge-charge and cycling tests. The tests were run at a current density of 50 $\mu A/cm^2$ and a capacity cutoff of 200mAh/gcathode. The cyclic voltammetry was performed using CHI600D electrochemical analyzer with a scan rate of 0.1mV/s. X-ray diffraction (XRD), X-ray photoelectron spectroscopy (XPS), and scanning electron microscope (SEM) were utilized to characterize the cathode. The XRD was acquired using Scintag Theta-Theta X-ray diffractometer. The XPS was obtained using a Surface Science Instruments SSX-100 with operating pressure approximately 1 ×10-8 Torr. The SEM images and EDX spectrum were obtained with LEO 1550-FESEM. Differential electrochemical mass spectrum (DEMS) was used to analyze the gas phase product. The DEMS set-up has been described elsewhere [6, 7]. The scan rate of DEMS is 0.5mV/s.

2. Formation of silica particle layer on the anode

Due to the interaction between the tethered imidazolium ionic liquid and the sodium metal, the tethered silica nanoparticles tend to form a layer on the anode surface, which can be proved by the ex-situ XPS (Figure 4.S1). After discharge, the XPS on the anode clearly shows a Si 2p peak at 103.23eV, which corresponds to SiO_2 compound. This indicates the formation of silica layer on the anode surface.

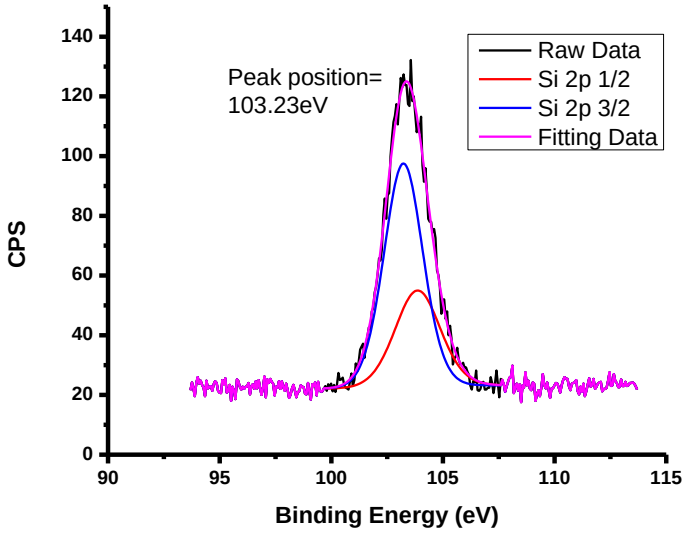

Figure 4.S1 XPS results on anode after discharge in Na-O_2/CO_2 cell with ionic liquid tethered silica nanoparticles.

3. Characterization of discharge products

X-ray Differaction (XRD)

Figure 4S2 shows the XRD patterns of cathode after discharge in different cathode gas compositions. It is clear that for O_2:CO_2=1:1 case, the spectrum shows characteristic peaks of $NaHCO_3$ (2θ=30.421, 34.467), while for the other cases, the spectra show no clear peaks, meaning the discharge product in these cases are amorphous.

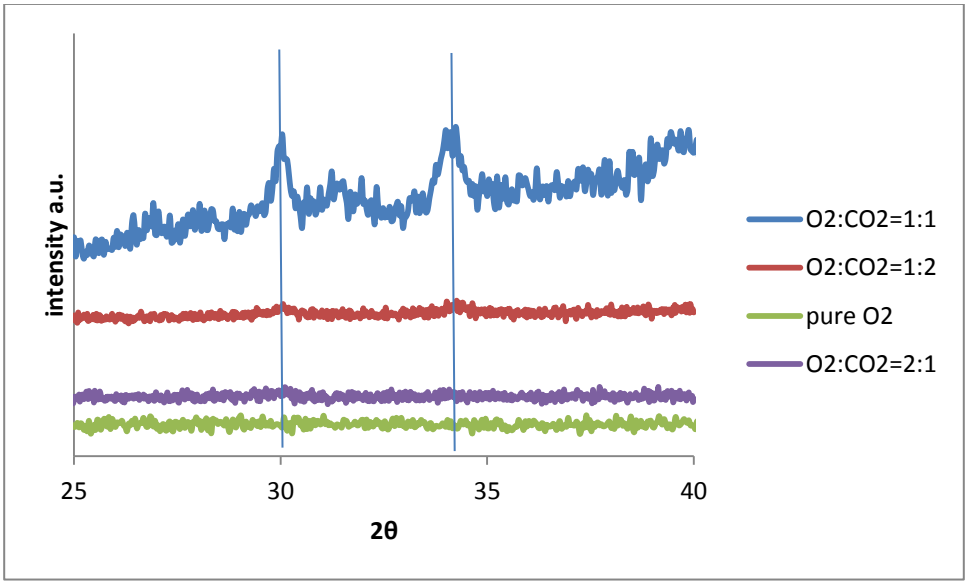

Figure 4.S2 XRD patterns of cathodes after discharge in different cathode gas compositions.

Energy Dispersive X-ray Analysis (EDX)

Figure 4S3 shows the EDX profile of cathode discharged in Na-O_2/CO_2 battery with the O_2/CO_2 ratio 1:1. There are clearly the peaks of Na, C and O which are from the discharge product, whereas the peaks of Ni and Si are from the cathode substrate and remaining electrolyte respectively. Table 4S1 shows the atomic percentage of Na, C and O. The Na:C:O ratio is close to 1:1:3, which indicates the discharge product to be $NaHCO_3$.

Table 4S1. Atomic percentage of Na, C and O on the cathode after discharge in Na-O_2/CO_2 battery with 1:1 O_2 to CO_2 ratio.

Element	at.%
Sodium	20.35039
Carbon	16.9053
Oxygen	62.74431

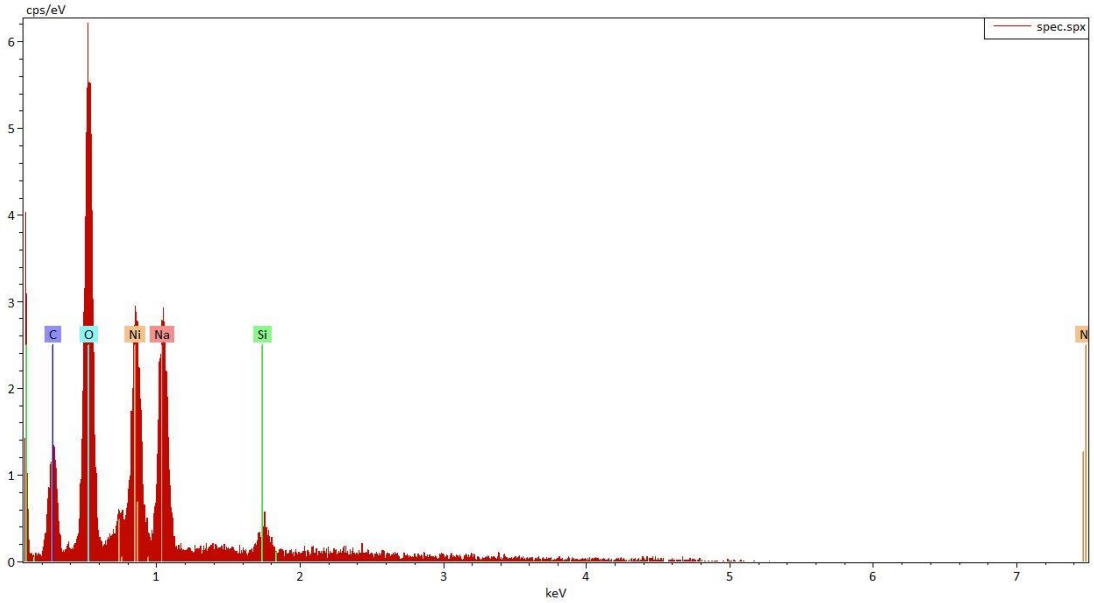

Figure 4.S3 EDX spectrum of cathode after discharge in Na-O_2/CO_2 battery with 1:1 O_2 to CO_2 ratio.

X-ray Photoelectron Spectroscopy (XPS)

Figure 4S4 shows the XPS spectrum of cathodes discharged in different atmospheres. The cathode discharged in 1:1 O_2 to CO_2 ratio shows only one $NaHCO_3$ peak (BE=1071.5EV), while the peak of the cathodes discharged in 1:2 and 2:1 O_2 to CO_2 ratio can be deconvoluted into two characteristic peaks. For O_2:CO_2=2:1 case the peaks correspond to Na_2O_2 (BE=1073EV) and $NaHCO_3$ (BE=1071.5EV) respectively, whereas for For O_2:CO_2=1:2 case the peaks correspond to $Na_2C_2O_4$ (BE=1070EV) and $NaHCO_3$ (BE=1071.5EV) respectively.

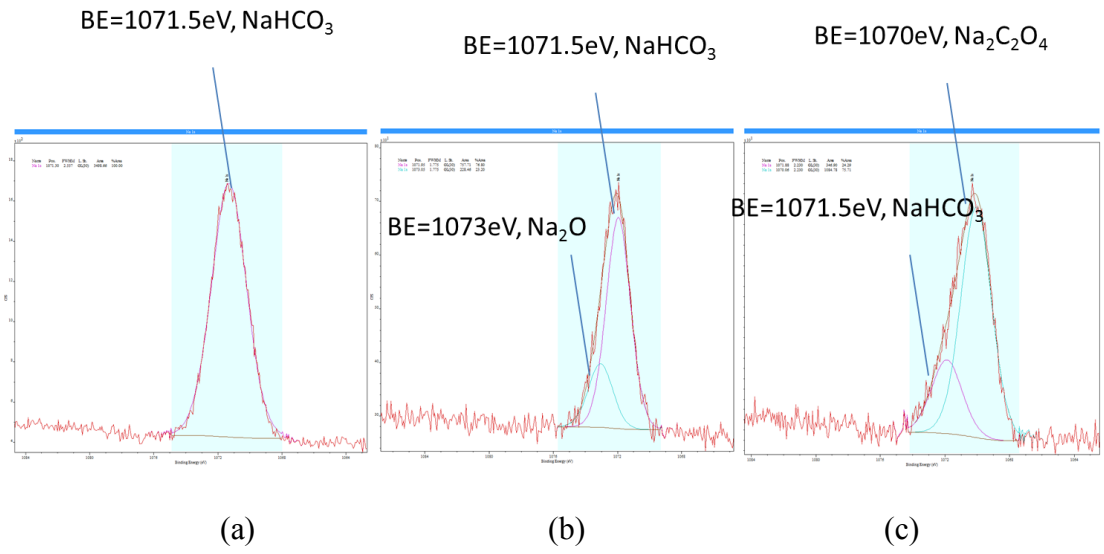

Figure 4.S4 XPS spectra of cathodes after discharge in (a) O_2:CO_2=1:1, (b) O_2:CO_2=2:1 and (c) O_2:CO_2=1:2.

4. Determination of Water Content in the Electrolyte

Because of the introduction of SiO_2 nanoparticle in the electrolyte, it is inevitable that trace amount of water would be introduced to the electrolyte. In order to determine the water content in the electrolyte, Mettler Toledo C20D Karl Fisher Coulometer was used. It is found that the water content in the electrolyte is 56ppm. Due to the relatively large amount of electrolyte used in the battery, even this small amount of water can cause the discharge product to convert from Na_2CO_3 to $NaHCO_3$ based on the reaction $\boldsymbol{Na_2CO_3 + CO_2 + H_2O \rightarrow 2NaHCO_3}$.

5. Reference

1. S. K. Das, S. Xu and L. A. Archer, *Electrochem. Commun.,* **27**, 59 (2013).
2. S. Xu, Y. Lu, H. Wang, H. D. Abruña and L. A. Archer, *J. Mater. Chem. A*, **2**, 17723 (2014).
3. S. K. Das, S. Xu, A. Emwas, Y. Lu, S. Srivastavaa and L. A. Archer, *Energy Environ. Sci.,* **5**, 8927 (2012).
4. S. Xu, S. K. Das and L. A. Archer, *RSC Advances*, **3**,6656 (2013).
5. Y. Lu , S. K. Das , S. S. Moganty and L. A. Archer, *Adv. Mater.,* **24**, 4430 (2012).
6. H. Wang, E. Rus and H. D. Abruña, *Anal. Chem.,* **82**, 4319 (2010).
7. H. Wang, E. Rus, T. Sakuraba, J. Kikuchi, Y. Kiya and H. D. Abruña, *Anal. Chem.,* **86**, 6197 (2014).

CHAPTER 5

A High Temperature Primary Lithium-CO_2 Battery Enabled by an Ionic Liquid Electrolyte

5.1 Abstract

This chapter focuses on a novel primary Li-CO_2 system that consumes pure CO_2 gas as its cathode. An imidazolium based ionic liquid electrolyte is utilized in this system. The ionic liquid has high CO_2 solubility and good stability under high temperature. The cell exhibits a high discharge capacity of around 2500mAh/g at moderate temperatures. At 100 ℃ the discharge capacity is close to 1000% higher than at 40 ℃, and the temperature dependence is significantly weaker for higher surface area carbon cathodes. Ex-situ FTIR and XRD analysis convincingly show that lithium carbonate (Li_2CO_3) is the main component of the discharge product. The feasibility of similar primary metal-CO_2 cells based on earth abundant metal anodes, such as Al and Mg, is demonstrated. The metal-CO_2 battery platform provides a novel approach for simultaneous capturing of CO_2 emissions and producing electrical energy.

5.2 Introduction

Mankind's total energy consumption is currently 14TW and is projected to roughly triple by the year of 2050 [1]. In 2009 it was estimated that close to 83% of current energy needs are met by combustion of fossil fuels (coal, natural gas, and petroleum products), all of which introduce large amounts of carbon dioxide into the

environment. Carbon dioxide is now understood to be one of the leading greenhouse gases. The emissions are on the order of thousands of metric tons per annum. Coal fired power plants provide the largest portion of CO_2 production [2-6]. The most widely employed technology for CO_2 capture uses aqueous alkanoamine (e.g. monoethanolamine (MEA) and Diethanolamine (DEA)) solutions to chemically bind the CO_2 in a mixed effluent gas stream [7-9]. The captured CO_2 is then liquefied, stored, and eventually pumped into the subsurface or into the deep ocean for long-term sequestration [10].

This approach to carbon dioxide capture is attractive for its simplicity and efficiency (each amine group can bind up to 1 mol of CO_2). It nonetheless has several perhaps obvious disadvantages. First, the capture solutions are unstable at the elevated temperatures characteristic of most flue gas streams. This means that the gas must first be cooled in an energy intensive process before treatment. Second, the alkyl-amines are unstable under the conditions needed to regenerate the capture fluid, which causes a gradual deterioration in performance over time. Additionally, sulfur-containing impurities in the effluent gas can react irreversibly with the capture fluid, also reducing its efficacy over time. Finally, sequestration of CO_2 in underground reservoirs will in most cases require large, government-scale levels of economic investment for construction and long-term monitoring, but makes no demands on the energy content of the CO_2. The cumulative effect of these drawbacks is that the cost of CO_2 capture and sequestration is prohibitive for the vast majority of utilities. These realities are fueling a global search for cost effective, benign and efficient technologies

for capturing CO_2 and for utilizing the captured CO_2 gases to improve process economics. There are many reports suggesting approaches for utilizing captured CO_2 as a reagent for chemical synthesis based on formation of C-N bonds [11]. Strategies based on feeding CO_2 to microalgae to produce organic materials and energy are also growing in popularity [12].

Recently the lithium-air battery has become the subject of intensive investigation worldwide as a promising technology for meeting growing energy demands for transportation [13-16]. Interest in the lithium air battery is fueled by its exceptionally high theoretical specific energy (11680 Wh/kg Li), which is around 90% that of commercial grade gasoline (13000 Wh/kg). The high energy density of Li-air battery comes from the fact that the cathode - oxygen harvested from the ambient air - is not a part of the battery cell. Therefore, the discharge process is not limited by the consumption of the cathode material. Recently, researchers at Toyota reported that combining CO_2 gas with oxygen in a lithium-air battery could increase the batteries capacity by a factor of three [17]. Our work in chapter 2 [18] showed that Na-CO_2/ O_2 and Mg-CO_2/O_2 cells exhibit 200%-300% increases in capacity at CO_2/O_2 molar compositions close to 0.5, but that these cells also exhibit measurable, small capacities when pure CO_2 is used as the cathode in metal-air batteries. Further development of such metal-CO_2 batteries would be attractive for their potential dual attributes as platforms for carbon capture and electrical energy generation.

The chemical reaction between lithium metal and CO_2 gas has been known for a very long time [19]. Lithium metal can react with CO_2 to form lithium oxalate at room temperature. At high temperature, lithium oxalate decomposes to form lithium carbonate and carbon monoxide gas:

$$\boldsymbol{Li + CO_2 \rightarrow Li_2C_2O_4 \xrightarrow{high\ temp.} Li_2CO_3 + CO \uparrow}$$

It has been reported that at room temperature the discharge capacity of Li-CO_2 and Na-CO_2 batteries are well below their respective theoretical values [17-18]. Our recent research on the Li-air battery shows that build-up of an insulating coating of discharge products may be responsible for this observation. Increasing the cell operation temperature was previously shown to influence the coating thickness and topology, which increases both the discharge voltage and discharge capacity [20].

In this chapter, we first show that the imidazolium based ionic liquid (IL) has desirable carbon capture capability. PEG is used to reduce the viscosity of the ionic liquid, which increases the carbon capture efficiency. Since the ionic liquid has high CO_2 solubility and is stable at high temperature, it is a good candidate for the electrolyte of the high temperature Li-CO_2 battery. Building upon these ideas, we report a high capacity primary Li-CO_2 battery able to operate stably at high temperatures (100 ℃) with an ionic liquid based electrolyte. We also show that the concept can be extended to other anodes to create primary metal-CO_2 batteries based on magnesium and aluminum.

5.3 Experimental

This chapter discusses both the CO2 capture capability of the ionic liquid as well as a high-temperature Li-CO2 system based on the ionic liquid as the electrolyte. Therefore, this section describes the experimental protocol of both studies.

5.3.1 CO_2 Capture by an Ionic Liquid

A schematic of the experimental setup used to study CO_2 capture is shown in Figure 5.1. At the beginning of the experiment, the target gas was introduced into a feed tank, a 150mL stainless steel cylinder (HOPE: DOT 3E1800). The feed tank allows the pressure of the gas to be regulated within a narrow range. The solubility experiment was performed in a stainless steel chamber, a 1-way (¼ in.) with the bottom port plugged. A sample of ionic liquid (1-butyl-3-methylimidazolium acetate, [bmim][acetate]) was placed in the container, which was immersed in a temperature-controlled water bath (Fisher Scientific ISO-temp Refrigerated Circulator, Model: 901). The container was sealed by Swagelok one-way ball valves. An ultra-high accuracy pressure transducer (Sensotec Sensors: FP-2000, 0-50 Psia) was connected to the upper port of the container. The accuracy of the pressure transducer was 0.10 % of the full span. The output from the transducer was sent to a USB-based data acquisition board and recorded with TacerDAQ^{TM} software. The container was evacuated to vacuum before each experiment using a vacuum pump (Brand Tech Scientific Inc, Diaphragm vacuum pump) with ultimate vacuum level of 7 torr (9 mbar).

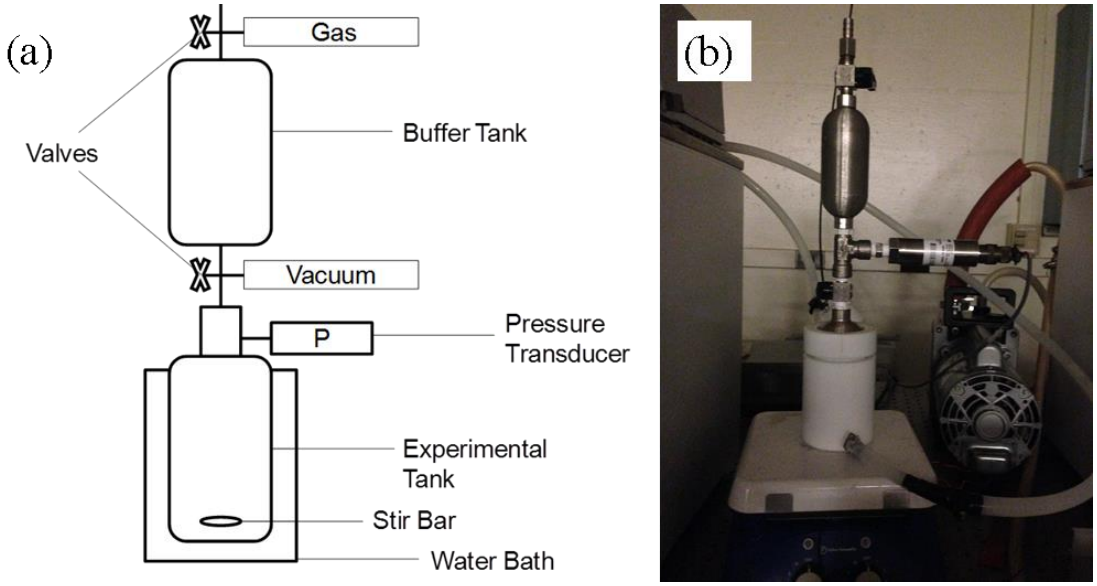

Figure 5.1 (a) Schematic of the carbon capture experimental apparatus and (b) Photo of the sesetup

The experimental procedure comprises four steps: system leak detection, sample drying, CO_2 absorption and solvent regeneration. The detailed procedure is described below. 15 ml of PEG (polyethylene glycol, MW=550g/mol, Sigma Aldrich)/IL([bmim][acetate]) blend was introduced into the chamber, which was sealed with a pressure transducer on the top and a stir bar was used to facilitate mixing and a faster equilibrium. Teflon PTFE thread seal tape was applied to each connector to prevent leaks. The vacuum pump was turned on and valve opened to evacuate the chamber. The pressure sensor monitored the pressure of the gas in the container. If the pressure of the container did not change for 10- 12hrs, then it was confirmed that there was no leak and the container was sealed completely. After the system leak test, the temperature-controlled water bath was set to 70^oC and top valve was opened. The vacuum pump was turned on and the sample was degassed under vacuum for at least 8 hours. The feed tank was then filled with the CO_2 gas under study and valve was opened to introduce CO_2 into the chamber as a function of time. The computer controlled pressure transducer recorded the pressure in chamber. The duration of the experiment was typically 8 hrs, depending upon the sample. The capture fluid was regenerated after the gas absorption experiment at multiple temperatures, by introducing nitrogen in to the chamber and evacuating the system at high temperature ($70^\circ C$) to draw the absorbed CO_2 out.

CO_2 pressure decay in the experimental chamber is recorded as a function of time at constant temperature, and the ideal gas law used to determine the moles of CO_2 absorbed by the PEG/IL blends. Since the CO_2 pressure (~2atm) and moles absorbed

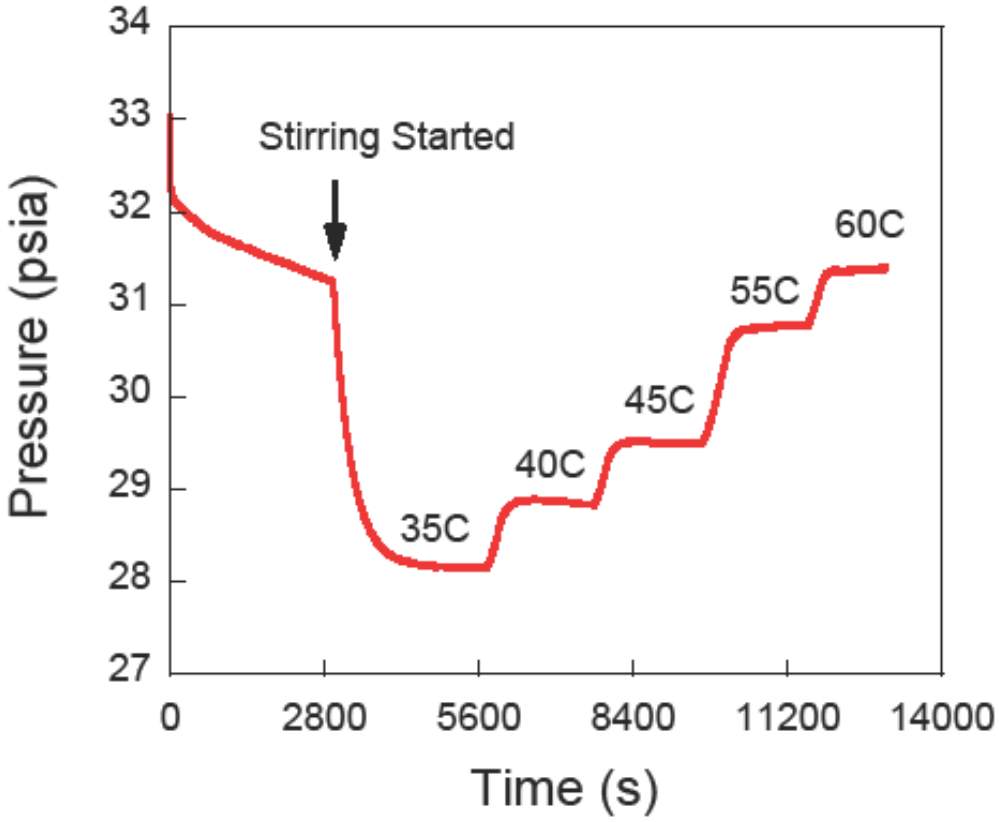

Figure 5.2 Pressure versus time plot for carbon dioxide in PEG/IL at different temperatures. The equilibrium pressure at a given temperature represents the solubility of CO_2 at that temperature.

were also low, it is reasonable to assume that the volume expansion of the blends is negligible. Equilibrium between the CO_2 and the blends were determined when the pressure decay curve reaches a steady-state as illustrated in Figure 5.2. Using ideal gas law, the concentration of CO_2 in moles of CO_2 absorbed in PEG/IL blends was determined from the pressure decay (ΔP) in the experimental chamber volume ($V_{chamber}$). Henry's law relates the fugacity of a gas dissolved in a liquid with its concentration in the diluted region, $p = Hx$, where p is the pressure of the gas, H is the Henry's constant and x is the concentration of the dissolved gas in the liquid. Hence, the Henry's law constant for CO_2 in the PEG/IL blends was calculated from mole fraction of CO_2 in the blends and the final pressure in the chamber. Experiments were conducted at different temperatures and repeated at least three times.

5.3.2 High Temperature Li-CO_2 Battery

The investigated Li-CO_2 battery configuration is similar to the Li-air and Na-CO_2/O_2 cells reported in previous chapters [18, 20]. In particular, coin-type cells mechanically perforated on the cathode side were used for electrochemical experiments. The cathode material was created by blending conductive carbons with varying porosities, pore size distributions, and surface area with a PVDF polymer binder in NMP. A fixed mass ratio of carbon to PVDF of 9:1 was used for all of the systems studied. The NMP slurry was cast on an aluminum mesh substrate (diameter 1.6 cm) and dried. In order to maintain the uniformity of the anion in the electrolyte, the electrolyte comprised of 1M LiTFSI in the ionic liquid 1-butyl-3-methylimidazolium bis(trifluoromethanesulfonyl) imide ([bmim][TFSI]) was used for the Li-CO_2 cells.

The Mg-CO_2 cells employed 1M $Mg(ClO_4)_2$ in propylene carbonate (PC) and the Al-CO_2 cells used $AlCl_3$ dissolved in 1-Ethyl-3-Methylimidazolium Chloride ([EMIm]Cl) in a 1.1:1 molar ratio [21]. The cells were assembled in an argon filled glove box. The assembled cells were then sealed into a customized stainless steel chamber filled with CO_2 gas (1atm pressure) and connected to the battery test stand.

5.4 CO_2 Capture with PEG/IL Blend

5.4.1 CO_2 Solubility in PEG/IL Blend

The Henry's law constant is most widely used in literature for representing the solubility of CO_2 in ILs at low pressures. The Henry's law constants for CO_2 in PEG/IL blends are presented in Table 5.1. It is important to note the inverse relation between Henry's law constant and solubility. It is evident that the CO_2 solubility increases with increase in concentration of IL, due to high affinity of IL towards CO_2. Figure 5.3 compares the Henry's law constants for different ILs with our blends. The Henry's law constant values for the IL/PEG blends are smaller compared to pure ILs.

Table 5.1 Experimentally measured Henry's law constants for carbon dioxide in PEG/IL blends at different temperatures.

Solvent	Henry's Law Constant (atm)			
	25 ℃	40 ℃	50 ℃	60 ℃
PEG	21.9	2.7		35.5
1 wt% IL	20.9	2.7	30.7	34.4
5 wt% IL	24.1	3.1	36.8	40.1
10 wt% IL	20.4	2.6	29.8	33.7
20 wt% IL	15.8	2.0	23.5	26.3
40 wt% IL	8.8	1.2	13.7	16.1
50 wt% IL	6.3	0.9	11.4	14.0
60 wt% IL	6.0	0.8		12.0
80 wt% IL	3.7	0.6	7.1	8.9

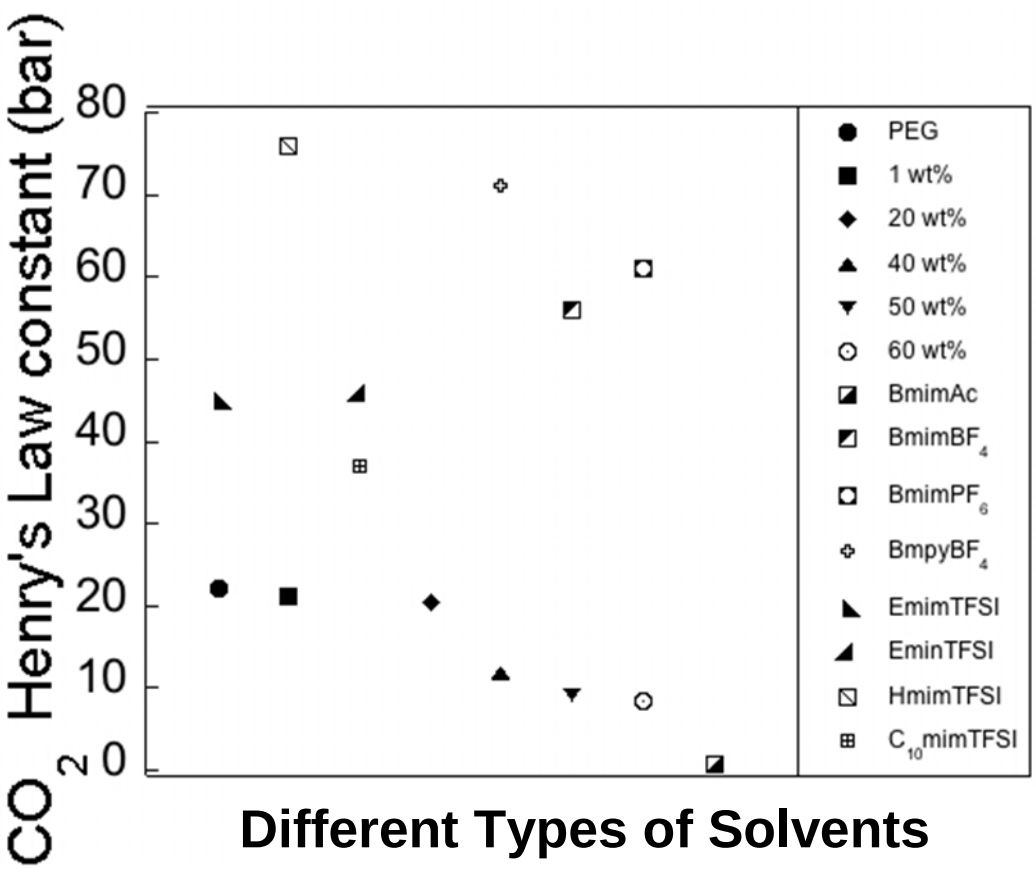

Figure 5.3 Comparison of carbon dioxide Henry's law constant for different ILs and the PEG/IL blends studied in the present study at 40 ℃.

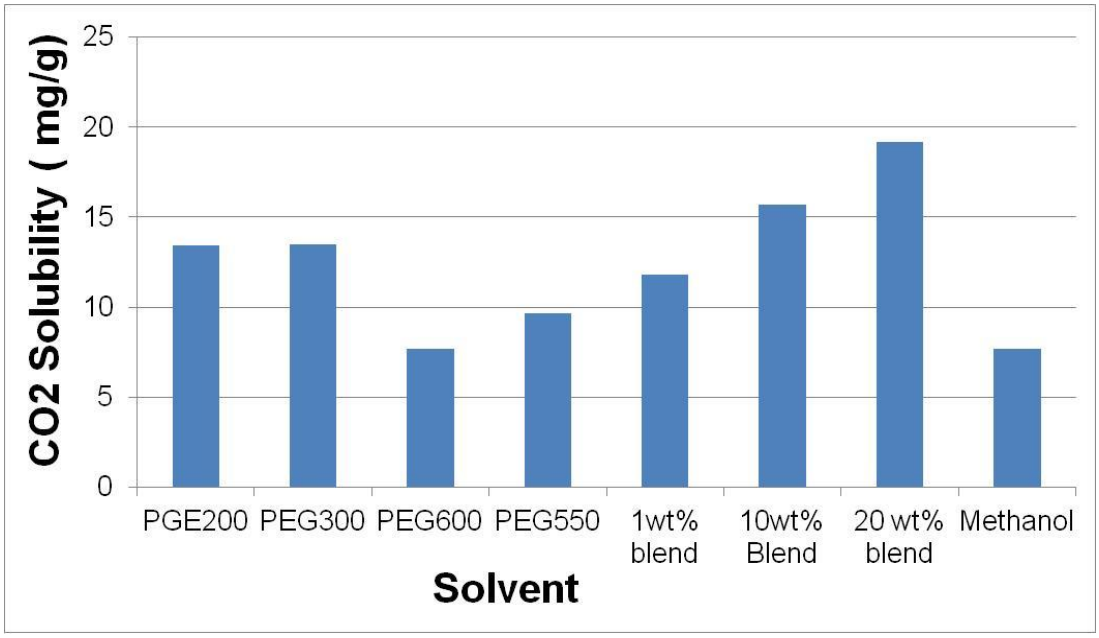

Figure 5.4 Comparison of carbon dioxide at 25 ℃ in different solvents.

There are few studies on CO_2 solubility in PEGs. Henni *etal* [25] reported CO_2 solubilities in PEGDME 250 and in other solvents at three different temperatures. Their reported Henry's law constants are in agreement with our measured values for pure PEG. In another study [26], Aschenbrenner and Strying reported CO_2 solubilities at 25 ^oC in different molecular weight PEGs using thermogravimetry. They reported that CO_2 solubility, *mg CO_2/g*, decrease with molecular weight of PEG. Figure 5.4 compares the CO_2 solubility at 25^oC in different solvents; this clearly shows the values from the present work are in good agreement with the literature reports.

Table 5.2 Carbon dioxide solubility in PEG/IL blends at different temperatures at 1 atm CO_2 pressure.

	Solubility (mmol/g)			
Blends (IL wt%)	25 ℃	40 ℃	50 ℃	60 ℃
0	0.22	0.19		0.16
1	0.27	0.22	0.21	0.18
5	0.26	0.22	0.19	0.19
10	0.36	0.30	0.28	0.26
20	0.44	0.38	0.34	0.32
40	0.68	0.61	0.56	0.52
50	0.80	0.71	0.64	0.59
60	0.82	0.75	0.70	0.65
80	1.01	0.93	0.87	0.82

It is convenient to express the carbon dioxide solubilities in terms of molality (moles of CO_2 absorbed per kilogram of the solvent), to access the efficiency of our materials for CO_2 capture instead of using the conventional mole fraction basis. The amount of CO_2 absorbed by the IL/PEG blends was determined from the difference between the

initial pressure and equilibrium pressure at four different temperatures as a function of IL concentration. The values of CO_2 solubility in IL/PEG blends are summarized in the Table 5.2. It is clearly evident from the results that the CO_2 solubility increased with concentration IL in the blends and the solubility decreased with temperature for the entire spectrum of the blends investigated in the present work. The increase in CO_2 solubility or the absorption capacity with IL concentration in the blends is the consequence of the increased amount of IL concentration. Ionic Liquid, [bmim][acetate], chemically reacts with the CO_2 and hence has high CO_2 solubility than the other blend component, PEG, which is a physical solvent.

However, the CO_2 capture capacity of the IL/PEG blends is relatively poor compared with the aqueous amine solutions. It can be seen from Table 5.2, that one gram of IL-PEG blends can absorb up to around 1 mmol CO_2, which is pretty low compared with the CO_2 capture ability of aqueous amine solutions, which is around 3 to 4 mmol CO_2/g.

One of the major draw backs of the aqueous amine solutions is the evaporation of water during the regeneration and thereby reducing the capture capacity. Due to very low vapor pressure of IL and PEG, the evaporation problem can easily be mitigated. To evaluate the effectiveness of the blends, the absorption efficiency was tested by regenerating and reusing the same material. Figure 5.5 shows the CO_2 solubility in 20 wt% IL/PEG blends at 25^{o}C for 30 regeneration cycles. The solubility was found to be invariant with number of cycles. This indicates that the blends are completely

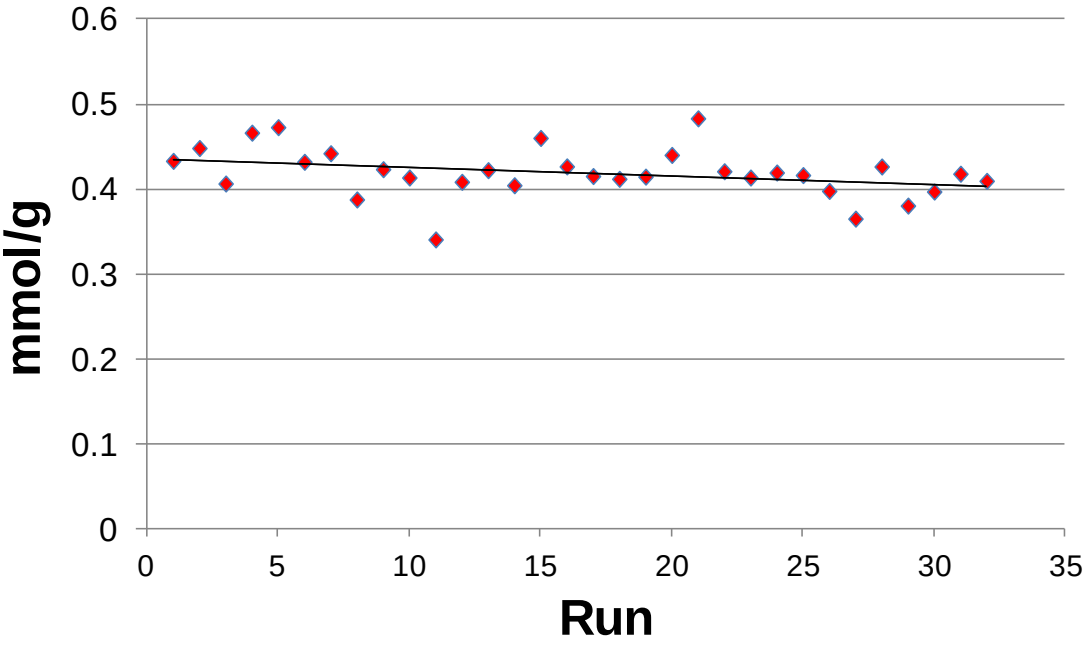

Figure 5.5 Recycle efficiency of PEG/IL blends. The experimental data was collected for 20 wt% IL blends at 25 ℃ for 30 regeneration cycles.

regenerated and there is no degradation or loss of material during the regeneration process.

5.4.2 Effect of Temperature

CO_2 solubility was found to decrease with increasing temperatures for all the blends studied in the present work. This observation is in agreement with literature reports for CO_2 solubility in ILs. The temperature derivative of the CO_2 solubility, CO_2 mole fraction, is related to either the partial molar enthalpy or the partial molar entropy of the CO_2 in the blends.

$$\Delta h_{CO_2} = -R\left(\frac{\partial \ln x_{CO_2}}{\partial 1/T}\right)$$

$$\Delta s_{CO_2} = R\left(\frac{\partial \ln x_{CO_2}}{\partial \ln T}\right)$$

The values for Δh_{CO_2} indicate the energetic interactions of CO_2 in blends, and Δs_{CO_2} represents the ordering of CO_2 molecules in the blends, were calculated from the corresponding plots of the CO_2 solubility versus temperature. These values were shown in Figure 5.6 as a function of IL concentration in PEG. Both Δh_{CO_2} and Δs_{CO_2} were found to decrease with increase in IL concentration, indicating the higher energetic interactions and ordering of CO_2 with IL. The negative values for Δh_{CO_2} and Δs_{CO_2} are thermodynamically consistent with the observed inverse relation between solubility and temperature. The enthalpy of CO_2 absorption for amine solutions is on order of -80 to -100 kJ/mol, which is much higher than the values for blends studied in the present work. In other words, less energy is required to remove CO_2 from IL+PEG

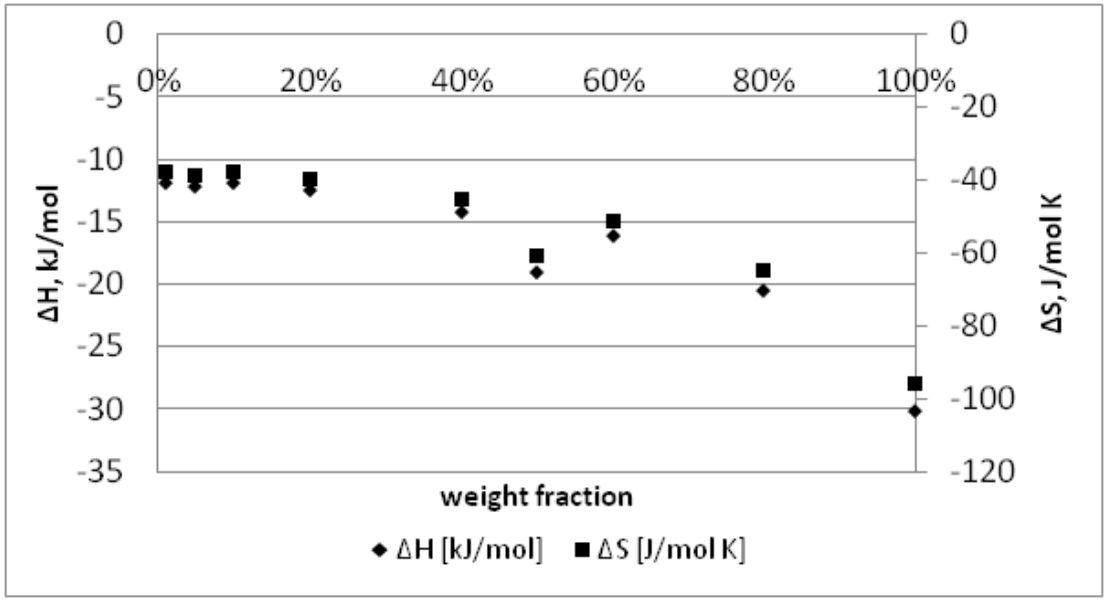

Figure 5.6 Partial molar enthalpy and partial molar entropy of absorption for CO_2 in PEG/IL blends.

blends compared to amine solutions. Hence, these materials open a wide range of possibilities for tuning the enthalpy of absorption and thereby making the process less energy intensive.

The IL-PEG blend has decent solubility of CO_2 and very good cycle ability under high temperature. With the increase of ionic liquid concentration, the solubility increases. The high CO_2 solubility and the good stability under high temperature make the imidazolium based ionic liquid the ideal electrolyte material for the high temperature Li-CO_2 battery system.

5.5 High Temperature Li-CO_2 Battery

In order to avoid the side interactions introduced by having different anions in the electrolyte, the ionic liquid used in the high temperature Li-CO_2 battery is 1-butyl-3-methylimidazolium trifluoromethanesulfonimide ([bmim][TFSI]), which has the same anion as the salt LiTFSI, instead of [bmim][actate], which is used in the CO_2 capture study. However, the anion of the ionic liquid does not have much effect on the CO_2 solubility.[27] Therefore, it is anticipated that the [bmim][TFSI]electrolyte still maintains the high CO_2 solubility and good stability under high temperature.

5.5.1 Electrochemical Analyses

Figure 5.7 shows the galvanostatic discharge curves of Li-CO_2 batteries at temperatures in the range of 60 ℃ to 100 ℃ at a fixed current density of 0.05mA/cm^2 and final potential of 2V. It is apparent from the figure that the discharge potential

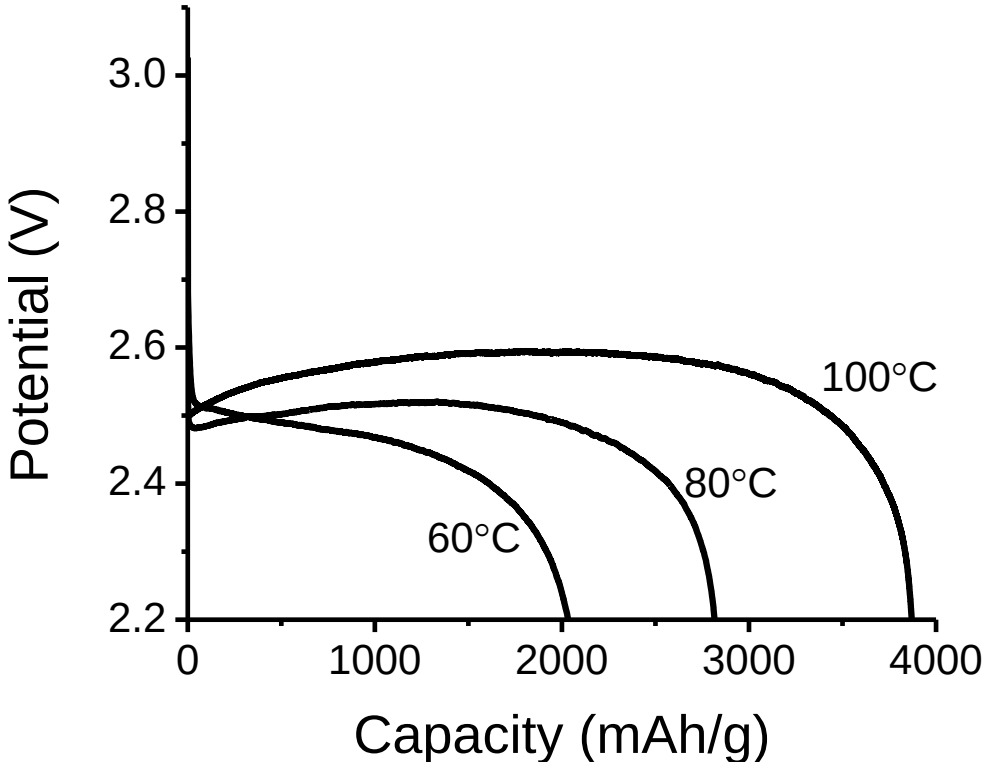

Figure 5.7 Galvanostatic discharge curves of Li-CO_2 cells operated at various temperatures in the range 60 ℃-100 ℃ at a current density of 0.05mA/cm^2 to the potential of 2.2V

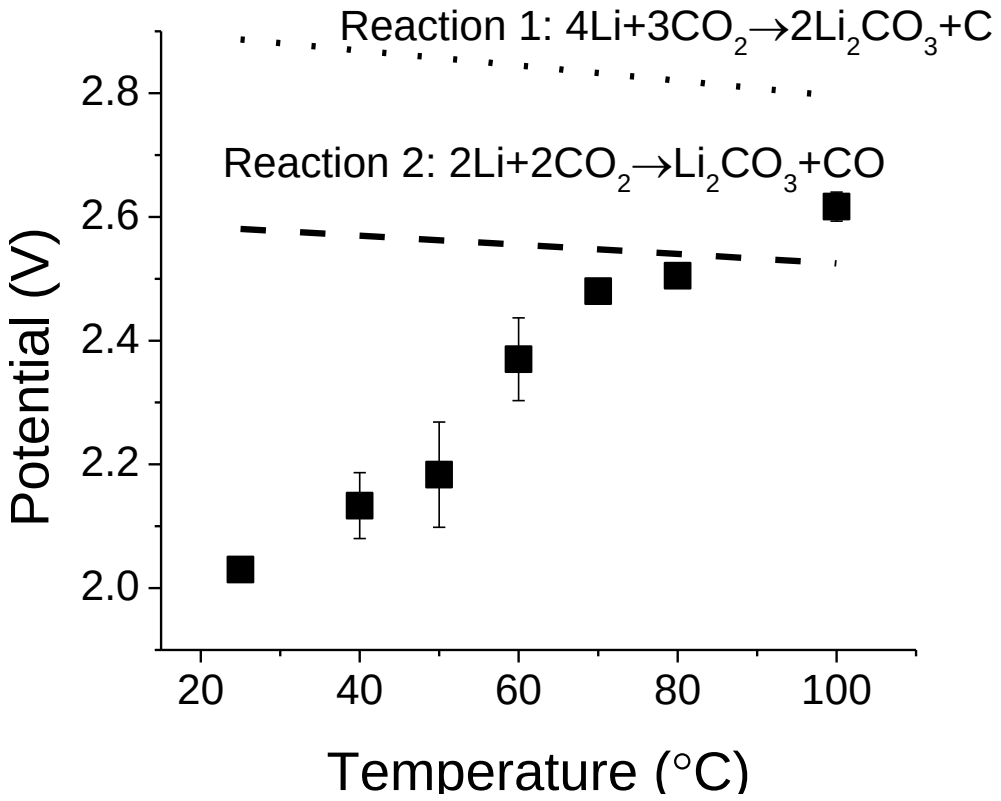

Figure 5.8 The comparison of theoretical equilibrium potential with actual discharge potential. The theoretical equilibrium potential 1 was calculated based on the reaction: $2Li + 2CO_2 \rightarrow Li_2CO_3 + CO$. The theoretical equilibrium potential 2 was calculated based on the reaction: $4Li + 3CO_2 \rightarrow 2Li_2CO_3 + C$

increases with temperature. Figure 5.8 shows that the increase is not monotonic, but rather there is a "thermal trigger" region in the 40°C to 60°C temperature range where the largest changes in the cell discharge potential are observed. It is possible to estimate the Li-CO_2 cell potential theoretically from knowledge of the electrochemical reactions underway using the formula $\mathbf{E = -\Delta G/zF}$ [22]. If we assume, for example, that the simplest known reaction between Li and CO_2 dominates the discharge process,$\mathbf{2Li + 2CO_2 \rightarrow Li_2CO_3 + CO}$, the cell potential is estimated based on thermodynamic data [23] and shown in Figure 5.8 dashed line. It is evident that the measured cell potential initially approaches the calculated equilibrium potential, but then surpasses it. Based on Tafel theory, the actual discharge potential cannot exceed the theoretical equilibrium potential, implying that the proposed reaction is likely only partially correct. Additional insight into the electrochemical reaction can be obtained from analysis of the gas phase composition in a Li-CO_2 cell using Differential Electrochemical Mass Spectrometry (DEMS) (see supporting information). These measurements indicate that CO is not a significant reaction product, which provides further evidence against the proposed cell reaction. It is known that CO disproportionates in an exothermic reaction to produce CO_2 and carbon $\mathbf{2CO \rightarrow CO_2 + C}$, but under normal conditions, the reaction rate is slow. This process is relevant in the present case because it provides a natural mechanism to explain the absence of CO in the gas phase product. Its consideration leads to the overall reaction, $\mathbf{4Li + 3CO_2 \rightarrow 2Li_2CO_3 + C}$, where lithium carbonate is again a principal discharge product. The cell potential estimate based on this reaction is provided in Figure 5.8 as the dotted line. It

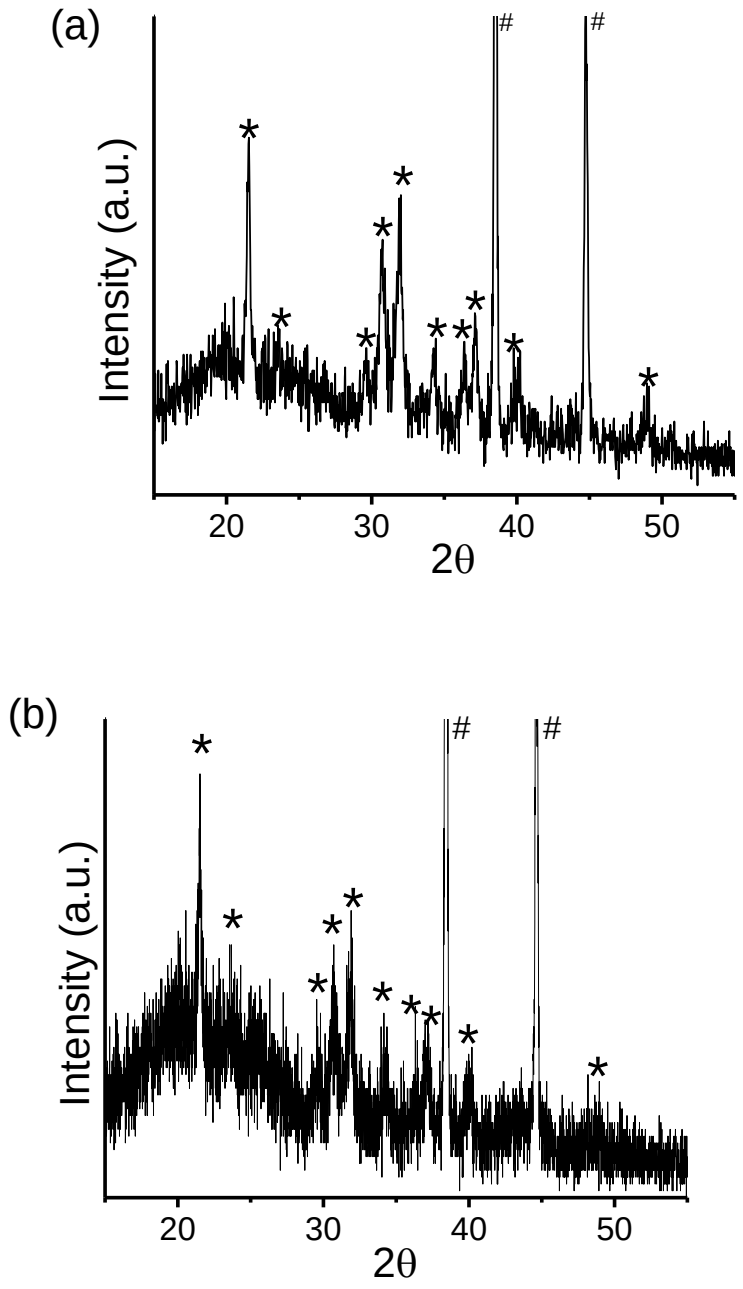

Figure 5.9 Ex-situ XRD results of the cathodes after discharge at (a) 70 ℃ (b) 100 ℃. Peaks with symbol (*) are the characteristic peaks of Li_2CO_3 and peaks with symbol (#) are from the aluminum substrate.

is apparent that the measured cell discharged potentials at elevated temperature is consistently lower than the equilibrium potentials estimated for the two proposed mechanisms, implying that this reaction could be relevant for understanding the electrochemistry of the Li-CO_2 cell. Li_2CO_3 is also evidently the principal solid discharge product for both reaction mechanisms hypothesized for the Li-CO_2 battery. This expectation is directly confirmed by ex-situ x-ray powder diffraction (XRD) (Figure 5.9) and FTIR analysis (Supporting Information, Figure 5S1) conducted on the cathode following discharge. These measurements clearly show that Li_2CO_3 is an important, perhaps even the most important component of the Li-CO_2 battery discharge product.

5.5.2 Effect of Temperature

Figure 5.10 are SEM images of the carbon cathode in the Li-CO_2 cell following discharge at varying temperatures. It is clearly apparent from the figure that as the operating temperature is increased, a progressively thicker film of the Li_2CO_3 product accumulates on the carbon cathode, eventually covering it with a contiguous-polymer like coating.

Commensurate with the increases in the cell discharge potential, Figure 5.7 also clearly shows that the discharge capacity of the Li-CO_2 cells rise with temperature. This result is illustrated more clearly in Figure 5.11, where the discharge capacity is reported as a function of temperature for Li-CO_2 cells utilizing porous carbon anodes

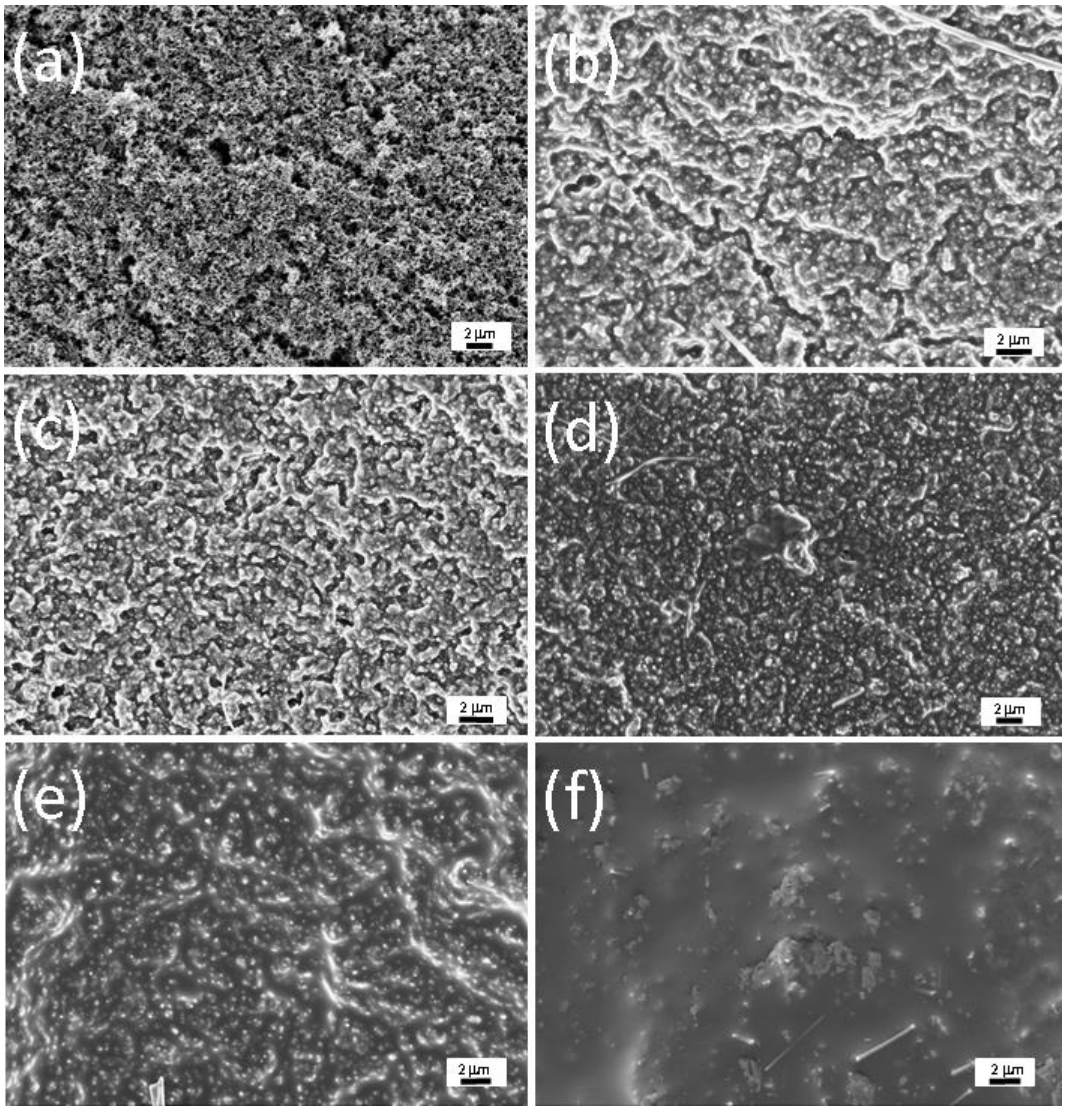

Figure 5.10 Scanning electron micrographs of super P electrodes after discharging at different temperatures (a) pristine electrode (b) room temperature (c) 40 ℃ (d) 60 ℃ (e) 80 ℃ (f) 100 ℃

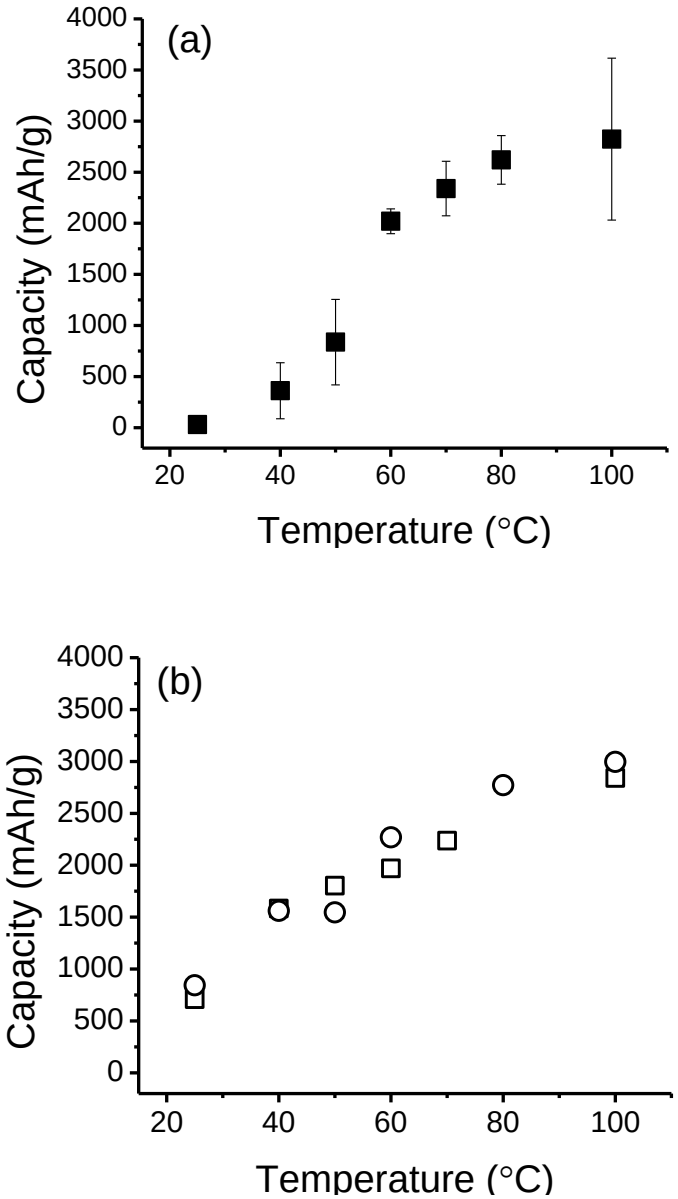

Figure 5.11 Variation of Li-CO_2 cell discharge capacity with temperature (a) super P carbon black (SA≈60 m^2/g, PV=0.3 cm3/g) as cathode (b) high surface area carbon as cathode (square symbol: SA=1020m^2/g, PV=4.45cm3/g, circle symbol: SA=1300m^2/g, PV=2.2cm3/g)

with differing surface areas and pore volumes. The figure shows that irrespective of the cathode surface area and pore volume, moderate increases in the cell temperature consistently produce higher discharge capacities. However, the rate of increase is considerably lower for cells based on high surface area cathodes.

It is also noteworthy from the results in Figure 5.11 that, as is the case for the cell potential, the lowest surface area super P-based carbon cathode shows a thermal triggering effect in its performance. In particular, at temperatures between 40 ℃ and 60 ℃, the discharge capacity of Li-CO_2 cells based on these cathodes rise rapidly. This finding is remarkably similar to our previous report of a thermal triggering event in Li-O_2 cells [20]. In that case, the effect was attributed to the beneficial effects of temperature in limiting electrode passivation produced by the electrically insulating Li_2O_2 discharge product. Like Li_2O_2, Li_2CO_3 is an electrical insulator and deposition of a layer of the material on the carbon cathode may have a similar negative effect on electron transport at the cathode/electrolyte interface, prematurely ending the discharge reaction. Again as was the case for the Li-O_2 cell, the operating temperature can have at least two beneficial effects. First it might increase the solubility of Li_2CO_3 in the electrolyte, which limits the thickness of its deposits on the cathode. Second, a higher temperature could also reduce transport barriers at the cathode/electrolyte interface. The fact that the discharge capacity of the Li-CO_2 cell at 40 ℃ increases by a factor of around seven for a fifteen to twenty-fold increase in the cathode surface area and pore volume are consistent, at least qualitatively, with expectations based on this explanation.

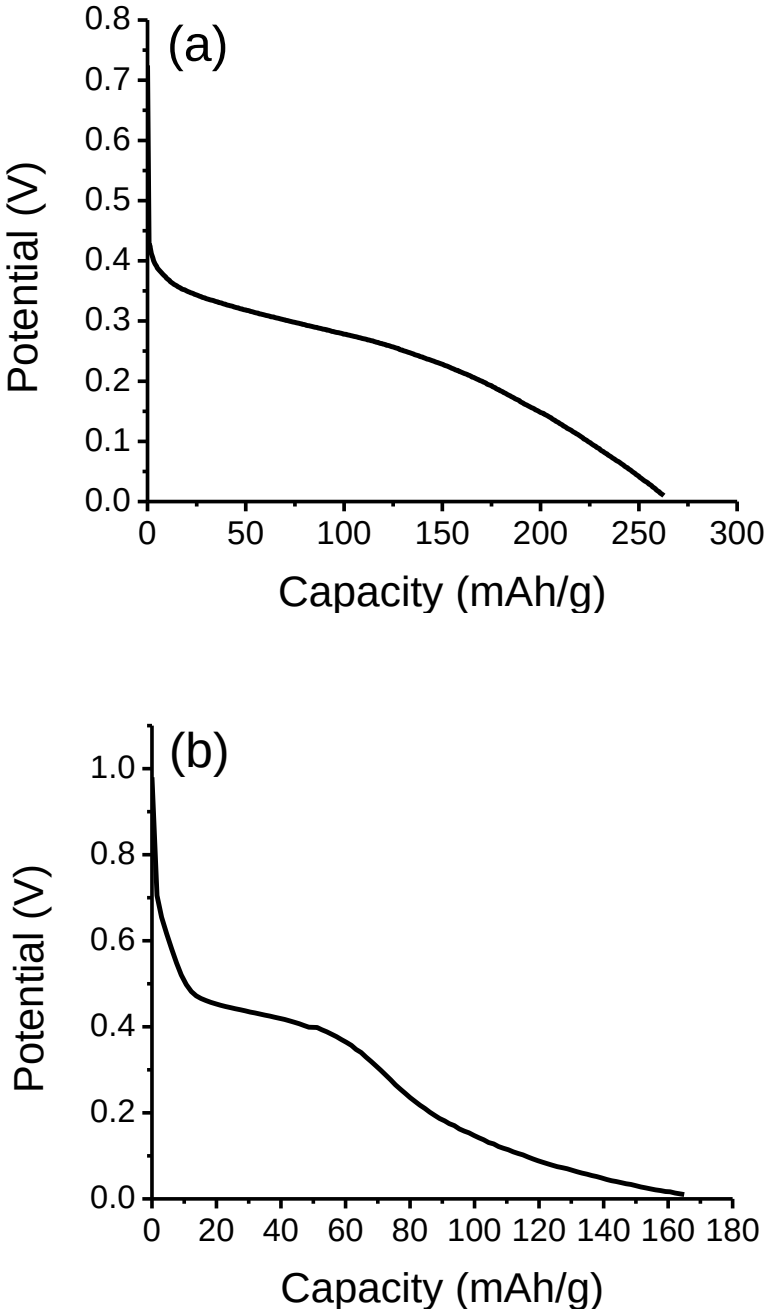

Figure 5.12 Galvanostatic discharge curves of (a) Mg-CO_2 battery and (b) Al-CO_2 battery operated at room temperature at a constant current density of 0.05mA/cm^2

5.6 Metal-CO_2 Batteries based on Other Metals

In closing, we point out that the behaviors reported here are not unique to metal-CO_2 cells based on metallic lithium anodes. Similar observations have been made for cells based on Magnesium (Mg), Aluminum (Al), and Sodium (Na) [18] anodes (Figure 5.12). All of these materials are advantageous for their greater earth-abundance and lower cost than Li. As in the case of Li-CO_2, however, these cells manifest low discharge capacities at room temperature, but these values can be made substantially larger using a combination of moderately higher cell operating temperatures and cathode materials with higher surface areas and pore volumes. The cell discharge potentials are also commensurately (for electrochemical reactions that produce the appropriate metal carbonates).

5.7 Conclusions

In summary, we investigated a primary Li-CO_2 battery as a platform for capturing CO_2 and producing electrical energy. The discharge capacity of Li-CO_2 battery shows an enhancement of about 200 times at 100 ℃ compared with operated at low temperature. Based on preliminary ex-situ analyses, Li_2CO_3 can be concluded as an important component of the discharge products. Besides lithium, other more abundant metals like Mg and Al also show the potential to work as the anode material of the metal-CO_2 battery.

REFERENCES

1. P. B. Weisz, *Phys. Today*, **2004**, 57, 47; B. Richter, D. Goldston, G. Crabtree, L. Glicksman, D. Goldstein, D. Greene, D. Kammen, M. Levine, M. Lubell, M. Savitz and D. Sperling, "Energy Future: Think Efficiency" *American Physical Society Report*: College Park, MD, **2008**
2. D. P. Scharg, *Science*, **2007**, 315, 812
3. S. M. Benn, and F. M. Orr, Jr., *MRS Bull*, **2008**, 33, 30.
4. C. Gough, *Int. J. Greenhouse Gas Control*, **2008**, 2, 155.
5. P. Luby and M. R. Susta, *Power*, **2007**, 151, 40.
6. H. Balat and C. Ox, *Energy Explor. Exploit.*, **2007**, 25, 357.
7. M. L. Gray, Y. Soong, K. J. Champagane, H. W. Peennline, J. Baltrus, R.W. Stevens, R. Khatri and S. S. C. Chuang, *Int. J. Environ. Tech. & Management*, **2004**, 4, 82.
8. G. T. Rochelle, *Science*, **2009**, 325, 5948.
9. H. Yang, Z. Xu, M. Fan, R.B. Gupta, R.B. Slimane, A. E. Bland and I. Wright, *J. Environ. Sci.*, **2008**, 20, 14.
10. H. Herzog, B. Eliasson and O. Kaarstad, *Sci. Am.*, **2000**, 282, 72-29
11. Z. Yang, L. He, J. Gao, A. Liu and B. Yu, *Energy Environ. Sci.*, **2012**, 5, 6602.
12. M. Arhaman, L. Cheng, X. Xu, L. Zhang and H. Chen, *Renew. Sust. Energy. Rev.*, **2011**, 15, 4002.
13. K. M. Abraham and Z. Jiang, *J. Electrochem. Soc.*, **1996** 143,1.

14. T. Ogasawara, A. Débart, M. Holzapfel, P. Novák and P. G. Bruce, *J. Am. Chem. Soc.*, **2006**, 128, 1390.

15. P. G. Bruce, S. A. Freunberger, L. J. Hardwick and J. M. Tarascon, *Nat. Mater.*, **2012**, 11, 19.

16. G. Girishkumar, B. McCloskey, A. C. Luntz, S. Swanson and W. Wilcke, *J. Phys. Chem. Lett.*, **2010**, 1, 2193.

17. K. Takechi, T. Shiga and T. Asaoka, *Chem. Comm.*, **2011**, 47, 3463.

18. S. K. Das, S. Xu and L. A. Archer, *Electrochem. Commun.*, **2012**, In Press.

19. Z. H. Kafafi, R. H. Hauge, W. E. Billups and J. L. Margrave, *J. Am. Chem. Soc.*, **1983**, 105, 3886.

20. S. K. Das, S. Xu, A. Emwas, Y. Lu, S. Srivastava and L. A. Archer, *Energy Environ. Sci.*, **2012**, 5, 8927.

21. N. Jayaprakash, S. K. Das and L. A. Archer, *Chem. Comm.*, **2011**, 47, 12610.

22. K. J. Vetter, "Electrochemical Kinetics", Academic Press, New York, **1967**.

23. M. W. Chase Jr., "NIST-JANAF Thermochemical Tables, Fourth Edition", *J. Phys. Chem. Ref. Data*, **1998**.

24. P. Albertus, G. Girishkumar, B. McCloskey, R. S. Sánchez-Carrera, B. Kozinsky, J. Christensen and A. C. Luntz, *J. Electrochem. Soc.*, **2011**, 158, A343.

25. Henni, A.; Tontiwachwuthikul, P.; Chakma, A. Can. *J. Chem. Eng.* **2005**, 83, 358.

26. Aschenbrenner, O.; Styring. P. *Energy. Environ. Sci.*, **2010**, 3,1106.

27. Hou, Y. and Baltus, R. E., *Ind. Eng. Chem. Res.*, **2007**, 46, 8166

APPENDIX

Supporting Figures for Chapter 5

1. Ex-situ FTIR spectrum on the Cathode

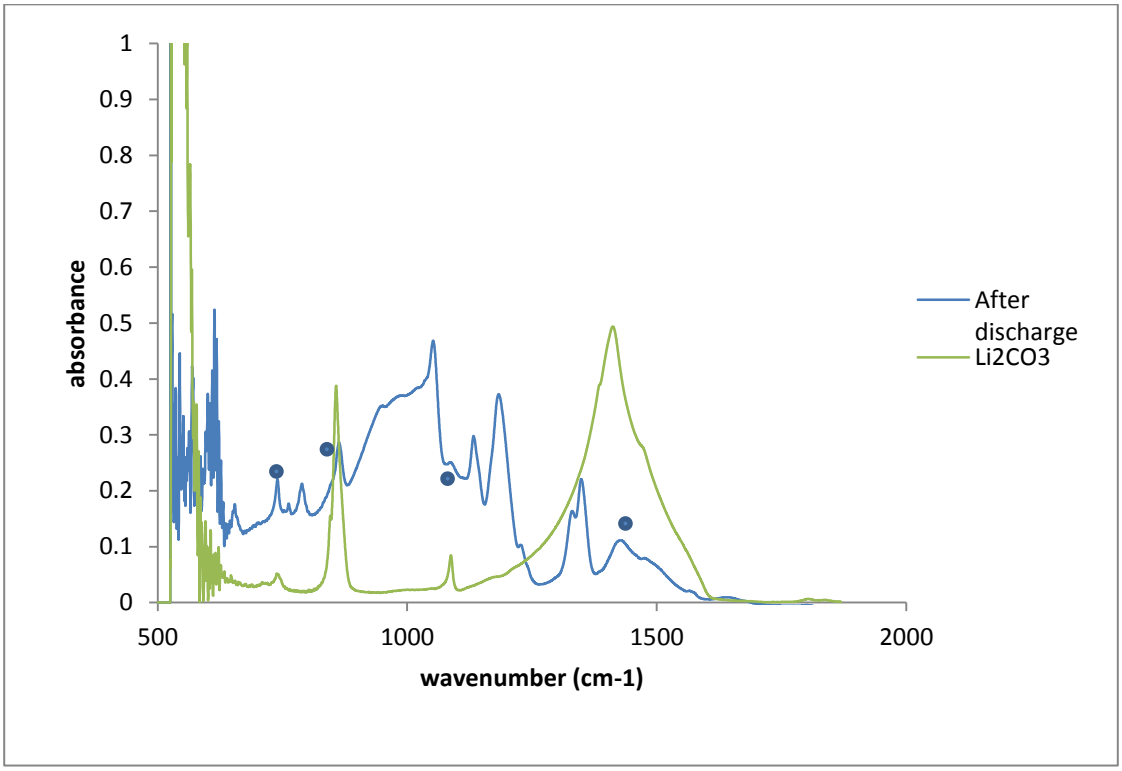

Figure 5S1 Ex-situ FTIR spectrum of the electrode after discharge at 100 ℃. The peaks emphasized with a blue dot are from the discharge product, Li_2CO_3. The other peaks are from the electrolyte.

2. *Differential Electrochemical Mass Spectrometry*

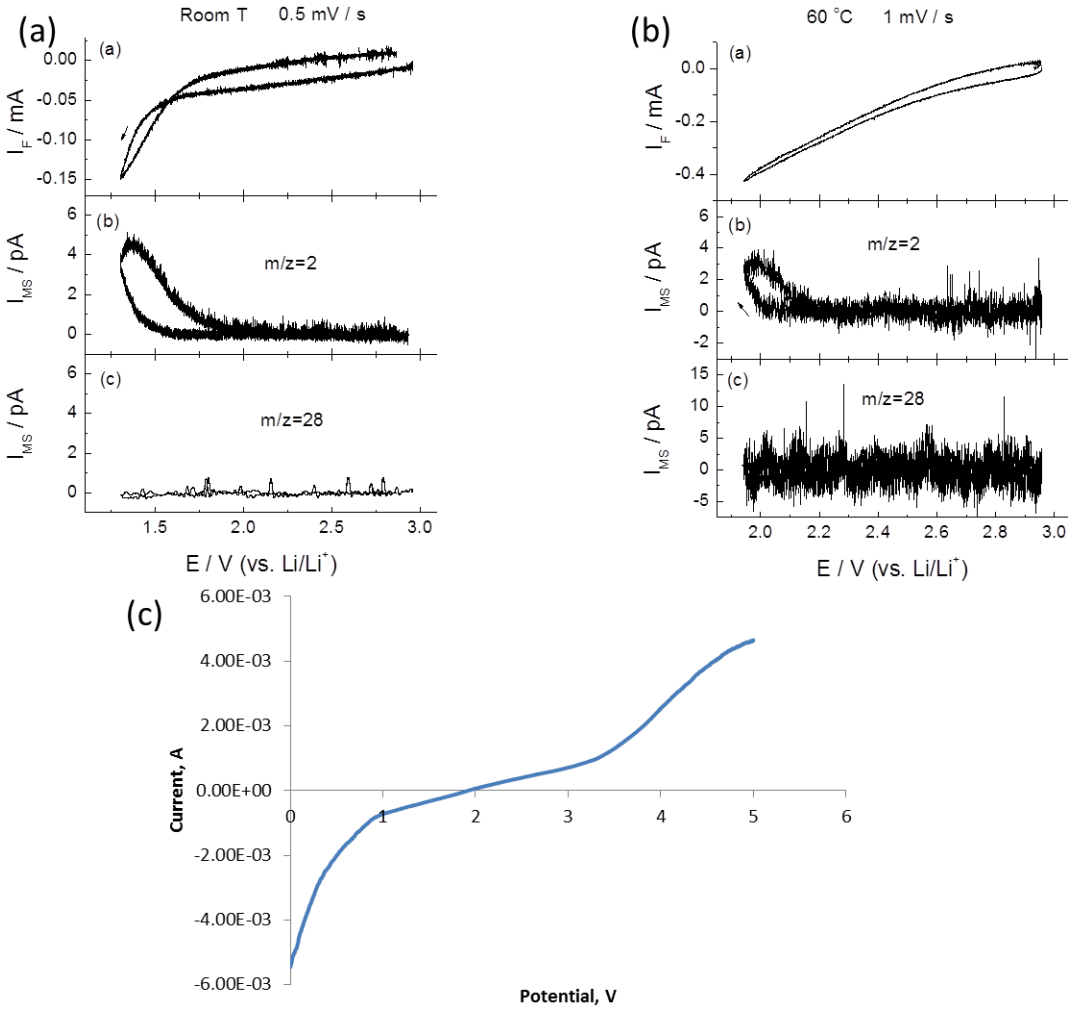

Figure 5S2 DEMS results at (a) room temperature (b) 60 ℃ and (c) cyclic voltammetry of Li-CO_2 battery. It can be easily seen that there is no CO(MW=28) evolution. However, the evolution of H_2 was detected at low potential. This is caused by the decomposition of the electrolyte, as shown in the cyclic voltammetry (Figure 5S2(c)).

3. *Adsorption Kinetics Analysis of the CO_2 Capture with IL/PEG Blend*

For high concentration blends, it would also take longer time to reach equilibrium state than low concentration blends, as shown in Figure 5S3.

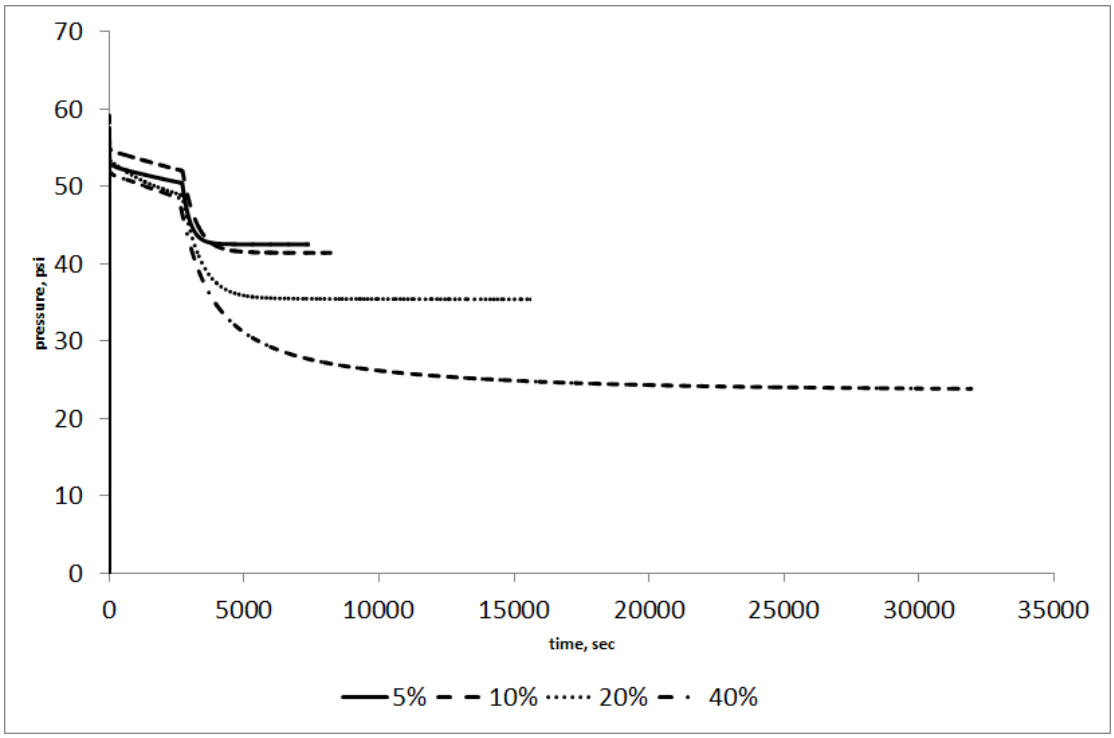

Figure 5S3 Pressure versus time plot for PEG/IL blends

In order to discuss the kinetics of the absorption process, the parameter ξ (non-dimensional pressure) and τ (blending time) are defined by the following equations:

$$\xi = \frac{P - P_{eq}}{P_{eq}} \qquad \tau = t - t_{start}$$

The pressure versus time plot using the new parameters are shown in Figure 5S4.

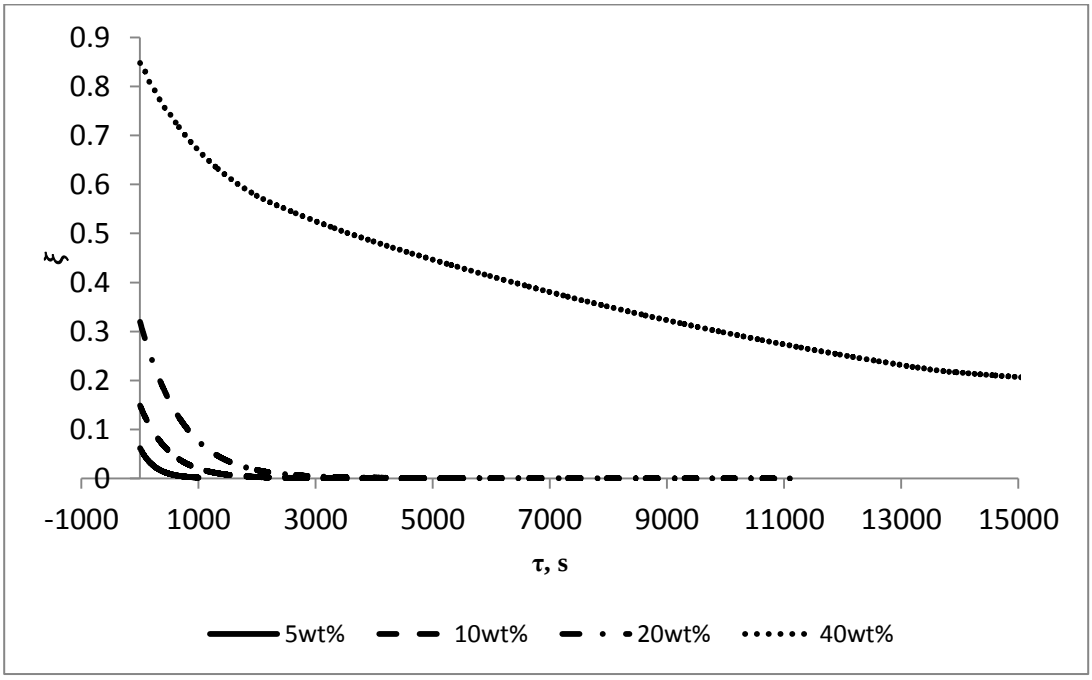

Figure 5S4 Normalized pressure versus time plots for PEG/IL blends.

It is clear that the normalized pressure changes exponentially with the blending time:

$$\xi = Aexp(-\tau/\lambda)$$

In this equation, the parameter A is determined by the CO_2 capture capability of the blends, while λ, the characteristic time, is determined by how fast the blend absorbs CO_2. The values of A's and λ's of some blends are shown in Table 5S1.

Table 5S1: Parameter A and Characteristic Time of Several Blends

wt%	5	10	20	40
A	0.0580	0.1284	0.3179	0.8230
λ, s	287.63	554.53	685.08	5215.71

It can be seen from Table 5S1 that the characteristic time increases with the concentration of ionic liquid in the blends. This means blends with high ionic liquid concentration absorb CO_2 more slowly than blends with low ionic liquid concentration.

4. Rheology of the IL/PEG Blend

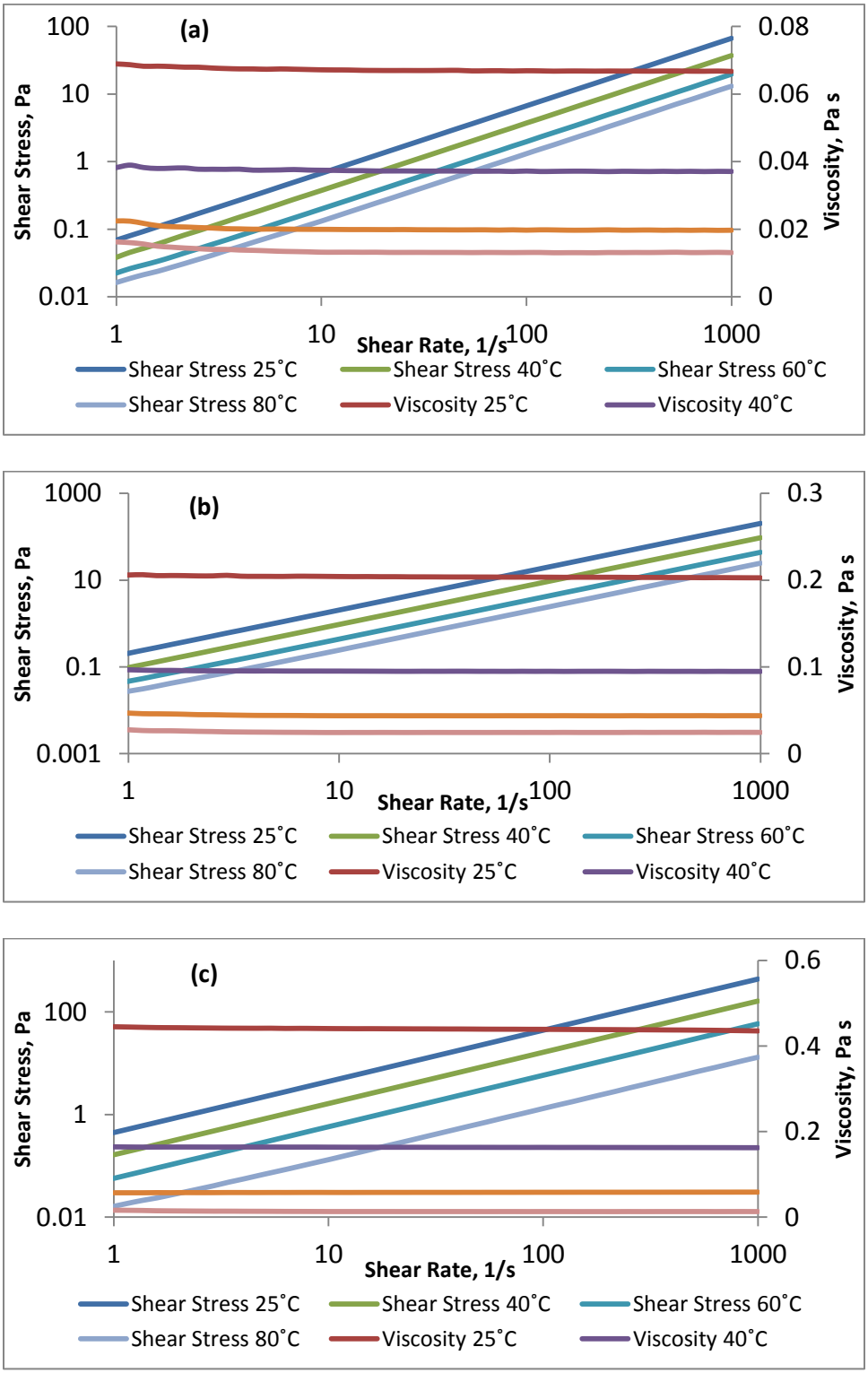

Figure 5S5 Rheology Properties of (a) Pure PEG, (b) 40wt% IL-PEG Blend and (c) Pure IL.

Figure 5S5 shows the results of rheology experiments for pure PEG, 40wt% IL-PEG blends, and pure IL. It is obvious in Figure 5S5(a)(b)(c) that the shear stress has a linear relation with shear rate and that the viscosity does not change with shear rate, which means PEG, [bmim][acetate], and the blends of them are all Newtonian liquid.

In Figure 5S6, the relation of viscosity and inverse temperature is shown in a log-linear coordinate. The linear relation shows that the viscosity of this IL-PEG system has an Arrhenius type behavior:

$$\eta = Aexp(E_a/RT)$$

The value of pre-exponential factor A and the viscosity activation energy E_a of different blends are shown in Table 5S2.

Table 5S2: Arrhenius Parameters of Different Blends

Weight fraction, %	Pre-exponential factor A, 10^{-7} Pa·s	Viscosity activation energy, E_a kJ/mol
0	38.72	23.89
5	39.77	23.86
10	41.86	24.74
20	17.72	27.81
40	7.94	30.49
60	2.52	34.36
80	1.80	35.41
100	0.43	39.51

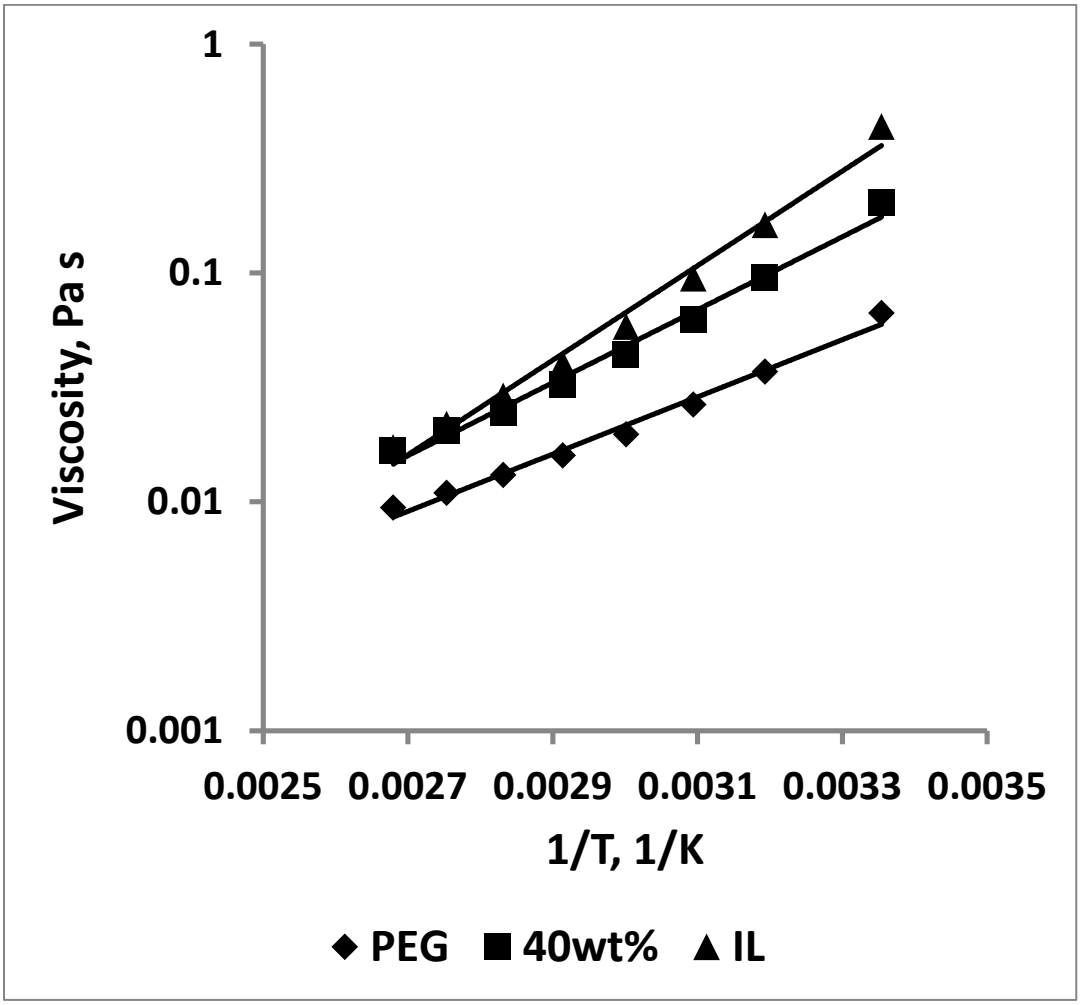

Figure 5S6 Arrhenius-type Behavior of Viscosityo of the PEG/IL Blends.

CHAPTER 6

Conclusion and Future Work

In conclusion, a high capacity, highly rechargeable Na-O_2/CO_2 electrochemical cell has been developed. The high capacity and rechargeability of the cell has been examined using electrochemical tests. The reaction mechanism of the cell has been analyzed by post-mortem characterization of the product, as well as the study of the effect of CO_2 concentration in the cathode gas. Further tunings to the electrolyte (ionic liquid tethered silica nanoparticle as additive) and the cathode (introduction of nickel cathode) have been utilized to improve the capacity and the rechageability of the cell. At this point we have an overall and detailed picture about the Na-O_2/CO_2 electrochemical cell.

Several as pects may be further explored as part of future work. One of these is the study on the methods of decreasing the charge overpotential. As was mentioned in chapters 3 and 4, the charge potential of Na-O_2/CO_2 electrochemical cell can be high than 4.5V, which leads to a low efficiency of the cell and is a crucial problem for real application. Some reports about Li-O_2 battery give light to potential solutions to this problem. It is suggested that catalysts or redox mediators can help lower the charge potential and help improve the efficiency of such systems.

i) Catalysts

Catalysts have been extensively investigated in Li-O_2 batteries. It is believed that catalysts can help improve the poor kinetics of the oxygen evolution reaction (ORR), which is the key reaction happening during the charge of the battery. Possible candidates include metal oxides [1, 2], noble metals [3], etc. It has been found that with addition of catalysts in the cathode, the capacity of the battery can be increased to 2700mAh/g and the charge potential can be lowered below 4V. [1, 3]

ii) Redox Mediators

Besides the poor kinetics of ORR, the insulativity of the discharge product is another key reason for the high charge potential of metal-air batteries. After discharge, the insulating discharge product form a thick layer on the cathode surface, which makes it very hard for electrons to diffuse through during recharge, thus leading to a high charge overpotential. A redox mediator is a chemical that can react with the insulating discharge product chemically, so it can work as a charge carrier that carries charge from electrochemically active surface to the insulating discharge product. The redox mediators that are studied in Li-air battery include tetrathiafulvalene (TTF) [4], TEMPO (2,2,6,6-tetramethylpiperidinyloxyl) [5], lithium iodide [6], etc. The introduction of redox mediators can significantly lower the charge potential to 3V [6]. The same concept may also apply to the metal-O_2/CO_2 cell. With the introduction of proper redox mediators, such as an iodide salt, the charge potential of the cell can be lowered to a reasonable vale and the cell can be more realistically applicable.

Another area for future work is the effect of other impurity. For a metal-air battery, CO_2 is one major destructive impurity. However, there are other impurities that are detrimental for the cell, such as moisture, SO_2, NO_x, etc. The effect of moisture [7, 8] and ambient air [9] has been previously reported. Similar to CO_2, the introduction of moisture in to the cell can help increase the discharge capacity, due to the effect that the added H_2O can help the solvation of the intermittent product. However, the effect of other species has yet been studied. In order to have a metal-air battery that can be utilized in an atmosphere such as flue gas, it is important to understand the effect of these species.

REFERENCE

1. D ébart, J. Bao, G. Armstrong, P. G. Bruce, *J. Power Sources*, **2007**, 174, 1177.
2. D ébart, A. J. Paterson, J. Bao, P. G. Bruce, *Angew. Chem. Int. Ed.*, **2008**, 47, 4521.
3. Y. Lu et al. *J. Am. Chem. Soc.* **2010**, 132, 12170.
4. Y. Chen et al. *Nat. Chem.*, **2013**, 5, 489.
5. J. Bergner et al. *J. Am. Chem. Soc.*, **2014**, 136 (42), 15054.
6. T. Liu et al. *Science*, **2015**, 350, 530.
7. N. B. Aetukuri et al. *Nat. Chem.* **2014**, 7 (1), 50.
8. Li, F.; Wu, S.; Li, D.; Zhang, T.; He, P.; Yamada, A.; Zhou, H. *Nat. Commun.* **2015**, 6, 7843.
9. Zhang T.; Zhou H., *Nat. Commun.* **2013**, 4, 1817